# Dynamic wetting of complex liquids

Dissertation

zur Erlangung des Grades
„Doktor der Naturwissenschaften“
am Fachbereich Chemie, Pharmazie und Geowissenschaften
der Johannes Gutenberg-Universität in Mainz

vorgelegt von

Daniela Fell
geboren in Idar-Oberstein

Mainz, den 02. Februar 2013

Die vorliegende Arbeit wurde in der Zeit von August 2009 bis Januar 2013 am Max-Planck-Institut für Polymerforschung in Mainz durchgeführt.

Tag der mündlichen Prüfung: 03. April 2013
Dekan:

1. Berichterstatter:
2. Berichterstatter:

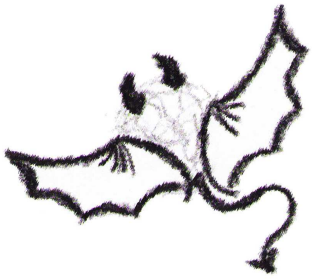

"God made the bulk; surfaces were invented by the devil."

*Wolfgang Pauli*

# Zusammenfassung

Für das Be- und Entnetzungsverhalten einfacher Flüssigkeiten wurde eine einfache Abhängigkeit des Kontaktwinkels $\theta$ von der Geschwindigkeit und der Oberflächenspannung vorhergesagt [1, 2]. Diese Abhängigkeit wurde von Cov und Voinov aufgrund der hydrodynamischen Theorie als $\theta \sim Ca^{\frac{1}{3}}$ ($Ca$: Kapillarzahl) beschrieben. Für komplexere Flüssigkeiten wie Tensidlösungen ist diese einfache Vorhersage allerdings nicht unmittelbar gegeben.

In der vorliegenden Arbeit präsentiere ich einen rotierenden Zylinderaufbau zur Untersuchung von Be- und Entnetzungsprozessen von Tensidlösungen anhand von geschwindigkeitsabhängigen Kontaktwinkelmessungen. Mit Hilfe dieses neuen Aufbaus konnte ich zeigen, dass das Be- und Entnetzungsverhalten von Tensidlösungen nicht der Cox-Voinov-Beziehung folgt, sondern eine stärkere Abhängigkeit von der Oberflächenspannung aufweist. Alle Tenside, unabhängig ihrer Ladung, wiesen diese Abhängigkeit auf, so dass ich elektrostatische Wechselwirkungen als Ursache hierfür ausschließen konnte. Vielmehr schlage ich die Ausbildung eines Oberflächenspannungsgradienten nahe der Dreiphasenkontaktlinie als Hauptursache für den starken Kontaktwinkelabfall mit steigender Tensidkonzentration vor. Oberflächenspannungsgradienten bilden sich nicht nur lokal nahe der Dreiphasenkontaktlinie, sondern auch global entlang der Luft-Wasser Grenzfläche aufgrund der kontinuierlichen Entstehung/Vernichtung der Grenzfläche durch das Auf-/Eintauchen des Zylinders in die Flüssigkeit. Durch systematisches Blockieren der Equilibrierungswege des globalen Gradienten entlang der Grenzfläche und/oder durch die Lösung habe ich die Bedeutung der Aufbaugeometrie für das Be-/Entnetzungsverhalten von Tensidlösungen genauer untersucht. Desweiteren hat die Oberflächenbeschaffenheit, wie beispielsweise die Rauigkeit oder chemische Homogenität, des zu be-/entnetzenden Substrats einen großen Einfluss auf das Verhalten der Flüssigkeit, d. h. die Dreiphasenkontaktlinie zeigt unterschiedliches Haftungsverhalten auf rauen/glatten oder homogenen/inhomogenen Oberflächen. Alles in allem habe ich gezeigt, dass das Be-/Entnetzungsverhalten von Tensidlösungen nicht von der Art des verwendeten Tensids (anionisch, kationisch, nichtionisch), sondern vielmehr von der Tensidkonzentration und -stärke, der Aufbaugeometrie und der Beschaffenheit der zu be-/entnetzenden Oberfläche abhängt.

Tensid hat nicht nur Einfluss auf das Be-/Entnetzungsverhalten von Lösungen, sondern auch auf das Aufprallverhalten von Tropfen auf freistehenden Filmen bzw.

Lösungen. In einem weiteren Teil der vorliegenden Arbeit habe ich mich mit der Stabilität des Luftpolsters zwsichen Tropfen und Film/Lösung beschäftigt. Damit der Tropfen mit dem Substrat verschmelzen kann, muss das Luftpolster zwischen Tropfen und Film/Lösung herausströmen und somit einen Kontakt zwischen den beiden Flüssigkeiten ermöglichen. Dabei wird das Herausströmen der Luft in Anwesenheit von Tensid aufgrund einer Änderung der Grenzbedingung von “slip” zu “no-slip” verlangsamt, d. h. das Verschmelzen von Tropfen und Substrat wird unterdrückt bzw. verlangsamt.

# Abstract

A simple dependency between contact angle $\theta$ and velocity or surface tension has been predicted for the wetting and dewetting behavior of simple liquids [1, 2]. According to the hydrodynamic theory, this dependency was described by Cox and Voinov as $\theta \sim Ca^{\frac{1}{3}}$ ($Ca$: Capillary number). For more complex liquids like surfactant solutions, this prediction is not directly given.

Here I present a rotating drum setup for studying wetting/dewetting processes of surfactant solutions on the basis of velocity-dependent contact angle measurements. With this new setup I showed that surfactant solutions do not follow the predicted Cox-Voinov relation, but showed a stronger contact angle dependency on surface tension. All surfactants independent of their charge showed this difference from the prediction so that electrostatic interactions as a reason could be excluded. Instead, I propose the formation of a surface tension gradient close to the three-phase contact line as the main reason for the strong contact angle decrease with increasing surfactant concentration. Surface tension gradients are not only formed locally close to the three-phase contact line, but also globally along the air-liquid interface due to the continuous creation/destruction of the interface by the drum moving out of/into the liquid. By systematically hindering the equilibration routes of the global gradient along the interface and/or through the bulk, I was able to show that the setup geometry is also important for the wetting/dewetting of surfactant solutions. Further, surface properties like roughness or chemical homogeneity of the wetted/dewetted substrate influence the wetting/dewetting behavior of the liquid, i. e. the three-phase contact line is differently pinned on rough/smooth or homogeneous/inhomogeneous surfaces. Altogether I showed that the wetting/dewetting of surfactant solutions did not depend on the surfactant type (anionic, cationic, or non-ionic) but on the surfactant concentration and strength, the setup geometry, and the surface properties.

Surfactants do not only influence the wetting/dewetting behavior of liquids, but also the impact behavior of drops on free-standing films or solutions. In a further part of this work, I dealt with the stability of the air cushion between drop and film/solution. To allow coalescence between drop and substrate, the air cushion has to vanish. In the presence of surfactants, the vanishing of the air is slowed down due to a change in the boundary condition from slip to no-slip, i. e. coalescence is suppressed or slowed down in the presence of surfactant.

# Table of Contents

# 1 Introduction and motivation

The wetting of a solid surface by a liquid is a basic element of many natural phenomena and technical applications, including spreading of liquid drops in coatings on metals, glass, or paper and the effective distribution of pesticides on leaf surfaces. The wetting of single-component liquids has been studied extensively resulting in several theories, e. g. molecular kinetic theory, hydrodynamic theory, etc. trying to describe the wetting/dewetting macroscopically as well as microscopically [3, 4]. Compared to single-component liquids, the wetting of more complex liquids, e. g. surfactant solutions, is less understood. Surfactant molecules can not only adsorb at the interfaces, but also influence the flow behavior of a liquid. While molecules adsorb at or desorb from the interfaces, concentration and therefore surface tension gradients can occur, leading to a flow along the interface - independent of the general flow behavior.

Surfactants are used to control the extent or the speed of wetting, due to their ability to reduce liquid-solid contact angles or to allow an aqueous solution to spread on nonpolar surfaces [3–7]. Most studies on the wetting of surfactant solutions are concerned with spontaneous spreading [8–14], i. e. wetting that is only driven by differences in surface tension, not by external forces. Further, they mostly concentrate on the thickness of the coated films [15] or on air entrainment at high velocities [16, 17], not directly on the velocity-dependent wetting and dewetting. But the velocity-dependent wetting/dewetting gets more and more important in technical applications such as printing and coating, since printing techniques become attractive to fabricate e. g. semiconductor devices cost-effective [18].

## 1.1 Dynamic wetting in printing techniques

Gravure printing is counted among the upcoming printing techniques used for fabricating semiconductor devices, although several unresolved issues are faced, e. g. ink viscosity, cavity size, and film stabilization [19]. The unresolved issues are connected to the wetting/dewetting processes involved in the gravure printing process.

Gravure printing is an intaglio process, where an engraved cylinder partially runs through an ink reservoir filling the cavities (Figure 1.1). During rotation, ink is

drawn out of the reservoir and excess ink is removed with a doctor blade.The substrate is pressed to the engraved cylinder by an impression roller, resulting in a homogeneous ink transfer from the cavities of the cylinder to the substrate [20, 21]. Because the printed lines are made of single dots placed closely together, the line quality depends on the resolution of the printing technique that ranges down to 15 µm or even less.

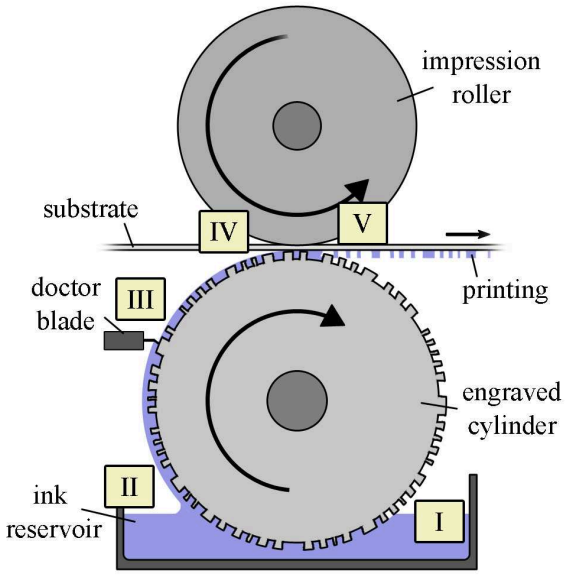


**Figure 1.1:** Sketch to illustrate the gravure printing technique. The engraved cylinder rotates through an ink reservoir drawing up an ink film that is removed via a doctor blade. The impression roller presses the substrate onto the engraved cylinder to allow for homogeneously transferring the ink from the cavities of the cylinder to the substrate.
Roman numerals indicate the dynamic processes involved in gravure printing.

So far, the gravure printing method as well as the necessary printing machines have only been optimized for visual image properties, e. g. magazine printing. But printing functional materials imposes more stringent requirements on the methods, machines as well as ink chemistry and rheology, e. g. high layer quality [21–23]. Therefore the basic specifications, e. g. wetting and dewetting steps during printing, have to be studied in further detail.

The wetting and dewetting steps involved in gravure printing can be divided as followed (Figure 1.1):

I *Wetting of the engraved cylinder*
When the cylinder enters the ink reservoir, the surface is wetted by the ink, depending on e. g. the ink and cylinder properties.

II *Dewetting of the engraved cylinder*
When the cylinder leaves the ink reservoir, the ink either dewets the cylinder or is drawn upwards as a (partial) film.

III *Removal of the excess ink*
The excess ink is removed by a doctor blade to ensure a homogeneous distribution of the ink in the cavities.

IV *Ink transfer from the cylinder to the substrate*
The ink gets in contact with the substrate and wets it. At the same time, the ink tear-off from the cylinder starts.

V *Ink tear-off from the cylinder*
During further rotation, the ink is transferred to the substrate and dewets the cylinder's cavities.

Each of those dynamic processes can influence the printing quality, e. g. a non-uniform filling of the cavities leads to an inhomogeneous printing or the ink can dewet on the substrate leading to unintended printing structures [23, 24] (Figure 1.2). Any irregularity or defect in the printed layers will lead to a reduced efficiency of the fabricated device or in the worst case to its failure [25].

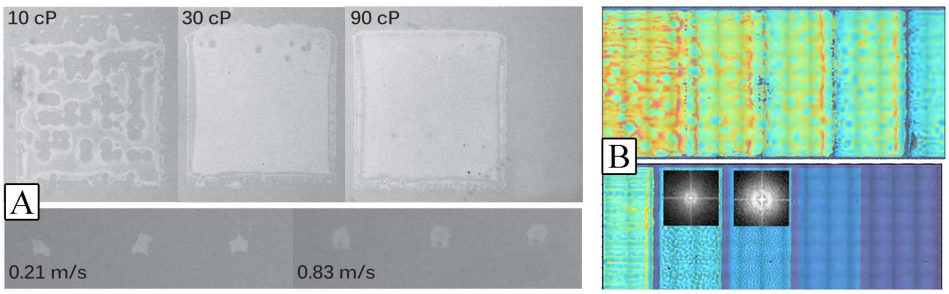


**Figure 1.2:** Influence of ink and printing properties on the quality of the printed layers, e. g. (A) ink viscosity (top) and printing velocity for printed poly-4-vinylphenol layers [23] as well as (B) cavity size (top: larger cavities) [19].

## 1.2 Surfactants influencing drop impacts

Drop impact on liquid surfaces is not only important for an understanding of fundamental fluid mechanics and wetting dynamics. But also numerous applications such as spray coating and distribution of pesticides and herbicides can profit from a better understanding of drop impact, e. g. spreading, complete wetting. Drop impact on liquid surfaces has been studied for more than 100 years [26–30] and with the development of high-speed cameras further studies contributed to the understanding of the phenomena involved in drop impact on a liquid pool [31–37] or free-standing surfactant films that can be strongly deformed during impact leading to softer impacts [38].

Surfactants do not only complicate the dynamic wetting/dewetting of aqueous solutions, but they can also influence the impact behavior of drops on liquids. Pure

water drops coalesce almost immediately with a pure water surface, while the presence of surfactant either in the drop or the liquid surface can alter this process dramatically - drops can float on the liquid surface [39]. This floating is promoted by a more efficient separating between drop and liquid surface in the presence of surfactant than when surfactant is absent. Already in the early works by Reynolds [40] and Lord Rayleigh [41, 42] the role of an air cushion was mentioned as a barrier between drop and liquid preventing coalescence, but they could not determine the detailed mechanism. Still, the mechanism of an air cushion preventing drops and liquid surface from coalescence is not clear, but surfactants seem to enhance its stability beside a motion of the liquid surface [31, 43].

## 1.3 Aim of the present work

The processes involved in gravure printing are not yet completely understood and face several additional issues, e. g. ink viscosity, stabilization of the printed film, or dewetting problems [19]. Largely, this thesis focuses on the understanding of wetting and dewetting processes involved in gravure printing. Therefore the wetting/dewetting of aqueous surfactant solutions on unstructured surfaces (Chapter 3) as well as the influence of the setup geometry on the wetting/dewetting of those surfaces (Chapter 4) is studied via a rotating drum setup. As solutions, pure water as well as different surfactant solutions are investigated. The viscosity of those solutions can be seen as constant, while the surface tension and the solid-liquid interactions are varied. Further, the influence of surface roughness as well as chemical homogeneity on the wetting/dewetting of aqueous surfactant solutions are investigated (Chapter 5).

A further part of this thesis focuses on the understanding of the surfactant influence on drop impact and especially on the stability of the air cushion preventing drops from directly coalescing with the film/liquid pool (Chapter 6). Therefore drop impact experiments on motionless liquid surfaces as well as on free-standing surfactant films, as softer substrates, are performed.

# 2 Fundamentals, materials and methods

In the following chapter fundamentals about dynamic wetting as well as the methods and materials used for the present work are described and discussed[1].

## 2.1 Surfactants

Surfactants are amphiphilic molecules [49] present in everyday life, e. g. children blowing soap bubbles or detergency, and in many industrial processes, e. g. emulsifier in food industry. The term "amphiphilic" originates from the Greek amphis (both) and philia (love) and describes a molecule consisting of a hydrophilic (water-loving) as well as a hydrophobic (water-hating) moiety. Due to these properties, surfactants support the mixing of two basically immiscible liquids, e. g. oil and water, by adsorbing at the liquid-liquid interface and therefore decreasing the interfacial tension (Figure 2.1). Respect to this property of decreasing the interfacial tension respectively the surface tension of the liquid $\gamma$ is shown by the name "surfactant" as a short version of "surface active agent". Other notations for surfactants are detergents, tensides or soap, but surfactant is probably the most descriptive one.

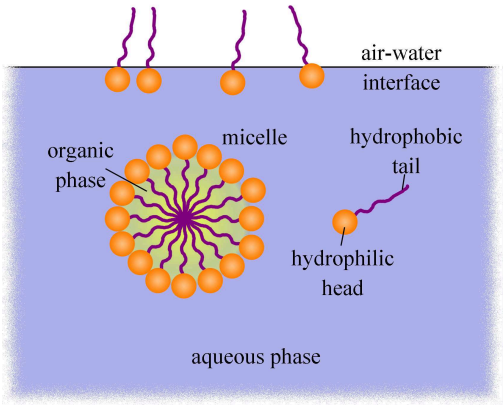


**Figure 2.1:** Surfactant molecules have a hydrophilic head (orange) and a hydrophobic tail (purple). They organize at the air-water interface or in micelles shielding an organic phase (yellow) from the aqueous phase.

[1] fundamentals are based on [44–48]

Surfactant molecules orient with the hydrophilic headgroup towards the more polar liquid/solid, while the hydrophobic tail orients towards the apolar liquid/solid. The hydrophobic part usually consists of a long straight alkyl chain $C_nH_{2n+1}$ with $n$ the number of carbon molecules ($8 < n < 20$). Completely or partially fluorinated chains are used to increase the hydrophobic character of the chains and to introduce even an organophilic character of the molecule. Depending on the hydrophilic headgroup, surfactants are divided into four groups:

- The headgroup of an **anionic** surfactant is negatively charged after dissociation. Sodium dodecyl sulfate (SDS), $C_{12}H_{25}OSO_3Na$, is one widely used anionic surfactant (Figure 2.2 A).
- After dissociation of a **cationic** surfactant, the headgroup carries a positive charge. One of the most important cationic surfactants is cetyl trimethyl ammonium bromide (CTAB), $C_{16}H_{33}N(CH_3)_3Br$ (Figure 2.2 B).
- **Nonionic** surfactants are not charged. They gain their hydrophilic behavior from highly polar groups as polyglycoles. A common type of nonionic surfactants is the group of alkyl glycoles ($C_nE_m$), with a hydrophobic alkyl chain $C_n$ and a hydrophilic glycole chain $E_m$ (Figure 2.2 C-E).
- An **amphoteric** surfactant has a positive as well as a negative charge, but the net charge is neutral.

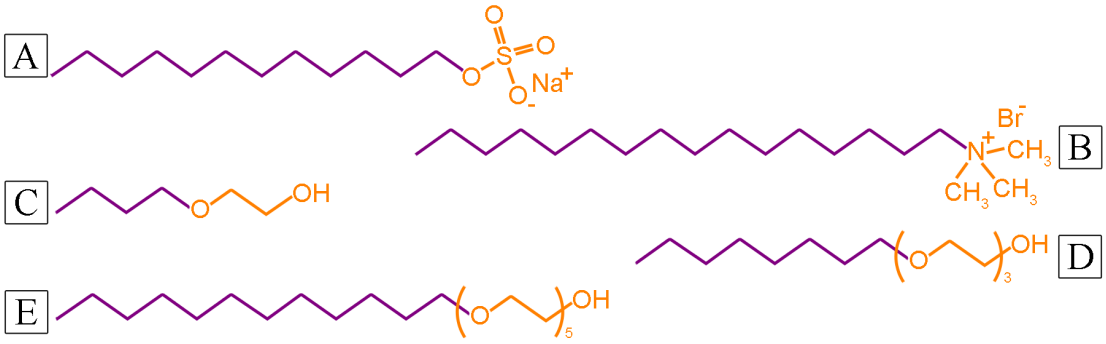


**Figure 2.2:** Chemical structure of the used surfactants showing the hydrophilic and hydrophobic moiety in orange and purple respectively: (A) sodium dodecyl sulfate SDS, (B) cetyl trimethyl ammonium bromide CTAB, (C) butyl glycole $C_4E_1$, (D) octyl triglycole $C_8E_3$, and (E) dodecyl pentaglycole $C_{12}E_5$.

### 2.1.1 Critical micelle concentration

Being soluble at low concentrations, above a certain concentration surfactant molecules can aggregate spontaneously in water and form well-defined structures like

spherical micelles, cylinders, etc. [50]. To form the aggregates, a certain number of surfactant molecules bundles together, depending on the surfactant properties, e. g. size, charge, concentration, shape of the molecules, etc. The hydrophobic tails congregate, while the hydrophilic headgroups orient towards the aqueous phase (Figure 2.1). The concentration above which aggregate formation takes place is called **critical micelle concentration (cmc)**.

At low concentrations (well below cmc) most of the surfactant molecules are dissolved as individual molecules, but some micelles already exist (Figure 2.3 A, purple). The surfactant molecules adsorb at the air-water interface resulting in a strong decrease in surface tension with increasing surfactant concentration (Figure 2.3 B). When the concentration reaches cmc, the decrease in surface tension flattens. At the same time, surfactant molecules no longer prefer adsorbing at the air-water interface, but spontaneously congregate to micelles. The concentration of non-congregated molecules keeps constant, while that of micelles increases (Figure 2.3 A, orange). With a further increase in surfactant concentration, the surface tension does not change significantly - further micelles are formed (Figure 2.3 A, blue).

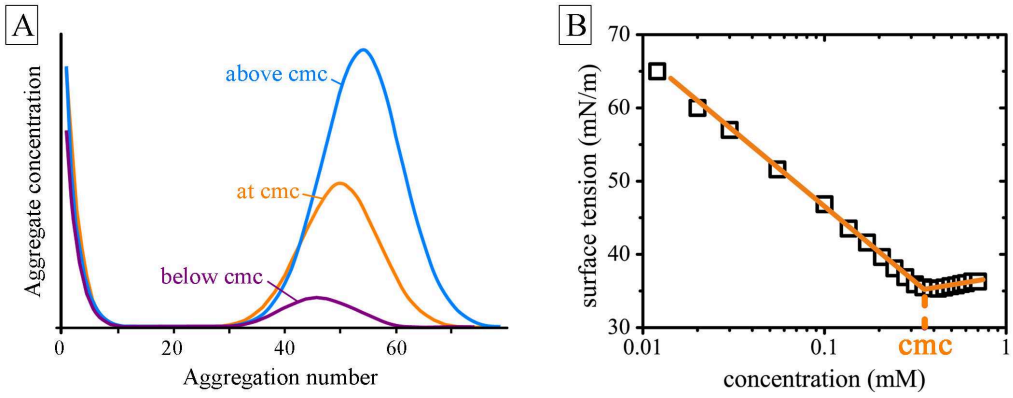


**Figure 2.3:** (A) Schematic distribution of the surfactant aggregate concentration as a function of the aggregation number for concentrations below, at and above cmc. Redrawn from [47, 51]. (B) Concentration-dependent surface tension measurement to determine the critical micelle concentration of a surfactant solution.

In parallel to the increasing number of micelles, the capacity of surfactants to solubilize hydrophobic substances, e. g. oil in water, increases with increasing surfactant concentration. The molecules, which usually form the micelles, adsorb at the oil-water interface and make the two liquids miscible [47].

Critical micelle concentrations as well as surface tensions were measured with the DCAT11 tensiometer from DataPhysics using the Wilhelmy-plate method (Section 2.3.2.1). Before every measurement, the platinum/iridium plate was cleaned

using a burner to remove all organic traces and insure a zero contact angle. For measuring critical micelle concentrations, the surfactant concentration in the liquid was subsequently increased while measuring surface tensions.

### 2.1.2 Adsorption

Adsorption describes the accumulation of molecules or dissolved solids at an interface [46]. Thereby the molecules or dissolved solids going to adsorb are called **adsorpts**, while the interface is referred to as **adsorbent** (Figure 2.4). Already adsorbed molecules are termed **adsorbates**. Depending on the dominating interaction between adsorbate and adsorbent, the adsorption process can be referred to as physisorption or chemisorption. During physisorption, adsorption is dominated by physical interactions, like van der Waals attraction, while chemisorption is dominated by chemical bondings. Physically adsorbed molecules are reversibly bound to the interface and are free to diffuse and rotate at the adsorbent [47], i. e. they can desorb again while chemically adsorbed molecules are bound to the interface.

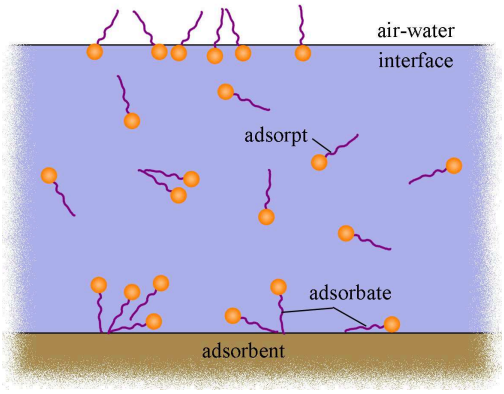


**Figure 2.4:** Scheme to illustrate the adsorption of surfactant molecules. The substrate respectively the interface, where the molecules adsorb to, is referred to as adsorbent. Adsorbate describes the already adsorbed molecules. The not yet adsorbed molecules are named adsorpts.

While working with substances adsorbing at interfaces, one important question is, how much of the substance is adsorbed. The adsorption function $\Gamma = f(\mathrm{p,T})$ indicates the number of adsorbed molecules per unit area and can be determined experimentally. $\Gamma$ depends on temperature T and either pressure p for adsorption of gas molecules or concentration c for adsorption from solution. Graphs of $\Gamma$ versus p respectively c at a constant temperature are called **adsorption isotherms** [47, 52].

Adsorption from solution is always an exchange process, e. g. the adsorption of surfactant molecules. Molecules adsorbing to the interface have to replace solvent molecules located at the interface. For surfactant molecules this exchange is preferable, because of the surfactant's amphiphilic character - one side in the solvent (mostly water) and one side at the solid substrate, in the vapor or additional liquid phase. The driving force for surfactant molecules going to the interface is the increasing entropy of the solvent molecules, known as entropy effect.

### 2.1.3 Used surfactants

During this work anionic, cationic, and neutral surfactants were used. The chemical structure of the surfactants are given in Figure 2.2 while the properties are summarized in Table 2.1.

| | surfactant | type | cmc / mM | $\gamma^*$ / mN/m | Figure 2.2 |
|---|---|---|---|---|---|
| SDS | sodium dodecyl sulfate | anionic | 8 | 38.2 | A |
| CTAB | cetyl trimethyl ammonium bromide | cationic | 1 | 36.7 | B |
| $C_4E_1$ | butyl glycole | neutral | 500 | 34.7 | C |
| $C_8E_3$ | octyl triglycole | neutral | 7.5 | 29.4 | D |
| $C_{12}E_5$ | dodecyl pentaglycole | neutral | 0.07 | 30.3 | E |

* at cmc

**Table 2.1:** Summary of the surfactants used during this work with according critical micelle concentration and surface tension $\gamma$.

## 2.2 Contact angles

A drop placed on a solid substrate shows a characteristic angle between the air-liquid and solid-liquid interface - the **contact angle** $\theta$ (Figure 2.5). The drop can either spread completely along the surface or form finite contact angles [4] (Figure 2.6).

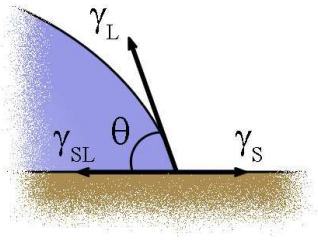


**Figure 2.5:** Sketch of a drop sitting on a substrate with the contact angle $\theta$ and the interfacial tensions of the solid-liquid $\gamma_{SL}$ as well as of the air-solid $\gamma_S$ and air-liquid interface $\gamma_L$.

For $\theta \neq 0°$, the liquid, air, and solid phases are in contact at the edge of the drop. The line formed by these three phases is called **three-phase contact line**, that does not only exist for drops, but for any liquid wetting a substrate.

Contact angles do not only depend on material properties of the liquid and of the substrate, but also on the interactions between liquid-liquid and solid-liquid molecules (Figure 2.6).

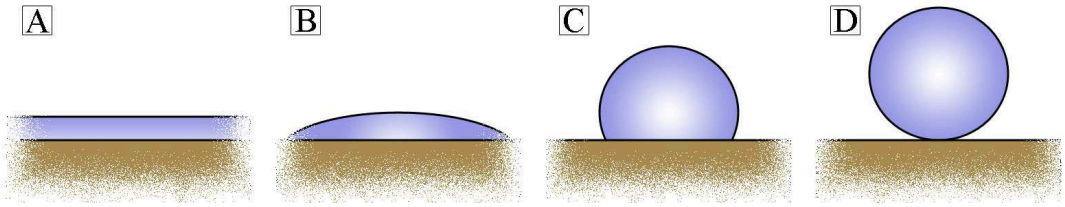


**Figure 2.6:** The contact angle is a measure of wettability - low contact angles for highly wettable substrates and high contact angles for hardly wettable substrates. (A) complete wetting ($\theta = 0°$); (B) highly wetting ($\theta < 90°$); (C) low wetting ($90° < \theta < 180°$); (D) non-wetting ($\theta = 180°$).

The strength of the interaction between liquid molecules themselves compared to the interaction of solid molecules with liquid molecules influences the contact angles (Table 2.2). These interactions are described by the interfacial tensions of the solid-liquid $\gamma_{SL}$ and the air-solid interface $\gamma_S$ as well as the surface tension of the air-liquid interface $\gamma_L$ originating from the cohesive forces between liquid molecules pulling molecules at the various interfaces towards the bulk liquid. The surface tension, given as the ratio of performed work $\Delta W$ and resulting change in surface area $\Delta A$

$$\gamma = \frac{\Delta W}{\Delta A}, \tag{2.1}$$

leads in absence of gravity to sphere-like drops due to a minimized surface.

The drop wets the surface completely in case of weak liquid-liquid interactions compared to solid-liquid interactions. In the opposite case, the drop forms an almost ideal sphere on the substrate ($\theta \approx 180°$). Regarding the influence of liquid-liquid and solid-liquid interactions on the contact angle, the contact angle can be seen as a measure of wettability and described by interfacial and surface tensions.

Young used the interfacial tensions to describe the equilibrium contact angle $\theta_{eq}$. He assumed the forces respectively tensions acting on the three-phase contact line and therefore influencing the contact angle to be balanced (shown as arrows in Figure 2.5). Laplace formulated this relation described by Young as [53, 54]

$$\gamma_L \cdot \cos\theta_{eq} = \gamma_S - \gamma_{SL} \tag{2.2}$$

with the interfacial tensions instead of the forces. This relation is known as “Young’s equation” and only valid for all forces being balanced.

| contact angle | degree of wetting | type of interaction | | Figure 2.6 |
|---|---|---|---|---|
| | | liquid-liquid | solid-liquid | |
| $\theta = 0°$ | complete | weak | strong | A |
| $0° < \theta < 90°$ | high wettability | weak | weak | B |
| | | strong | strong | |
| $90° < \theta < 180°$ | low wettability | strong | weak | C |
| $\theta = 180°$ | non-wetting | strong | weak | D |

**Table 2.2:** Correlation between contact angle, wettability, and molecule interactions.

### Dynamic contact angle

When the Young's equation is not valid, i. e. the three tensions are not balanced, the three-phase contact line moves. Upon this movement the contact angle changes - now called dynamic contact angle. Depending on the movement of the three-phase contact line, the resulting dynamic contact angle is referred to as **advancing** $\theta_{adv}$ or **receding contact angle** $\theta_{rec}$. The advancing contact angle describes the contact angle, when the liquid wets the surface, while the contact angle of a dewetting liquid is referred to as receding contact angle (Figure 2.7). Advancing and receding contact angles are not necessarily identical due to slight variations in surface roughness and contamination leading to local variations in interfacial tensions.

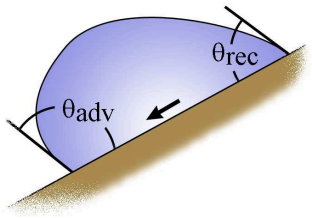


**Figure 2.7:** A drop sliding down an inclined surface has usually two different contact angles - the advancing $\theta_{adv}$ and receding contact angle $\theta_{rec}$. The difference $\theta_{adv}$ - $\theta_{rec}$ is called hysteresis.

The difference between advancing and receding contact angles is called **hysteresis** and typically in the order of 5 to 20°. But the hysteresis can also be significantly higher or even about 0° (for superhydrophobic surfaces), depending on the substrate, e. g. roughness or homogeneity.

$$\text{hysteresis} \quad = \quad \theta_{adv} - \theta_{rec} \quad \geq \quad 0° \tag{2.3}$$

### Apparent and microscopic contact angle

When the three-phase contact line is not in equilibrium, contact angles depend strongly on the length scale, i. e. on the distance from the contact line [4]. The length scale of a spreading drop that partially wets a substrate can be divided into three regions leading to two different contact angles depending on the observed regions (Figure 2.8):

- In the macroscopic region (millimeters) the macroscopic respectively apparent contact angle $\theta_{ap}$ is observed.
- When looking at an intermediate scale of the three-phase contact line region (micrometers), the contact line turns from concave to convex (orange blow-up) as experimentally confirmed by Marsh et al. [55] among others. The resulting (microscopic) contact angles $\theta_m$ are smaller than the apparent ones.
- The region close to the three-phase contact line (nanometers) feels interfacial fluctuations of liquid molecules and the substrate's corrugation described by computer simulations [56] (purple blow-up).

Conventional contact angle measurements lead to the determination of the apparent contact angle.

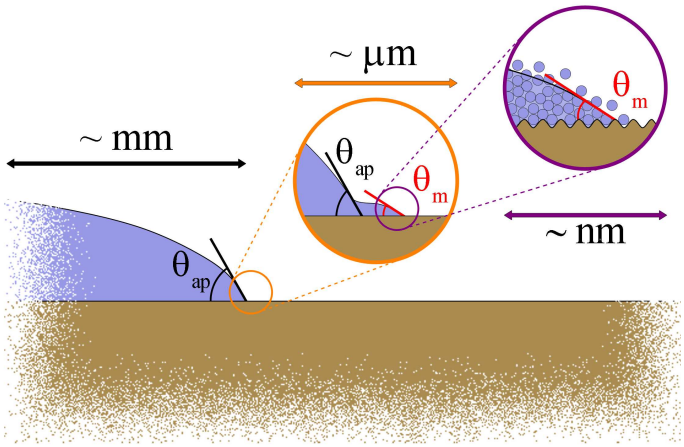


**Figure 2.8:** A partially wetting drop spreads along a surface (millimeter-sized). The measurable contact angle is called apparent or macroscopic contact angle $\theta_{ap}$. Going to a micrometer scale, the interface close to the three-phase contact line is curved differently leading to a smaller microscopic contact angle $\theta_m$ compared to $\theta_{ap}$ (orange blow-up). On a nanometer scale (purple blow-up), the interface fluctuates and the substrate's corrugation can be seen. Adapted from [4].

### Precursor film

Drops deposited on a solid substrate often show a molecularly thin film of adsorbed liquid molecules in front of the three-phase contact line, the so-called **precursor film** [57, 58] (Figure 2.9). This precursor film is formed in case of a volatile liquid by adsorbing liquid molecules from the vapor phase onto the solid substrate (A). In this case, the drop is in thermal equilibrium with its vapor leading to an elongated precursor film. When a non-volatile liquid is considered, the vapor is not saturated and therefore an adsorption of molecules from the atmosphere is not very likely (B). The precursor film is formed by liquid molecules from the drop migrating in front of the three-phase contact line [59]. Therefore the film size is restricted to several micrometers and the film thickness is below 0.1 µm.

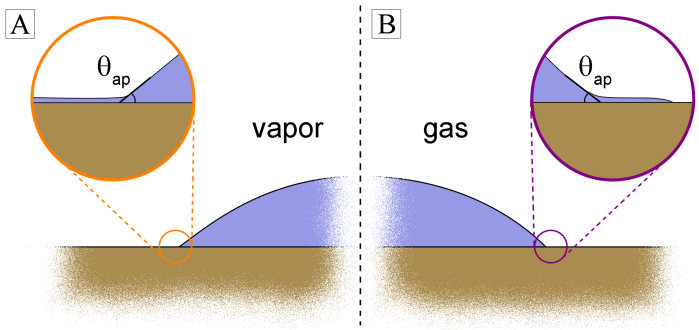


**Figure 2.9:** Schematic drawing either of a volatile drop in equilibrium with its vapor (A) or of a non-volatile drop (B) spreading on a substrate. The insets show the precursor films emerging during the spreading. Adapted from [58].

### Measuring static contact angles

Observing sessile drops is a common method for measuring static contact angles $\theta_s$. Thereby a light source is positioned behind the drop, so that it appears dark. Either a direct determination of the contact angle with a goniometer or an indirect determination with video recording is possible (Figure 2.10). For the indirect determination, a fitting of the contour using the Laplace equation is necessary.

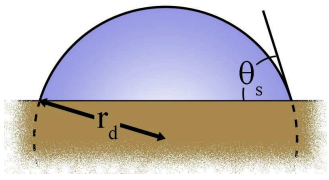


**Figure 2.10:** Sessile drop method to determine static contact angles $\theta_s$ by fitting the drop's contour with the drop radius $r_d$.

### Measuring dynamic contact angles

Sessile drops can also be the beginning of dynamic contact angle measurements, e. g. the tilting plate method (Figure 2.11 A). The drop sits on the surface, that is inclined subsequently from 0 to 90°. The contact angle on the downhill side ($\theta_{adv}$) increases due to gravity, while the contact angle on the uphill side ($\theta_{rec}$) decreases. They are measured just before the drop rolls off. The tilting angle of the plate is called roll-off angle $\alpha$ and provides as well as the hysteresis some information about surface roughness, chemical and topological heterogeneity. Another method uses the movement of the contact line due to increasing/decreasing the drop volume (Figure 2.11 B).

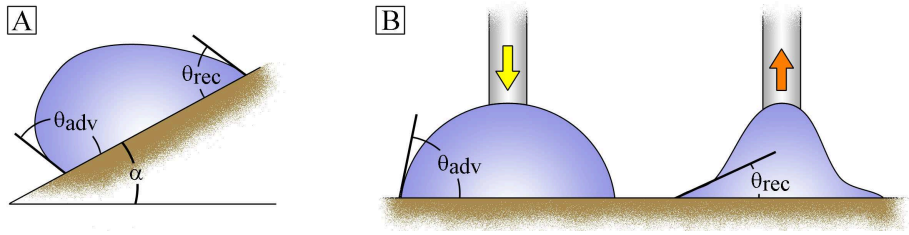


**Figure 2.11:** Dynamic contact angles measured by tilting the substrate (A) or increasing/decreasing the drop volume (B).

The values of the measured contact angles depend on the measurement technique, i. e. the values can differ between the tilting plate method and the increasing/decreasing the drop volume method.

The optical contact angle measurement device from DataPhysics OCA35 was used to measure static and dynamic contact angles. Dynamic contact angles were measured using the tilting plate method. For both measurements, the initial drop volume was about 3 µl.

## 2.3 Dynamic wetting

The wetting of a solid surface by a liquid is a basic element of many natural phenomena and technical applications. Examples include the spreading of liquid drops in coatings on metals, glass, plastics, or paper and the effective distribution of pesticides on leaf surfaces. During dynamic wetting, a liquid displaces another fluid (liquid or gas) from a solid surface. Two types of wetting can be distinguished - forced and spontaneous wetting:

- In **forced wetting**, external forces are applied to increase the solid-liquid interfacial area beyond the static equilibrium.
- The **spontaneous wetting** (or spreading) of a drop is caused by liquid-solid interactions heading towards thermodynamic equilibrium.

Forced wetting is important in, e. g. industrial printing processes, where a thin liquid layer is deposited continuously onto a moving surface. At a certain velocity, the liquid fails to replace the air from the substrate so that air is entrapped in the coated film. This limits the coating velocity to a critical velocity. Not only forced wetting is of practical relevance, but also spontaneous spreading, e. g. application of paints, adhesives, or lubricants.

To describe the dynamic wetting/dewetting of moving liquids, the apparent contact angle, which then depends on velocity, can be used [60] (Figure 2.12). When the three-phase contact line is advancing, $\theta_{ap}$ becomes higher with increasing velocity while in the receding case, it decreases. The difference at zero velocity between advancing and receding contact angle is called hysteresis.

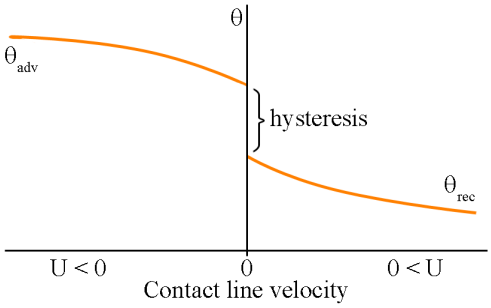


**Figure 2.12:** Sketch of the velocity dependency of experimentally determined apparent contact angles. $\theta_{adv}$ increases with increasing velocity $U$, while $\theta_{rec}$ decreases with increasing velocity. Adapted from [60].

$\theta_{ap}$ during forced wetting does not only depend on the velocity of the liquid $U$, but also on the viscosity of the liquid $\eta$ and the liquid's surface tension [61, 62]. These parameters can be correlated by the dimensionless **Capillary number** $Ca$:

$$Ca = \frac{U\eta}{\gamma} \tag{2.4}$$

Dynamical aspects of wetting are far from being understood, due to their inherent complexity. Observations of wetting phenomena usually involve only macroscopic quantities, e. g. wetting speed, surface tension, apparent contact angle, etc., while dynamic wetting also operates at a molecular level. Furthermore, the diversity of the possible materials and involved liquids at velocities ranging from a few micrometers per second up to several meters per second, complicate the understanding. Materials can be soft or hard, smooth or structured, homogeneous or heterogeneous, etc. while a huge variety of liquids have to be covered, e. g. an aqueous solution versus a viscous polymer solution.

### 2.3.1 Theories

The precise mechanism of a three-phase contact line motion across a surface is not yet understood. Different theories and models based on different length scales have been developed, but none of them fits the wetting/dewetting in its entire range. Models for fitting dynamic wetting experiments are highly discussed [61, 63–69]. Two popular theories are described below, the molecular kinetic theory and the hydrodynamic theory. In none of these models, precursor films, microscopic changes of the contact angles or surfactant-laden interfaces are an issue.

#### 2.3.1.1 Molecular kinetic theory

The **molecular kinetic theory** focuses on energy dissipation due to molecules attaching to or detaching from the solid surface close to the moving three-phase contact line [63] (Figure 2.13, blow-up). When the adsorption rate does not equal the desorption rate, the three-phase contact line tends to move, either in advancing direction for liquid molecules replacing adsorbed gas molecules or in receding direction for replaced liquid molecules [64]. The disturbance of adsorption/desorption equilibria leads to changes in the local surface tension and, hence, to a movement of the three-phase contact line across the solid surface [63].

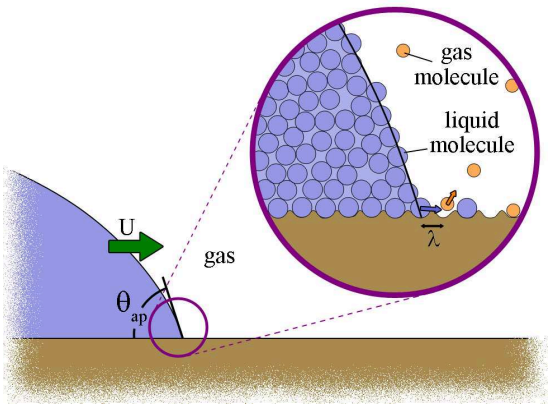


**Figure 2.13:** Liquid molecules replace gas molecules at the solid surface and change therefore the adsorption equilibrium, leading to a movement of the three-phase contact line. Adaptation from [63].

The assumption of local changes in surface tension due to the moving three-phase contact line and therewith velocity-dependent contact angles [70] leads to

$$U = \frac{\gamma\left(\cos\theta_{eq} - \cos\theta_{ap}\right)}{\zeta}, \tag{2.5}$$

with the three-phase contact line friction coefficient $\zeta$ given as

$$\zeta \sim \eta \left( \frac{V_m}{\lambda^3} \right) \exp(W_a). \tag{2.6}$$

The average displacement $\lambda$ is typically in the nanometer range, while viscosity, molecular flow volume $V_m$, and work of adhesion $W_a$ depend on the system.

This theory can describe parts of the velocity-dependent behavior of contact angles, but misses the link to hydrodynamics [63], which is discussed in the hydrodynamic theory.

#### 2.3.1.2 Hydrodynamic theory

The **hydrodynamic theory** describes the motion of liquid during forced wetting with respect to energy dissipation due to a viscous flow near the three-phase contact line [63].

For describing flow near a moving three-phase contact line, the classical hydrodynamic approach does not give an acceptable solution. The assumption of a moving contact line and the conventional no-slip boundary condition between solid and liquid lead to unbound stresses at the three-phase contact line and infinite forces exerted by the liquid to the solid [71]. Different approaches to deal with this singularity are possible, e. g. truncation of the solution [1] or relaxing the no-slip condition close to the three-phase contact line [60, 71]. In both cases, the air-liquid interface far from the contact line adopts the static shape of the interface. The viscous bending of the interface becomes only important on the mesoscale [63] (Figure 2.14). The apparent contact angle can be determined by extrapolating the static interface to the solid surface, while the microscopic contact angle is said to remain constant, although a velocity-dependency can not be excluded [1].

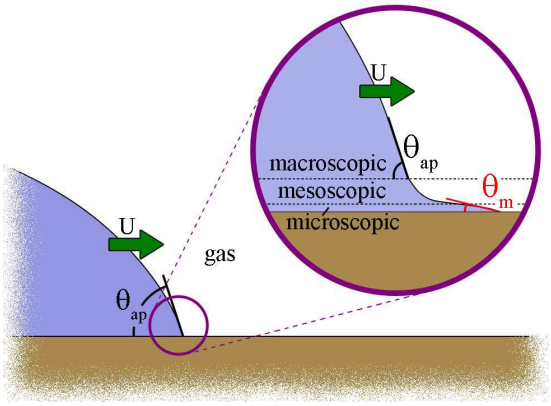


**Figure 2.14:** Different length scales of an advancing meniscus, illustrating the viscous bending of the air-liquid interface on the mesoscale. Adapted from [63].

The change in dynamic contact angle due to viscous bending of the air-liquid interface can be described in terms of the Capillary number in the limit of the lubrication approximation (parabolic flow profile and low contact angles) [1, 2, 60, 63] as

$$\theta_{ap}^3 - \theta_m^3 \quad = \quad 9\ Ca\ \cdot\ \ln\left(\frac{L}{L_m}\right) \tag{2.7}$$

with the macroscopic $L$ and microscopic lengths $L_m$, usually in the range of 10 µm respectively 1 nm. As the molecular kinetic theory, also the hydrodynamic theory has its limitations - this time at the molecular length scale. Therefore several combined theories are developed, e. g. by Shikhmurzaev [65, 66] or Billingham [67, 68], containing approaches from both theories.

#### Cox-Voinov relation

In the **Cox-Voinov relation** the velocity field in the hydrodynamic theory is eliminated and a completely wetting liquid ($\theta_{eq} \approx 0°$) is assumed, i. e. $\theta_m \approx 0°$ [1, 2]. Then Equation (2.7) simplifies and results in

$$\theta_{ap} \quad \sim \quad U^{\frac{1}{3}} \qquad \text{and} \qquad \theta_{ap} \quad \sim \quad \gamma^{-\frac{1}{3}}. \tag{2.8}$$

These relations hold for simple (single-component, Newtonian) liquids and low contact angles ($\theta_{eq} \approx 0°$). But what happens in the presence of complex liquids, e. g. surfactant solutions, or absence of a precursor film? The influence of surfactant solutions will be discussed in Chapter 3.

### 2.3.1.3 Landau Levich Derjaguin-theory

Above a certain velocity, a solid substrate is not completely dewetted when pulled out of a liquid, i. e. a liquid film is pulled upwards (Figure 2.15).

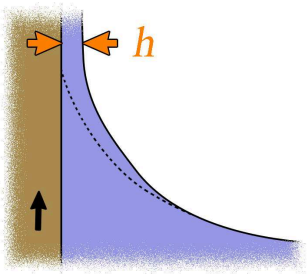


**Figure 2.15:** Scheme of the static meniscus (dashed line) as well as of the withdrawn film (straight line) with film thickness $h$. Adapted from [72].

This transition from a complete dewetting, i. e. a finite contact angle, to a film pulled up is called **Landau Levich Derjaguin**-transition and described in the according theory. At velocities below this velocity, a static meniscus can be observed (Figure 2.15, dashed line), while for higher velocities a thin liquid film is pulled upwards [15, 72, 73]. Surfactants present in the liquid cause surface tension gradients in the entrained film [74].

The Landau Levich Derjaguin-theory provides information about the film thickness $h$ dependent on the surface tension and density $\rho$ of the liquid as well as the Capillary number and gravity constant g

$$h = 0.94\sqrt{\frac{\gamma}{\rho g}} \cdot Ca^{\frac{2}{3}}. \tag{2.9}$$

## 2.3.2 Measurement techniques

A continuous motion of either the liquid along the substrate or the substrate through the liquid is essential for measuring dynamic contact angles. Contact angles can then be measured either optically or via force measurements.

### 2.3.2.1 Wilhelmy plate method

The principle of the **Wilhelmy plate method** goes back to Ludwig Wilhelmy [75]. A thin plate is vertically placed into the liquid and the force required to prevent the plate from being drawn into the liquid is measured (Figure 2.16).

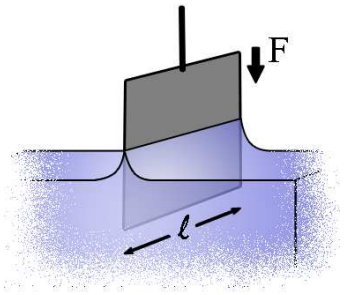


**Figure 2.16:** Sketch of a Wilhelmy plate tensiometer, with resulting force $F_{\gamma,\theta} = 2l\gamma \cdot \cos\theta$ from which either surface tension $\gamma$ or contact angle $\theta$ can be calculated.

Besides the gravitation and buoyancy, this force is given as

$$F_{\gamma,\theta} = 2l\gamma \cdot \cos\theta, \tag{2.10}$$

with the plate length $l$ [47]. For zero contact angle plates, like platinum ($\cos\theta = 1$), the surface tension can be calculated. Contact angles on plates are measurable when the surface tension of the wetting liquid is known. Therefore the plate has to be connected to the force balance. For measuring dynamic contact angles, the plate is uniformly moved into ($\theta_{adv}$) or out ($\theta_{rec}$) of the liquid while the force acting on the plate is measured. In consequence of the limited plate geometry and requirement for a uniform plate or beaker motion, the velocity range is limited to a range up to a few millimeters per second.

#### 2.3.2.2 Plunging tape method

In the **plunging tape method** a continuous tape, usually a polymer tape, is guided via rollers through a tank filled with liquid [61, 76–78]. The dynamic contact angle, usually the advancing contact angle, between tape and liquid is photographed and then optically analyzed. But also observing receding contact angles with this kind of setup is feasible. The achievable velocity in this type of setup typically covers a huge range - from $10^{-5}$ to more than 5 m/s. The tape has to fulfill special requirements, like flexibility and a certain length. Depending on the question, the geometry of the entering tape varies either in the angle it plunges into the liquid or in the curvature of the tape.

Blake for example (Figure 2.17) used a poly(ethylene terephthalate) tape entering the pool vertically. Before the tape was allowed to enter the pool, it was slightly bent (inset) to allow for focusing on a single point of the three-phase contact line [61].

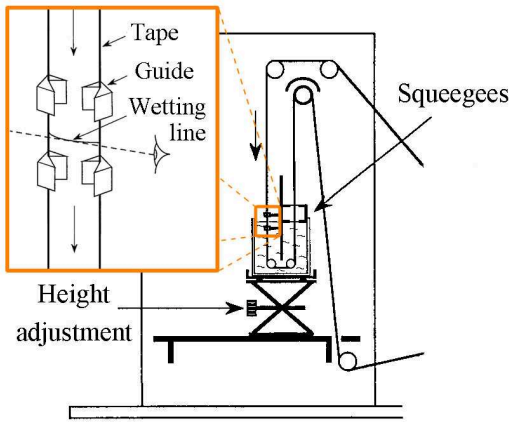


**Figure 2.17:** Schematic drawing of a plunging tape apparatus to determine static and dynamic contact angles. The inset magnifies the bending of the tape by guides. Adapted from [61].

This method does not only allow for observing dynamic contact angles, but also for observing air entrainment to the liquid at the three-phase contact line [76].

### 2.3.3 Different measurement technique - Rotating drum

For studying dynamic wetting and dewetting processes involved in gravure printing, a new setup - similar to the gravure printing setup - was designed. It contains a drum rotating in a bath allowing for imaging dynamic contact angles (advancing and receding) as well as three-phase contact lines depending on the rotation velocity. Not only a huge range of rotation velocities can be achieved, but also the drum's surface properties can be altered by applying different coatings. For studying air entrainment, comparable setups have been used earlier [16, 17, 55, 79, 80].

#### 2.3.3.1 Basic specifications

The rotating drum setup consists of an exchangeable drum placed horizontally in a bath filled with liquid (Figure 2.18 A). The bath (10 cm in width, 17 cm in depth, and 15 cm in height) has three windows - one at the front to allow for observing the three-phase contact line (B) and one at each side of the bath to observe the contact angles (C).

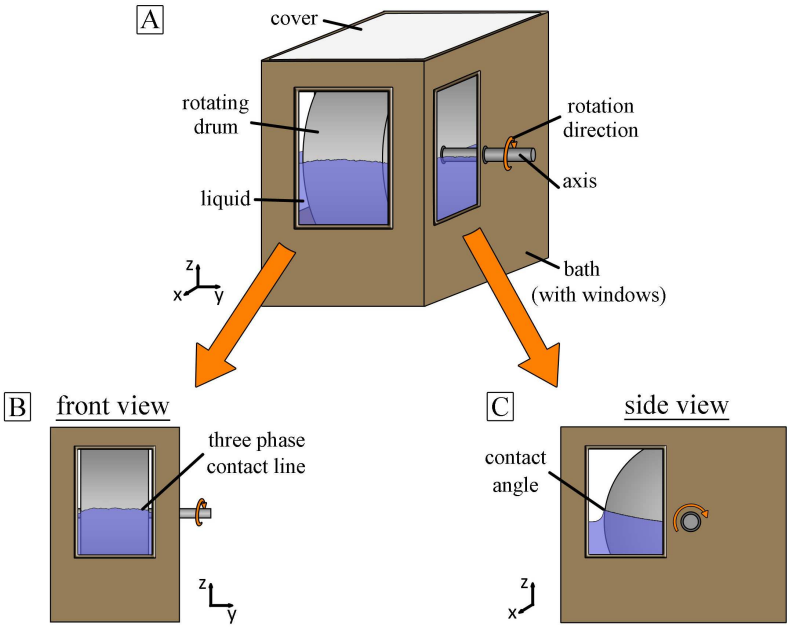


**Figure 2.18:** (A) Scheme of the rotating drum in a closed cell with observation windows. (B) Front-view imaging is used for visualizing the three-phase contact line. (C) Dynamic contact angles are observed via side-view imaging.

The exchangeable drums are made of polished stainless steel with 12 cm in diameter and 5 cm in width, but they differ in their radius of curvature:

- A planar drum is used for observing three-phase contact lines (no additional curvature added to the drum, Figure 2.19 A).
- Contact angles are measured by using a barrel-shaped (slightly convex) drum with a curvature of $0.2\,\mathrm{cm}^{-1}$ (spherical segment, Figure 2.19 B).

The planar drum with its constant radius all over the surface allows for a constant rotation velocity of the drum's surface independent of the observation postion. The rotation velocity of the barrel-shaped drum depends on the position of observation in contrast to the planar drum - higher velocity at the drum's center compared to the edges. The focal plane in case of the barrel-shaped drum is in the middle of the drum (Figure 2.19 B, dashed red line).

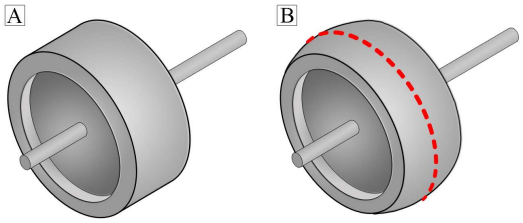


**Figure 2.19:** Sketch of the planar, cylindrical (A) and the barrel-shaped, convex drum (B). The dashed red line symbolizes the focal plane for observing contact angles using the barrel-shaped drum.

The rotation direction can be changed, so that either the advancing or the receding contact side can be observed. Rotation velocities ranging from $10^{-4}$ to 1 m/s are achievable with the help of four different motors - each motor covering one order of magnitude with different velocity increments available (Table 2.3).

| velocity range / m/s | velocity step / m/s |
|---|---|
| $10^{-4}$ - $10^{-3}$ | $5 \cdot 10^{-5}$ |
| $10^{-3}$ - $10^{-2}$ | $5 \cdot 10^{-4}$ |
| 0.01 - 0.1 | 0.005 |
| 0.1 - 1 | 0.05 |

**Table 2.3:** Four different motors with different step sizes allow for covering velocities ranging from $10^{-4}$ to 1 m/s.

During measurement the bath can either be closed to have an almost saturated atmosphere or open. In case of the closed bath, the relative humidity was about 95 % (Dostmann, P570), while for the open bath a humidity about 30 % was measured directly above the liquid. All measurements were performed at room temperature (about 21°C). The motion of the three-phase contact line as well as the change in contact angles are observed with the help of a high-speed camera, either a Photron,

Fastcam SA-1 or an Olympus i-SPEED LT. As objectives either a Navitar tube (up to 12 × magnification) or a macro zoom objective (6 × magnification) can be used.

#### 2.3.3.2 Three-phase contact line

For observing three-phase contact lines, the planar drum is inserted in the bath and the high-speed camera is placed at the front window (Figure 2.18 B), while light comes from the side. Due to its constant radius, the planar drum has a constant velocity all over its front surface in contrast to the barrel-shaped drum (Figure 2.19). This constant velocity simplifies the interpretation of the observed three-phase contact line, that is observed at a frame rate of 250 Hz (zoom objective) at a slight inclination (± 5°) of the camera - a downwards tilt for $\theta_{ap} < 90°$ and an upwards tilt for $\theta_{ap} > 90°$.

Depending on the rotation velocity, the shape of the receding three-phase contact line changes (Figure 2.20), while the advancing contact line is almost constant.

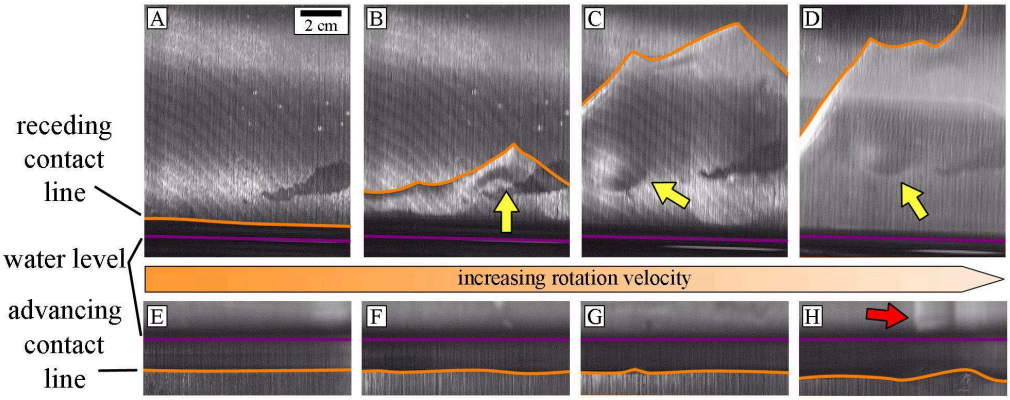


**Figure 2.20:** Velocity-dependency of the three-phase contact line. The receding contact line (A-D) changes significantly with increasing velocity, from a straight line, to a film transported along the drum (A-D: 1, 4, 8, 10 mm/s). The purple lines emphasize the water level, while the orange lines point out the contact line. Yellow arrows point to thicker parts of the film, originating from downflowing liquid. The advancing contact line is almost velocity independent (E-G). Only liquid transported from the receding to the advancing side disturbs its shape (H, red arrow points onto the liquid film). The rotation velocities are 1, 4, 8, and 10 mm/s (E-H). The system used is water wetting/dewetting a glass surface glued around the drum. The reflexes seen in A-D originate from reflected light at the liquid/glass/steel interface.

At low velocities, the receding contact line is roughly a straight line (A), while with increasing velocity a triangular shape is formed up to a critical velocity (B, C). At this critical velocity a film is drawn upwards (D) that is transported to the other

side, where it enters the liquid again (H). I observed this Landau Levich Derjaguin transition of films being pulled up, but measurements were always performed at lower velocities, i. e. at finite contact angles. The film drawn upwards has no uniform thickness (yellow arrows, B-D), because of liquid partially flowing downwards. In contrast to the receding contact line, the advancing contact line is almost velocity-independent and forms a straight line (E-G). It is disturbed at velocities above the critical velocity, when liquid is transported from the receding side along the drum to the advancing side (red arrow, H).

Similar to my observations, the three-phase contact line is described in literature as an almost straight line in case of low velocities [81, 82], while it adopts a triangular shape for higher velocities [83]. Above the critical velocity for film formation, the three-phase contact line is pulled upwards and forms an overhanging thicker ridge at the upper part as described in the Landau Levich Derjaguin-transition [73, 83]. Snoeijer et al. introduced surface defects, i. e. additional pinning sites, as a reason for the disturbance of the three-phase contact line [83], meaning that any inhomogeneity, roughness, etc. could influence the shape of the contact line.

#### 2.3.3.3 Dynamic contact angles

Contact angles are observed via side-view imaging typically at frame rates about 500 Hz (Figure 2.18 C). The camera is placed at a slight inclination for observing the contact angles, as done for observing the three-phase contact line. The light source is placed at the opposite window, to achieve a black and white image (Figure 2.21).

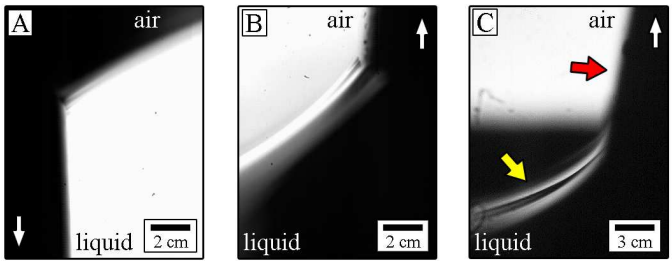


**Figure 2.21:** Imaged contact angles using either the barrel-shaped (A, B) or planar drum (C). While focusing on the planar drum, interferences with planes in front and behind the focal plane occur resulting in diffuse images of the drum's surface (C, red arrow). Also the imaged air-liquid interface does not appear as a single line, but resulted in a broad spectrum of possible interfaces (C, yellow arrow).

Both drums can be used for observing dynamic contact angles, although the barrel-shaped drum is more suitable. While focusing on the center of the barrel-shaped drum's surface (Figure 2.19 B, red line), a single plane is brought into focus without

any interference of other planes in front or behind the chosen one, what leads to unblurred images (Figure 2.21 A and B). Further, the focusing on the center of the barrel-shaped drum's surface is necessary (known radius) to allow for calculating the rotation respectively wetting/dewetting velocity of the drum. In contrast, by focusing on the planar drum, the interferences of the planes in front or behind the focal plane lead to blurred images (Figure 2.21 C), especially because the three-phase contact line is not a smooth straight line leading to slightly different contact angles along the drum.

Figure 2.22 shows a sketch of the advancing and receding contact angle in side view. When the drum moves out of the liquid, liquid is forced to dewet the drum's surface. The resulting contact angle is referred to as receding contact angle. The advancing contact angle describes the case, when the drum enters the liquid and its surface is wetted by the liquid.

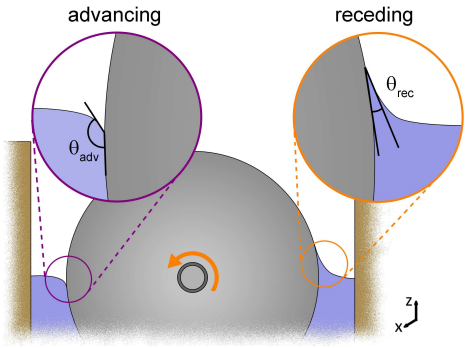


**Figure 2.22:** Sketch of receding and advancing contact angles. While the drum moves into the liquid, the liquid is forced to wet the drum. The corresponding contact angle is called advancing contact angle. The receding contact angle describes the case, when the drum moves out of the liquid and the liquid is forced to dewet the surface.

These velocity-dependent contact angle measurements are limited by the critical velocity of film formation not only on the receding, but also on the advancing side (Figure 2.20 D and H). On the receding side, some drops or even a film are pulled upwards - a finite contact angle does not exist anymore. This liquid is transported along the drum to the advancing side of the bath where it merges with the bulk liquid again. While the drops merge with the liquid, the three-phase contact line "jumps" upwards and the advancing contact angles change significantly.

#### 2.3.3.4 Altering the flow inside the bath

When the drum rotates in the liquid, a hydrodynamic flow arises at the surface as well as in the bulk. In the presence of surfactant molecules, a further flow can be observed due to concentration gradients - surfactant molecules will diffuse either along the surface or through the bulk to reduce these gradients. There are two different possibilities for a gradient formation - locally due to the upwards pulling of the three-phase contact line (Chapter 3) or non-locally between the advancing and receding side of the bath (Chapter 4).

The flow/diffusion along the surface or through the bulk can be altered by varying the liquid's filling level or by adding an external barrier (Figure 2.23). When the liquid is filled to half of the drum's height (static contact angle about 90°), the axis holding the drum, also half immersed in the liquid, hinders flow/diffusion along the surface (B). The axis immersed in the liquid does not influence the measurements because of its distance to the measured contact angles.

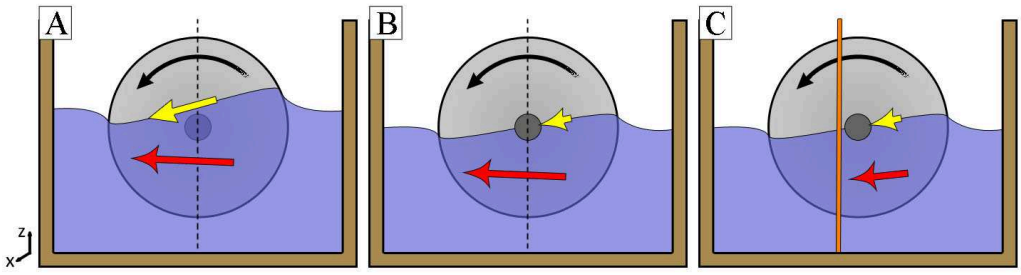


**Figure 2.23:** Illustration of the possible flow/diffusion depending on the setup geometry. (A) Liquid level above the axis allows for flow/diffusion along the surface (yellow arrows) as well as through the bulk (red arrows). (B) Liquid level up to the axis allows only for flow/diffusion through the bulk. (C) The external barrier (orange line) hinders any flow/diffusion.

By changing the liquid filling level to slightly above the axis, flow/diffusion along the surface can be allowed (A) without changing the resulting contact angles significantly. Not only flow/diffusion along the surface, but also through the bulk can be hindered by adding an external barrier (C). This barrier separates the advancing from the receding side, but a slight exchange between the two sides can not be completely excluded due to small gaps ($\approx 1\,\mathrm{mm}$) between barrier and bath/drum. Three different configurations of allowed flow/diffusion in the bath are achievable, as summarized in Table 2.4.

| | liquid filling level/ external barrier | flow/diffusion possible along the surface | flow/diffusion possible through the bulk |
|---|---|---|---|
| (A) | above axis | • | • |
| (B) | up to the axis | | • |
| (C) | external barrier | | |

**Table 2.4:** Depending on the liquid's filling level and the presence of the external barrier, flow/diffusion along the surface or through the bulk can be hindered.

In Figure 2.23 the different configurations of the rotating drum setup with the thereby resulting flow/diffusion along the surface (yellow arrows) and/or through the bulk (red arrows) are visualized. The barrier is shown as an orange line.

#### 2.3.3.5 Altering the drum's surface properties...

The drum's surface properties can be altered by changing the surface coating of the drum, either by a dip-coating-like process or a polishing step. Additionally, a glass slide or an engraved copper plate (as used in gravure printing) can be glued around the drum to modify the surface properties. Altering the surface allows for introducing surface roughness, hydrophilicity, homogeneity, etc.

##### ... by gluing a glass slide around the drum

The glass slides have dimensions of 5 cm in width, 20 cm in length and a thickness of 55 to 80 µm (Menzel, # 00). This low thickness allows for bending the glass slide around the planar drum, resulting in a well-defined, smooth surface, which can be easily chemically modified. The glass slide is glued at the beginning and end with the help of two components glue (UHU, Zweikomponentenkleber plus sofortfest), so that half of the drum is covered by the glass. The crossover from one material to the other (steel to glass or vice versa) modifies the contact angle and three-phase contact line close to these gluing points. But within half a rotation, undisturbed contact angle and contact line measurements are feasible.

Pure, clean glass has a static contact angle about 0°. To get finite contact angles, the surface has to be modified in a dip-coating-like process described below.

##### ... by coating the drum with a polymer or a silane

To coat the drum, a dip-coating-like process is used, where the drum rotates through the dissolved coating material. The rotation velocity of the drum is chosen to be above the critical velocity for film formation (about 10 cm/s) that a liquid film is drawn upwards and the drum is completely wetted. During solvent evaporation, a film of the coating material remains on the drum's surface that is dissolved again by entering the coating liquid. While coating the barrel-shaped drum, the coating solution has to be removed quickly. The drum's center would be longer immersed in the solution than the edges, leading to an inhomogeneous coating. This problem is less pronounced for the planar drum.

Such dip-coating-like processes were used for applying a polystyrene coating onto the steel or hydrophobizing the glass:

- Polystyrene coating onto the steel
  The drum rotated through a solution of 0.8 wt % of polystyrene in tetrahydrofuran (THF, Sigma-Aldrich) for 5 minutes. After quickly removing the solution, the drum was allowed to dry at ambient conditions for 1 hour before it was completely dried at 60 °C for 16 hours.
- Hydrophobizing the glass
  The glass glued to the drum rotated through a solution of 2.5 wt % of hexamethyl disilizane (HMDS, Aldrich, 99.9 %) in toluene (Sigma-Aldrich) about 7 hours before the solution was removed. After 1 hour of drying at room temperature, the drum was dried for at least 3 hours at 50 °C.

#### ... by polishing the drum with a sealant

As another method to modify the drum's surface, an additional polishing step can be used. For this, a sealant (NanoTec Felgenversiegelung, NIGRIN) is applied evenly onto the drum. After drying, the drum is polished with a soft lint-free cloth to remove the excess and smoothen the remaining sealant.

The used sealant was a polymer-based paste containing nanoparticles usually fabricated to protect metal parts on cars. It slightly hydrophobized the steel by increasing the static contact angle of water from 60° to about 80°.

#### ... by gluing an engraved copper plate around the drum

In gravure printing engraved copper plates are used to span around the printing cylinder. These plates consist of a basic copper plate plus a thin additional copper layer (copper skin). The inverse printing image is engraved in this copper skin and then coated with a thin chromium layer, to protect the gravure. Such copper plates are named Ballard skin after their inventor.

The Ballard skin[2] was glued around the drum at each end using tesa Powerstrips®.

### 2.3.4 Analysis of dynamic contact angles

The dynamic contact angles can be analyzed either manually or automatically. Both methods have their advantages and disadvantages (Table 2.5). The manual method allows for analyzing the contact angle of a limited number of frames ($\sim$ 5 frames per velocity) in a reasonable time leading to small statistics, but fast results without any image processing (Section 2.3.4.1). In contrast to the manual analysis, complete

[2]provided by the Institute of Printing Science and Technology, TU Darmstadt

videos (typically up to 200 frames) can be analyzed by using the automatic analysis (Section 2.3.4.2). But for this method, an image processing step, e. g. thresholding of the original video, is necessary before the analysis can be performed.

| | type of analysis | |
|---|---|---|
| | manual | automatic |
| statistics | $\sim$ 5 frames | $>$ 200 frames |
| contrast requirement | | black/white |
| image processing | - | • |
| time requirement (per data point) | $\sim$ 3 min | $\sim$ 10 min |

**Table 2.5:** Comparison of the manual and automatic analysis.

### 2.3.4.1 Manual analysis

To analyze the contact angles manually, the angle between solid-liquid and air-liquid interface is measured in case of the advancing contact angle (Figure 2.24 A). In case of the receding contact angle, the angle between air-liquid and air-solid interface is measured and then subtracted from 180° (Figure 2.24 B). The contact angles are determined for three to five random frames of the video and then averaged. The uncertainty of the contact angle determination is about 5° due to the difficulty in determining the air-liquid interface.

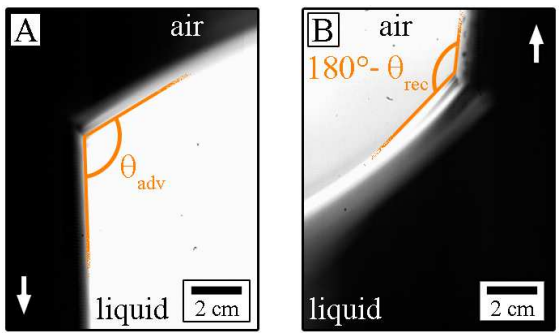


**Figure 2.24:** Manual analysis of the (A) advancing and (B) receding contact angle.

Irregularities in the wetting/dewetting can be seen in widely differing contact angles leading to a more precise analysis of the video via excluding any defects in the coating or dust on the surface causing the scattering contact angles.

#### 2.3.4.2 Automatic analysis

For automatically analyzing the dynamic contact angles, image processing of the original video is required to achieve black/white images (Figure 2.25). Based on these images, the interfaces can be determined - in the wetting case the air-liquid and the liquid-solid interface (A), in the dewetting case the air-liquid and the air-solid interface (B). The interface is determined as the transition from black to white using a program written in MATLAB[3]. First, each of these interfaces is fitted linearly using the regime further apart from the three-phase contact line (close to the image border, purple arrows) and then the point of intersection (yellow star) is determined. The intersection point is shifted along the drum's surface to the interface (Figure 2.25, yellow arrow).

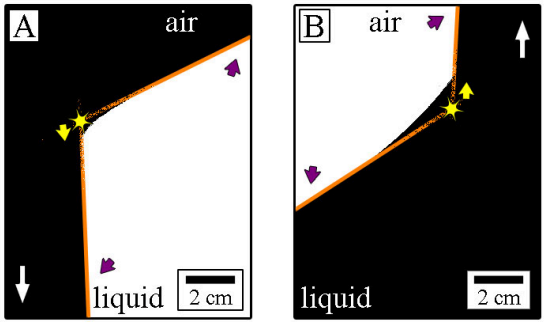


**Figure 2.25:** Threshold of the recorded videos with the first fitting of the interfaces (orange lines) from the image border (purple arrow) and the intersection point (yellow star). (A) Advancing and (B) receding side.

The shifted intersection point forms the origin for the following linear fitting of the interfaces (Figure 2.26, red lines). It can be understood as a point of the three-phase contact line and therefore the origin for the contact angle determination. The slopes of these fits allow for calculating the angle $\alpha$ between the two fitted lines and therefore for calculating the contact angles:

$$\theta_{adv} = \alpha \qquad \text{and} \qquad \theta_{rec} = 180° - \alpha \tag{2.11}$$

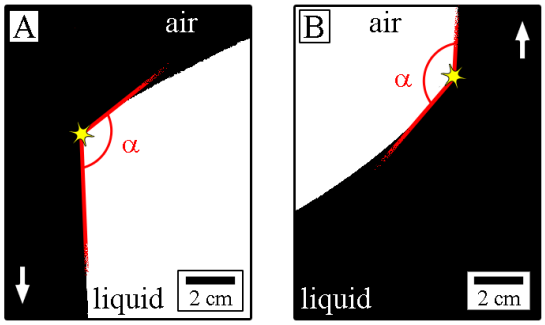


**Figure 2.26:** Determination of the contact angles from the second fit of the interfaces (red lines) with the shifted intersection point as origin.

[3]code was programmed by Marcel Weirich

For every frame in the video this contact angle determination is performed resulting in a plot of contact angle versus frame number respectively time (Figure 2.27) and an averaged contact angle (dashed orange line) with the standard deviation as uncertainty (orange shading).

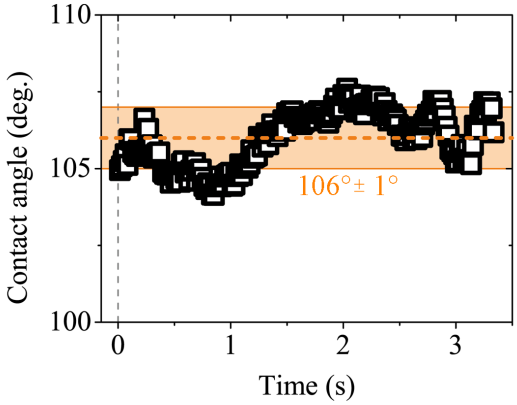


**Figure 2.27:** Automatic analysis of contact angles versus time. The average contact angle was 106° (dashed orange line) with an uncertainty of 1° (orange shading). The manually determined contact angle was about 105°.

One disadvantage of the automatic analysis is the averaging over all analyzed data, independent of the wetting/dewetting of the liquid, i. e. defects in the coating or dust could lead to pinning sites and thus locally to completely different contact angles (Figure 2.28).

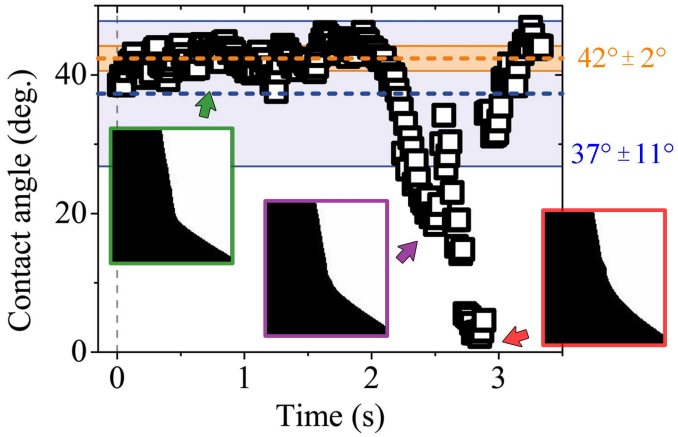


**Figure 2.28:** Defects in the surface, e. g. pinning sites or dust, could lead to locally completely different contact angles (2 - 3 s) resulting in too small averaged contact angles with large errors (37° ± 11°, blue line/shading) compared to the manually determined contact angle about 43°. In case of excluding the defect region comparable contact angle data could be obtained (42° ± 2°, orange line/shading).

Here, a defect in the polystyrene coating of the drum led to a pulling up of the three-phase contact line and therefore to a contact angle decrease to 0° and then

to an increase again (Figure 2.28, 2 - 3 s). Averaging over all analyzed data points resulted in a contact angle of $37° \pm 11°$, while a contact angle about 43° was observed manually. When the region of the defect taking place was excluded from the averaging, a contact angle of $42° \pm 2°$ was obtained also with the automatic analysis.

Further, the thresholding of the video can lead to frames, which have some defects, e. g. dirt as black dots in the white regime, leading to an insufficient determination of the interface and therefore to unreasonable contact angles. Large standard deviations hint to problems in the determination of the interfaces or to some wetting/dewetting instabilities. A closer look at the corresponding video allows for determining the reason of the large deviation and therefore for a possible exclusion of the frames causing the determination problems.

A comparison between the manually and automatically determined contact angles shows a good agreement of the two analysis types - automatically or manually (Figure 2.29). Thus, the manual determination with smaller statistics is sufficient to present the correct contact angle behavior. For the analysis of the contact angles, the manual method is used.

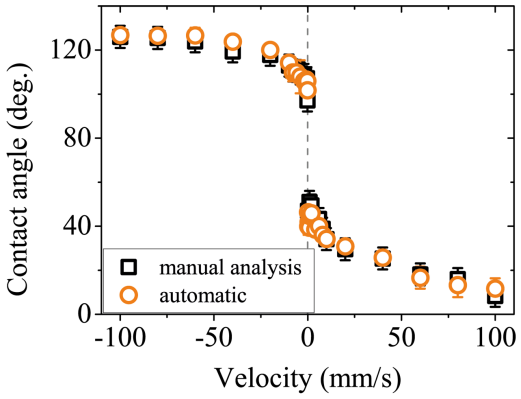


**Figure 2.29:** Comparison of the manually and automatically determined contact angles shows good agreement between both methods.

## 2.4 Scanning force microscopy

In scanning force microscopy (SFM) a sharp tip attached to a cantilever is used to probe sample surfaces. The topography of the sample as well as interactions between tip and sample lead to a bending of the cantilever. A focused laser beam on the back of the cantilever is reflected on a photodetector and allows for following the cantilever bending respectively tip movement while scanning the sample surface (Figure 2.30). This reflected beam does not only provide information about the topography of the sample, but also phase information [84]. The scanning can be performed either in contact, intermitted (tapping) or non-contact mode. While

contact mode SFM is suitable for scanning hard surfaces, softer surfaces like polymers are scanned in tapping mode. In tapping mode, the cantilever is vibrated at its resonance frequency and most of the time it is not in contact with the sample. This leads to less destruction of the sample, however, also the resolution slightly decreases [47].

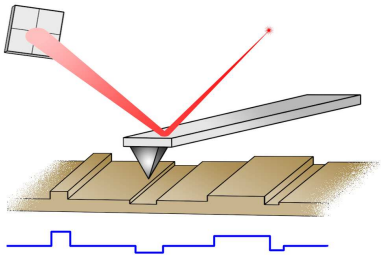

**Figure 2.30:** Sketch of a scanning force microscope. The cantilever tip rasters the sample surface resulting in a topography image.

The SFM technique was used to characterize the roughness of the drums used for dynamic wetting/dewetting experiments. The samples were scanned in tapping mode using the NanoWizard$^{TM}$ atomic force microscope by JPK instruments. OMCL-AC240TS cantilevers from Olympus with a nominal spring constant of 2 N/m and a resonance frequency of 70 kHz were used[4].

[4]measured by Thi-Huong Nguyen

# 3 Influence of surfactants on dynamic wetting/dewetting[5]

The wetting of single-component liquids has been studied extensively resulting in several theories, e. g. molecular kinetic theory, hydrodynamic theory, etc. (Section 2.3.1) trying to describe the wetting/dewetting macroscopically as well as microscopically. In the Cox-Voinov relation, a modification of the hydrodynamic theory, the contact angle is described as being proportional to $\gamma^{-\frac{1}{3}}$ respectively $U^{\frac{1}{3}}$ for single-component liquids (Section 2.3.1.2). This relation is valid for small contact angles and complete wetting ($\theta_{eq} \approx 0°$). But does this dependency hold true for multi-component liquids like surfactant solutions?

Chaudhuri and Paria used the Wilhelmy technique to measure dynamic contact angles in aqueous solutions of Triton X-100, sodium dodecylbenzene sulfonate, and CTAB on poly(tetrafluoroethylene) (PTFE) [85]. At velocities of 0.2 and 1 mm/s, they observed an initial decrease of the advancing respectively an increase of the receding contact angle (Figure 3.1). With increasing surfactant concentration, the advancing contact angles slightly decreased, while the receding contact angles remained constant. The hysteresis between advancing and receding contact angle decreased even at concentrations lower than 10 % cmc. Further, the addition of salt enhanced the decreasing effect of the surfactant on the advancing contact angle.

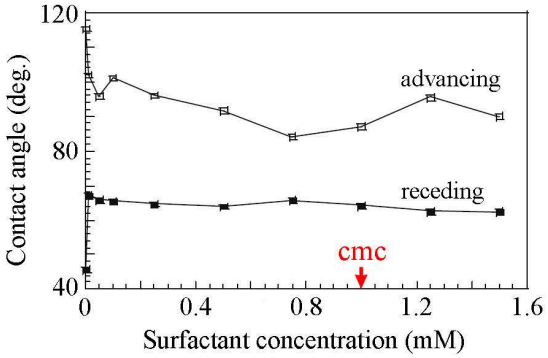


**Figure 3.1:** Dependency of the advancing as well as the receding contact angles of CTAB solutions at different concentrations on a PTFE surface measured by Chaudhuri and Paria [85].

[5]This chapter is based on "D. Fell, G.K. Auernhammer, E. Bonaccurso, C. Liu, M. Sokuler, H.-J. Butt, *Influence of Surfactant Concentration and Background Salt on Forced Dynamic Wetting and Dewetting*, Langmuir, **27** (2011) 2112".

These results give rise to the questions of how surfactant solutions behave at higher wetting velocities relevant for printing processes and how the hydrophobicity of the substrate influences wetting/dewetting. If the influence of higher wetting velocities and substrate hydrophobicity as well as the influence of different surfactants is understood, gravure printing processes can be optimized. Therefore I investigated the influence of different surfactant types (anionic, cationic and nonionic) and concentrations on the wetting/dewetting of aqueous solutions on a hydrophobized surface. In contrast to Chaudhuri and Paria, a rotating drum setup was used, which allowed for higher wetting velocities. The drum was coated with polystyrene, resulting in a homogeneous surface with an average roughness of $140 \pm 15$ nm measured by SFM (Figure 3.2). This high roughness which is correlated to the polystyrene coating just reflects the initial roughness of the lathed steel drum. Pure water gave a static contact angle of 86° at the polystyrene-coated drum.

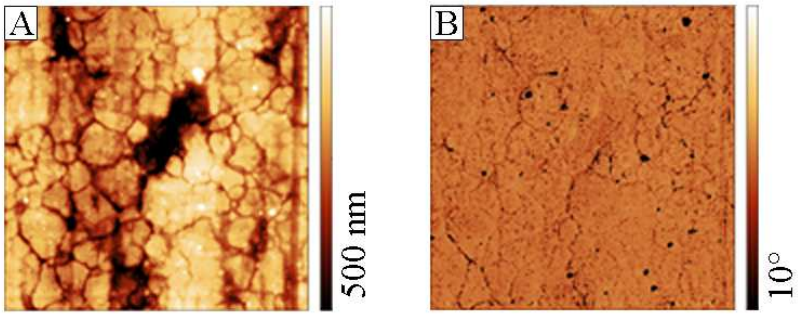


**Figure 3.2:** SFM images of the polystyrene coated drum. (A) Topography image shows a roughness of $140 \pm 15$ nm. (B) Phase image shows a quite homogeneous coating.

In this chapter, the influence of different surfactants (CTAB, SDS, $C_4E_1$, $C_8E_3$, and $C_{12}E_5$) on the wetting/dewetting of aqueous solutions on the polystyrene-coated steel surface at different concentrations are discussed.

## 3.1 Velocity-dependency of contact angles

Dynamic contact angles depend on the rotating velocity of the drum and are typically represented in contact angle versus velocity plots ($\theta - U-$plots). Following, the dynamic contact angle behavior is discussed considering the example of the polystyrene drum rotating through pure water. With increasing the drum velocity, the difference between apparent and static contact angles increased. In case of wetting (advancing contact angles, $U < 0$ mm/s), the apparent contact angle increased with increasing velocity, while receding contact angles (dewetting, $U > 0$ mm/s)

decreased with increasing velocity (Figure 3.3). The velocity-dependency found for pure water is similar to the velocity-dependency described by Dussan [60] (Figure 2.12). At low velocities ($|U| < 2\,\mathrm{mm/s}$) the trend of the advancing and receding contact angle is symmetric (green blow-up), while at higher velocities differences are observable. The advancing contact angles leveled off, while the receding contact angle steadily decreased until it reached 0° at the critical velocity. For the advancing as well as for the receding contact angle two different slopes are present - a high slope ($> 2°\,\mathrm{s/mm}$) for $|U| < 2\,\mathrm{mm/s}$ and a lower slope ($< 1°\,\mathrm{s/mm}$) for higher velocities. For U = 0 mm/s, two different contact angles exist (orange arrows) - one originating from dewetting, the other one originating from wetting measurements. This difference is called hysteresis and the static contact angle (blue star, measured via a sessile drop method) lies in between these two values: 86°. Above the critical velocity complete films were drawn up, known as Landau Levich Derjaguin film formation (Section 2.3.1.3), and wet the drum entirely (purple arrows).

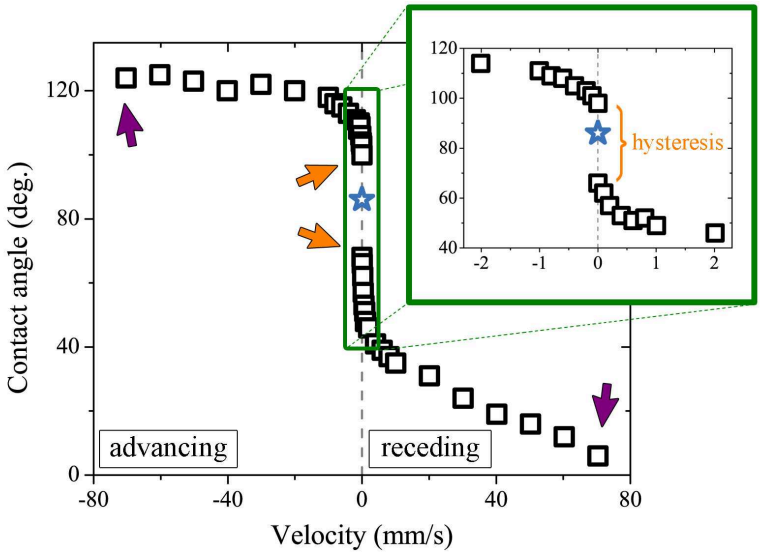


**Figure 3.3:** $\theta - U-$plot for pure water. $\theta_{adv}$ increased with increasing (absolute) velocity, while $\theta_{rec}$ decreased. The jump at $U = 0\,\mathrm{mm/s}$ reflects the hysteresis (orange arrows). The static contact angle lies in between this jump (blue star). Contact angle measurements had to stop at the Landau Levich Derjaguin-transition (purple arrows). The blow-up shows the symmetric behavior for low velocities ($|U| < 2\,\mathrm{mm/s}$).

At the critical velocity, the receding contact angle is 0°, leading to a liquid transport along the drum to the advancing side. This results in non-measureable advancing contact angles (Section 2.3.3.2). In case of an added doctor blade, advancing contact angles are measurable up to higher velocities. However, the usage of a doctor blade could lead to complications, including surface modification and contamination.

The observed velocity-dependent contact angle behavior could not be fitted with the existing theories (Section 2.3.1) - neither the molecular kinetic theory ($\cos\ \theta_{eq} - \cos\ \theta_{ap} \sim U$) nor the hydrodynamic model ($\theta_{ap}^3 - \theta_{eq}^3 \sim U$) resulted in a linear curve (Figure 3.4). Both plots show for the advancing as well as for the receding contact angle two different slopes - a high one for velocities up to 2 mm/s and a lower slope for higher velocities.

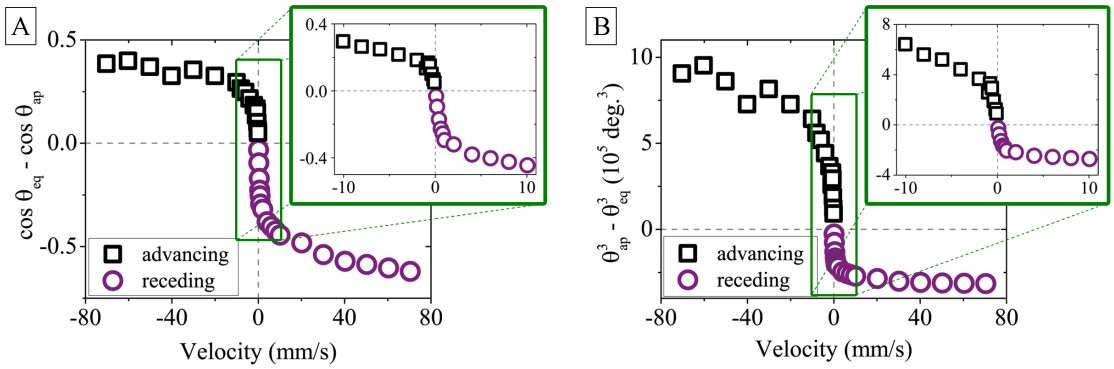


**Figure 3.4:** Plotting contact angle versus velocity according to theory should result in a linear curve for the contact angles. But for the (A) molecular kinetic theory ($\cos\theta_{eq} - \cos\theta_{ap}$ vs. velocity $U$) as well as for the (B) hydrodynamic model ($\theta_{ap}^3 - \theta_{eq}^3$ vs. velocity $U$) different slopes were found.

The existence of different slopes in the $\theta - U-$plots points to different influences, e. g. roughness, homogeneity, etc. on velocities above respectively below $|2|$ mm/s. Surface roughness could be more significant at low velocities, when the three-phase contact line has time to relax. The influence of surface roughness as well as surface homogeneity on the wetting/dewetting will be discussed in Chapter 5.

### Addition of surfactant changes contact angles

In the following experiments CTAB was used as surfactant as a model system to describe the influence of surfactant on the wetting/dewetting of aqueous solutions. CTAB has a critical micelle concentration of 1 mM and is completely soluble in water at the used concentrations. As a cationic surfactant, electrostatic repulsion between CTAB molecules/adsorbed layers can be observed.

When surfactant was added to the system, the overall behavior remained the same - contact angles depended on velocity, with a stronger dependency of the receding contact angle and a leveling off at high velocities for advancing contact angles. But the $\theta - U-$plots were shifted to lower contact angles with increasing surfactant concentration (Figure 3.5). This resulted in a steady decrease of the

contact angles with concentration at a constant velocity (6 mm/s, green blow-up). Additionally to the shifting of the plots, the slopes of the receding contact angle increased with concentration while the slopes of the advancing contact angles seemed to be independent of the CTAB concentration (for $|U| > 2$ mm/s).

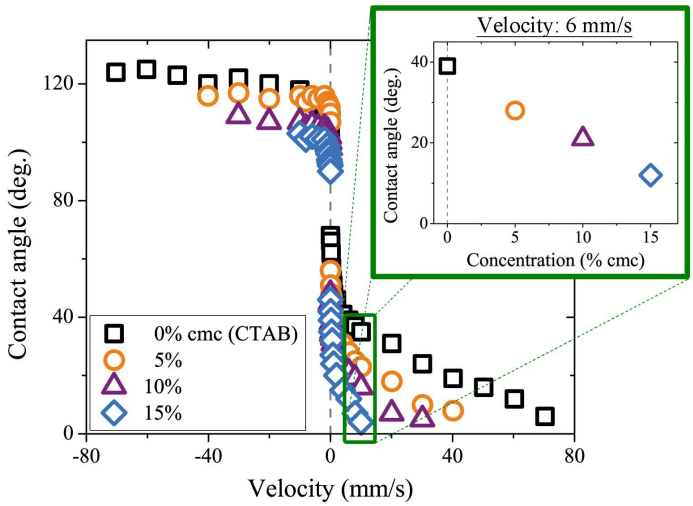


**Figure 3.5:** $\theta - U$ −plot of CTAB solutions well below cmc. Contact angles decreased with increasing wetting velocity as well as with increasing CTAB concentration (blow-up at 6 mm/s).

At a constant velocity of 6 mm/s, the receding contact angles decreased about 30°, when comparing pure water with a CTAB concentration of 15 % cmc. Not only the receding contact angles decreased with increasing CTAB concentration, but also the advancing contact angles decreased, however only about 10° (at 6 mm/s, comparison of 0 % to 15 % cmc). What affects the contact angles to decrease so significantly? And why is the difference between advancing and receding contact angle so significant? Following, I will focus on the receding contact angles, which show a more significant decrease than the advancing contact angles.

## 3.2 What causes the contact angles to decrease?

While increasing the CTAB concentration of the solution, the surface tension decreased due to the surface active effect of CTAB. This reduced surface tension could be the reason for an increased pulling up of the three-phase contact line at the receding side and therefore for a reduction of the receding contact angle. According to the relation between contact angle and surface tension predicted by Cox and Voinov ($\theta \sim \gamma^{-\frac{1}{3}}$, Section 2.3.1.2), contact angles should decrease with increasing surface tension . This means in case of contact angles plotted versus $\gamma^{-\frac{1}{3}}$, I expect a linear behavior with negative slope, if surfactant solutions follow the Cox-Voinov relation, plotted in (Figure 3.6).

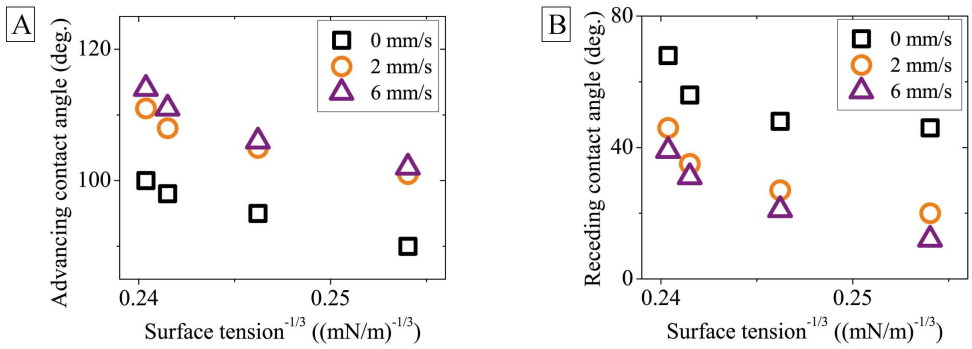


**Figure 3.6:** Testing of the Cox-Voinov relation ($\theta \sim \gamma^{-\frac{1}{3}}$) for CTAB solutions. The advancing contact angles might follow this relation (A), while the receding contact angles do not show a linear behavior when plotted versus $\gamma^{-\frac{1}{3}}$ (B).

Plotting $\theta$ versus $\gamma^{-\frac{1}{3}}$ did result in a behavior that could be seen as linear in the advancing case (Figure 3.6 A), but not in the receding case (B). This non-existence of a linear behavior between $\theta_{rec}$ and $\gamma^{-\frac{1}{3}}$ suggests surface tension not being the only reason for the contact angle decrease with increasing surfactant concentration.

To test this assumption, I measured the surface tension depending on the CTAB concentration (Figure 3.7). The measurements show that the surface tension up to a concentration of 15 % cmc (grey shading) was only reduced by 15 % of the initial surface tension of water (yellow shading).

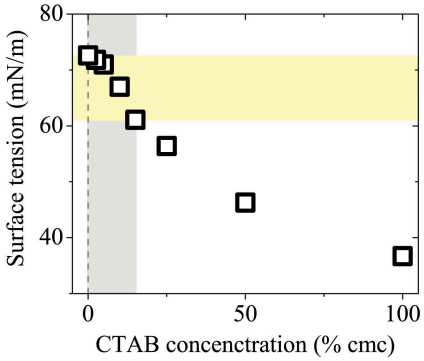


**Figure 3.7:** Surface tension of a CTAB solution at different concentrations in % cmc. The area shaded in yellow represents a surface tension decrease of 15 % compared to that of pure water. The surface tension stays within this area up to a CTAB concentration of 15 % cmc (grey area).

The observation of surface tensions of CTAB at the used concentrations being similar to those of pure water but receding contact angles decreasing significantly supports my hypothesis of something additional influencing the contact angles to decrease with increasing CTAB concentration. One possibility influencing the contact angles could be the ionic character of the CTAB molecules leading to electrostatic repulsion between molecules/adsorbed layers. How would this repulsion influence the wetting/dewetting of the surfactant solution?

### 3.2.1 Electrostatic repulsion?

The air-liquid and the solid-liquid interface merge at the three-phase contact line. When the distance between the two interfaces gets small ($< 100\,\text{nm}$), surface forces like van der Waals forces act between these interfaces. These forces can either be attractive or repulsive. A repulsive force would keep the interfaces apart and thus delay the dewetting on the receding side, while an attractive force would accelerate merging and therefore the dewetting process (Figure 3.8). The dewetting delay would lead to higher contact angles in case of repulsive forces being present between the interfaces, while attractive forces should lead to lower contact angles [86].

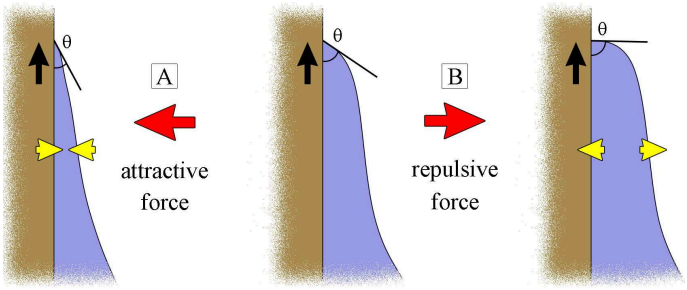


**Figure 3.8:** (A) Attractive as well as (B) repulsive forces (yellow arrows) between the air-liquid and solid-liquid interfaces can influence the wetting/dewetting leading to decreasing respectively increasing contact angles.

When CTAB is present in the solution, the surfactant molecules adsorb at the air-liquid as well as at the solid-liquid interface. Close to the three-phase contact line, this can result in a repulsion between these two interfaces due to the charged molecules. With increasing CTAB concentration, the electrostatic repulsion increases. At concentrations below cmc, as given in the experiments, added CTAB molecules adsorb preferentially at the interfaces to complete the adsorption layer leading to a higher negative charge at the air-liquid as well as at the solid-liquid interface. Tis should lead to a higher repulsion between these interfaces. Electrostatic repulsion should lead to higher contact angles with increasing CTAB concentration (Figure 3.8 B), but the result of the contact angle measurement at various CTAB concentrations (Figure 3.5) shows a different picture - the receding contact angles decreased. This observation is in clear contrast to the hypothesis of electrostatic repulsion leading to higher contact angles.

Is the assumption of increasing contact angles in case of electrostatic repulsion being present wrong? Do the contact angles decrease because of the electrostatic repulsion? If this hypothesis is true, a decrease of the electrostatic repulsion should lead to the original state, i. e. to increased contact angles.

#### 3.2.1.1 Adding salt to decrease electrostatic repulsion

The electrostatic repulsion between the charged molecules as well as between the interfaces can be decreased by adding ions, e. g. sodium chloride (NaCl), to the CTAB solution. The additional ions can shield the charged surfactant molecules as well as the charged air-liquid and solid-liquid interfaces from each other. Assuming that the electrostatic repulsion is responsible for the decreased contact angles, a reduction of the electrostatic repulsion should lead to higher contact angles (Figure 3.9).

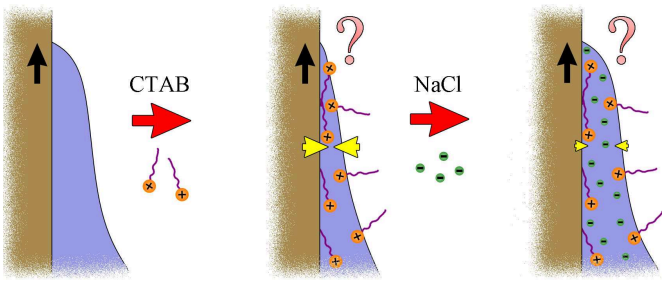


**Figure 3.9:** Illustration of the hypothesis that electrostatic repulsion (yellow arrow) leads to decreased contact angles while the reduction of the electrostatic repulsion by adding salt to the system should increase the contact angles again.

To test this hypothesis, I measured the contact angles of a 5 % cmc CTAB solution at three different NaCl concentrations: 0, 5, and 25 mM. While adding NaCl to the CTAB solution, the ionic strength $I$ increased from 0.05 mM to 5.05 respectively 25.05 mM with increasing NaCl concentration. The increased ionic strength leads to a decreased Debye length $\lambda_D$, given as

$$\lambda_D = \sqrt{\frac{\epsilon_0 \epsilon_r k_B T}{2 N_A e^2 I}}, \tag{3.1}$$

with the permittivity of free space $\epsilon_0$, the dielectric constant $\epsilon_r$, the Boltzmann constant $k_B$, the Avogadro number $N_A$, and the elementary charge $e$. The Debye length describes the length of effective shielding between charged molecules. For a 5 % cmc CTAB solution $\lambda_D$ equals 44 nm and decreases significantly with increasing NaCl concentration (Figure 3.10) showing a decreasing electrostatic repulsion.

The contact angles decreased with increasing NaCl concentration, i. e. with decreasing electrostatic repulsion (Figure 3.11). This means that the contact angles decreased independent of increasing or decreasing electrostatic repulsion, what implies that electrostatic has no significant influence on the wetting/dewetting of surfactant solutions. But why do the contact angles decrease with increasing NaCl concentration? Does the NaCl addition influence the wetting/dewetting of water

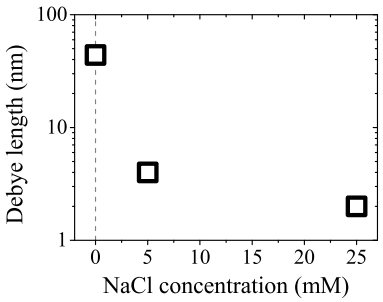


**Figure 3.10:** Debye length of a 5 % cmc CTAB solution at different NaCl concentrations as calculated from Equation (3.1).

and do the dynamic contact angles of CTAB solutions therefore decrease further with increasing salt concentration?

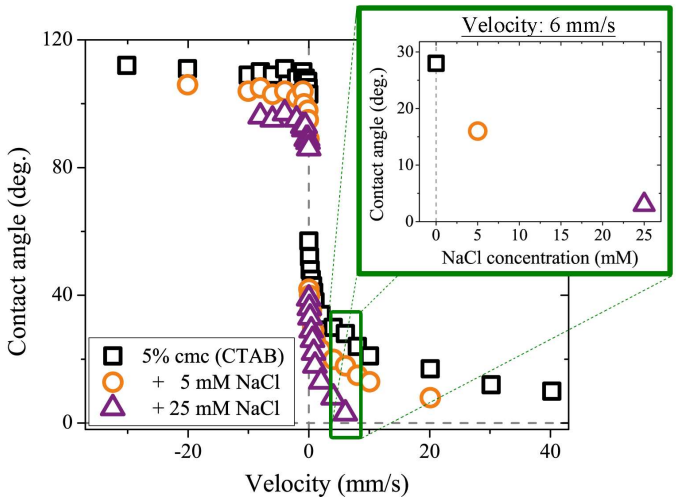


**Figure 3.11:** $\theta-U-$plot of a 5 % cmc CTAB solution. The contact angles decreased with increasing NaCl concentration. The $\theta-c-$plot shows a significant decrease at 6 mm/s (green blow-up).

To test the influence of salt on the wetting/dewetting of a liquid, NaCl was added to pure water. The contact angles did not change with increasing the salt concentration (Figure 3.12), in contrast to the observations made for salt added to CTAB solutions. This result implies that the NaCl addition altered the properties of the CTAB solutions leading to a decrease of the contact angles.

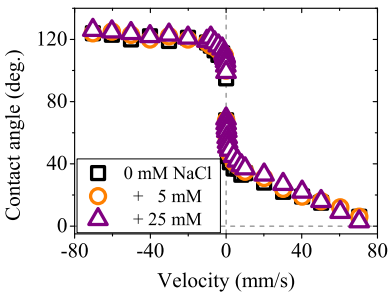


**Figure 3.12:** Influence of NaCl on the wetting/dewetting of pure water.

The hypothesis of changing the CTAB properties while adding salt was tested by measuring the critical micelle concentration in presence of NaCl. The results showed that the critical micelle concentration of a CTAB solution decreased significantly with increasing the NaCl concentration (Figure 3.13) - about 70 % for a 5 mM and about 85 % for a 25 mM NaCl solution. Not only the cmc of CTAB, but the cmc of ionic surfactants decrease in general with increasing salt concentration, i. e. with increasing ionic strength while non-ionic surfactants are unaffected [87].

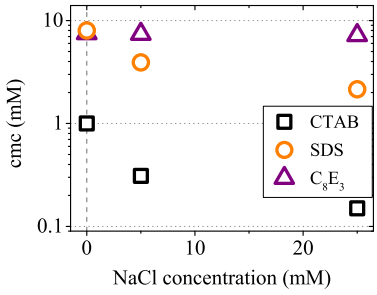


**Figure 3.13:** Influence of NaCl on the critical micelle concentration of CTAB, SDS, and $C_8E_3$.

The addition of salt decreased the cmc of CTAB and therefore increased the CTAB concentration in % cmc with increasing NaCl concentration:

$$5\,\%\ \text{CTAB}/5\,\text{mM NaCl} \longrightarrow \text{“10 \% cmc CTAB/NaCl solution”}$$

$$5\,\%\ \text{CTAB}/25\,\text{mM NaCl} \longrightarrow \text{“20 \% cmc CTAB/NaCl solution”}$$

By considering the “new” concentrations, the contact angle decrease with increasing concentration (in % cmc, Figure 3.11) is consistent with the earlier observations of decreasing contact angles with increasing surfactant concentration (Section 3.1). Further, the $\theta - U-$plot for the “10 % cmc CTAB/NaCl solution” is almost identical with that for the pure 10 % cmc CTAB solution (Figure 3.14 A).

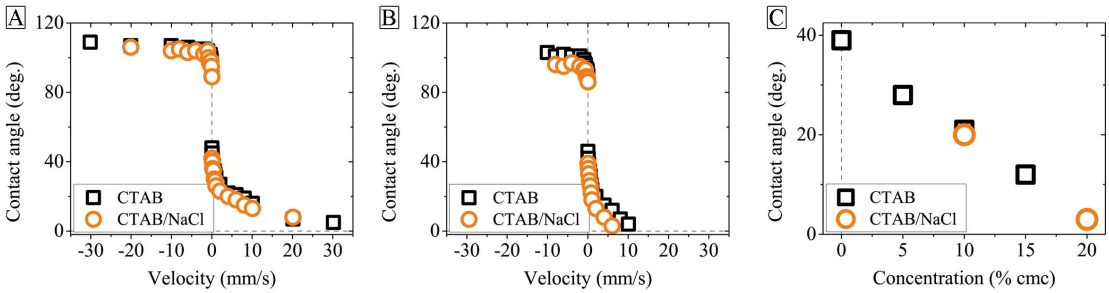


**Figure 3.14:** Comparison of $\theta - U-$plots for pure CTAB solutions and mixtures of CTAB/NaCl at (A) 10 % cmc and (B) 15 %/20 % cmc as well as a (C) $\theta - c-$plot, comparing the pure CTAB solutions with the CTAB/NaCl mixtures at 6 mm/s.

The plot for the "20 % cmc CTAB/NaCl solution" follows the general trend and shows smaller contact angles than that for a pure CTAB solution of 15 % cmc (B). The wetting/dewetting of the CTAB/NaCl solutions correspond to the behavior of the pure CTAB solutions in case of recalculated CTAB concentrations (Figure 3.14 C).

The fact that the $\theta - U-$plot of the "10 % cmc CTAB/NaCl" concentration fitted the plot of the pure 10 % cmc CTAB solution, suggests that electrostatic repulsion has no dominant - whether contributing nor counteracting - influence on the wetting/dewetting of aqueous CTAB solutions.

#### 3.2.1.2 Neglecting electrostatic repulsion

If electrostatic repulsion has no significant influence on the wetting/dewetting of ionic surfactants, the presence of nonionic surfactants should also result in a significant contact angle decrease with increasing surfactant concentration. Due to the neutral headgroup of the nonionic surfactants, an electrostatic repulsion between the air-liquid interface and the solid-liquid interface during merging can be excluded.

To further test the influence of electrostatic repulsion on the wetting/dewetting, the nonionic surfactant $C_8E_3$ was used at increasing surfactant concentration (Figure 3.15). $C_8E_3$ has a critical micelle concentration of 7.5 mM and a surface tension (at cmc) of 29.4 mN/m. With increasing the $C_8E_3$ concentration, the dynamic contact angles decreased (at a constant velocity), as they did for CTAB solutions.

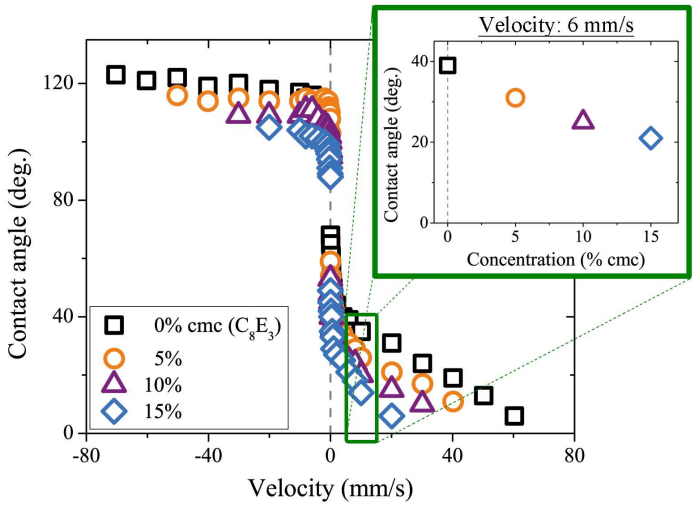


**Figure 3.15:** The $\theta - U-$ as well as the $\theta - c-$plots show decreasing contact angles with an increasing $C_8E_3$ concentration.

As expected, the addition of NaCl had no influence on a 5 % cmc $C_8E_3$ solution - the contact angles remained constant (Figure 3.16). This corresponds to the previ-

ous observations of the cmc of $C_8E_3$ being independent of the NaCl concentration (Figure 3.13).

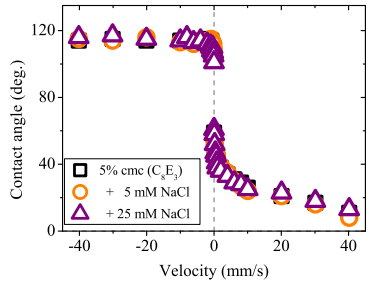


**Figure 3.16:** The $\theta - U-$plot of a 5 % cmc $C_8E_3$ solution showed no influence of increasing NaCl concentration on the dynamic contact angles.

Both, the ionic CTAB and the nonionic $C_8E_3$ solutions showed a significant contact angle decrease with increasing surfactant concentration. In case of the ionic CTAB, the decrease was more pronounced than for the nonionic $C_8E_3$ (Figure 3.17).

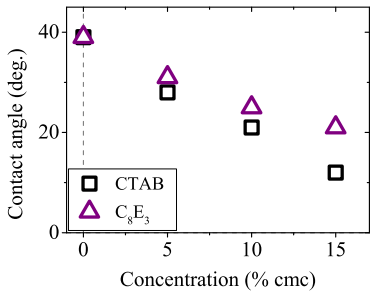


**Figure 3.17:** A comparison of the $\theta - c-$plots for CTAB and $C_8E_3$ at 6 mm/s showed a significant difference between these two surfactants - a stronger contact angle decrease for CTAB.

But what were the differences between these two surfactants, except of the charged/non-charged headgroup? One important difference was given by the strength of the surfactant - CTAB is the stronger surfactant with a cmc $\approx$ 1 mM compared to 7.5 mM for $C_8E_3$. As a consequence, the question arises if the surfactant strength influences the wetting/dewetting of surfactant solutions and therefore causes the differences in the $\theta - U-$plots for CTAB and $C_8E_3$.

#### 3.2.1.3 SDS - link between CTAB and $C_8E_3$

So far, two completely different surfactants were compared in terms of their influence on the wetting/dewetting of surfactant solutions - the stronger surfactant CTAB (ionic, cmc $\approx$ 1 mM) and the weaker $C_8E_3$ (nonionic, cmc $\approx$ 7.5 mM). To link these surfactants, I examined the anionic surfactant SDS. Like CTAB, SDS is an ionic surfactant allowing for electrostatic repulsive forces close to the three-phase contact line. At the same time, its surfactant strength (cmc $\approx$ 8 mM) is comparable to that of $C_8E_3$. This allows for studying the influence of electrostatic repulsion as well as surfactant strength on the wetting/dewetting of surfactant solutions.

SDS solutions followed the overall trend of decreasing contact angles with increasing surfactant concentration (Figure 3.18) as already described for CTAB and $C_8E_3$. The addition of NaCl to a 5 % cmc SDS solution led to a contact angle decrease (comparable to the CTAB/NaCl experiments) due to changed concentrations in multiples of cmc. Again, the $\theta - U-$plots of the recalculated concentrations fitted to those of the original concentrations - as described for CTAB/NaCl.

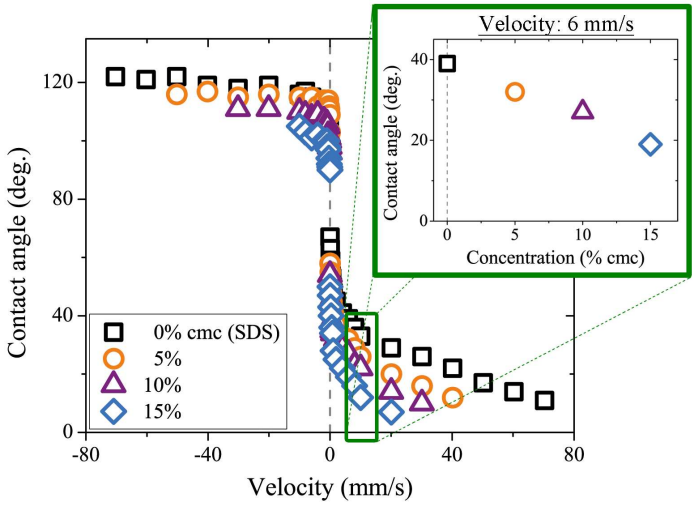


**Figure 3.18:** $\theta - U-$plot showing decreasing contact angles with increasing SDS concentration. Blow-up: $\theta - c-$plot at 6 mm/s.

Comparing the two ionic surfactants SDS and CTAB allows for judging the influence of the surfactant strength on the dynamic contact angles (while neglecting any contribution of the electrostatic repulsion to contact angle changes). The $\theta - c-$plot at 6 mm/s shows faster decreasing contact angles for CTAB than for SDS (Figure 3.19, black squares and orange circles). This faster decrease for the stronger surfactant hints to an influence of the surfactant strength - the stronger the surfactant, the faster the contact angle decrease with increasing concentration at constant velocity.

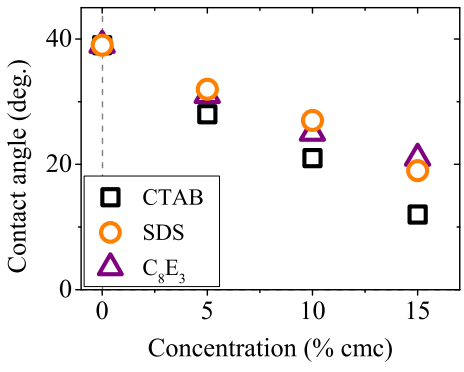


**Figure 3.19:** $\theta - c-$plots at 6 mm/s for CTAB, SDS, and $C_8E_3$ to test the influence of surfactant strength respectively electrostatic repulsion.

A comparison between SDS and $C_8E_3$, two surfactants of similar strength (cmc of 8 respectively 7.5 mM), could give some further information about the influence

of repulsive electrostatic forces. The $\theta - c-$plots at a constant velocity of 6 mm/s shows that both surfactants behaved identical (Figure 3.19, orange circles and purple triangles). This identical behavior of an ionic and a nonionic surfactant corroborates the assumption that electrostatic repulsion did not significantly add to the change in contact angles with increasing surfactant concentration.

Summarizing the results drawn from comparisons between SDS, CTAB, and $C_8E_3$ leads to the hypothesis that electrostatic repulsion is negligible (i. e. surfactants of any type can be compared), but surfactant strength plays an important role.

### 3.2.2 Marangoni effect?

After learning that electrostatic repulsion is negligible for the contact angle decrease with increasing surfactant concentration, one important question remains: What caused the contact angles to decrease?

In order to answer this question, I had a look at the regions close to the three-phase contact line on the advancing as well as on the receding side. The rotating drum generated a flow in the liquid bath. I assumed that this flow efficiently mixes the liquid and homogenizes the surfactant concentration. Far away from the contact line (at molecular length scale), a no-slip boundary condition of the liquid on the solid surface is assumed leading to a flow profile as sketched in Figure 3.20 [1, 2, 71].

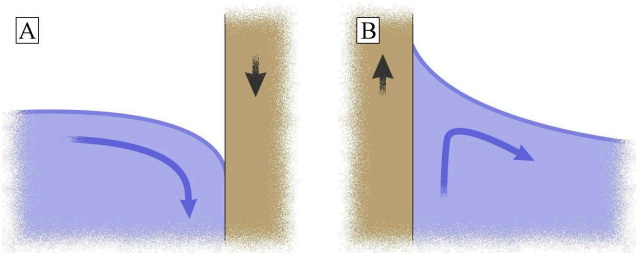


**Figure 3.20:** Sketched flow profile close to the (A) advancing and (B) receding contact line.

Due to this flow, on the side of the receding contact line ("receding side", Figure 3.20 B) a fresh liquid surface was constantly created and on the side of the advancing contact line ("advancing side", A) the liquid surface was constantly brought into contact with the cylinder. On the advancing side, surfactant adsorbed to the liquid surface was transferred to the cylinder surface. Consequently, the air-liquid interface close to the advancing contact line was constantly depleted of surfactant molecules. Assuming that on the receding side the freshly created liquid surface did not immediately have the equilibrium surfactant concentration, but a lower one, relaxing to the equilibrium concentration would transport more surfactant molecules to the surface to adsorb at the fresh surface. This would lead to a net flux of surfactant molecules from the bulk liquid to the air-liquid interface close to the receding contact line and therefore to a change in surface properties, e. g. surface coverage.

Local surface tension gradients would evolve from these changes in surface coverage. These gradients could lead to a force acting from the region of low to the region of high surface tension. This effect is known as **Marangoni effect**.

#### 3.2.2.1 Local surface tension gradients

The process described below reflects a stationary state where all processes take place at the same time, resulting in a new flow equilibrium. This process is described in several steps for simplification, while they occur at the same time.

First, I will discuss the process taking place at the receding side. When the drum moves at a constant velocity, the liquid is transported along the drum-liquid interface up to the stationary three-phase contact line (Figure 3.21 A, yellow star).

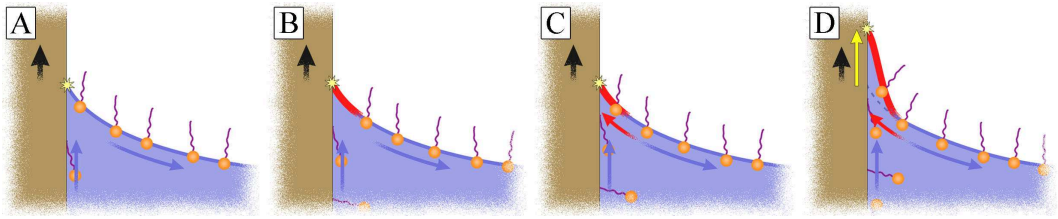


**Figure 3.21:** Sketch illustrating the formation of a local surface tension gradient leading to a contact angle decrease. For simplification, the sketched process is divided into several steps, although they take place at the same time. (A) Liquid is transported upwards along the drum, changes direction at the stationary three-phase contact line (yellow star), and flows downwards again (blue arrows). (B) Fresh surface is created (red interface), that is not immediately covered with surfactant molecules leading to a surface tension gradient. (C) This gradient implies a Marangoni force (red arrow) minimizing the initial flow. (D) As a consequence of the Marangoni force towards the drum, the three-phase contact line raises (yellow arrow) leading to lower contact angles.

There the liquid changes direction and flows towards the bulk (blue arrows). When the liquid changes direction and the three-phase contact line stays stationary, fresh surface is created that is not immediately covered with surfactant molecules (B, red interface). While the interface ages, the surfactant concentration at the air-liquid interface increases until it reaches the surface density given by the surfactant concentration in the bulk liquid. The inhomogeneous occupancy of the air-liquid interface leads to a surface tension gradient and therefore to a force counteracting the initial flow of the air-liquid interface (C, red arrow). This force can minimize respectively invert the initial flow, leading to an increased liquid amount close to the three-phase contact line. The increased liquid amount at the three-phase contact line can be compensated by an upwards movement of the three-phase contact line (D, yellow arrow) resulting in decreased contact angles [86].

The model about the upwards movement of the three-phase contact line is supported by observations of an increasing height difference between bulk liquid and three-phase contact line with increasing surfactant concentration (Figure 3.22 A). In addition, the decreasing critical velocity with increasing surfactant concentration points to a simplified raise of the three-phase contact line (Figure 3.22 B).

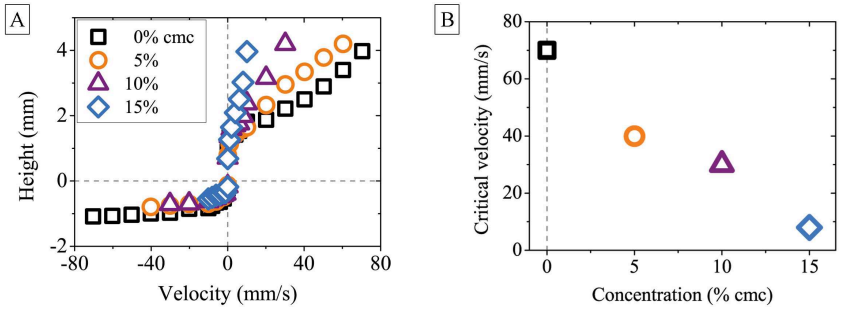


**Figure 3.22:** Increasing surfactant concentration favors the deformation of the air-liquid interface as shown for CTAB in (A) the height difference between the three-phase contact line and bulk liquid and (B) the decreasing critical velocity.

Second, I will discuss the processes taking place at the advancing side in detail. Figure 3.20 A illustrates the flow on the advancing side: The liquid is transported along the air-liquid interface towards the drum. At the drum, the air-liquid interface is transferred onto the drum, when the drum moves into the liquid. This transfer of the air-liquid interface to the drum-liquid interface can lead to an accumulation of surfactant molecules close to the three-phase contact line (Figure 3.23).

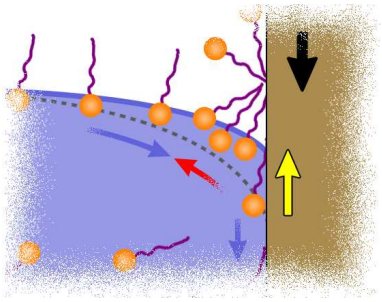

**Figure 3.23:** Surfactant molecules accumulating at the three-phase contact line can lead to a Marangoni force (red arrow) counteracting the initial flow (blue arrows). Thus, the three-phase contact line can rise (yellow arrow) due to a combination of reduced flow, reduced surface tension, and hydrophilized drum surface, leading to decreased contact angles.

This accumulation can lead to a Marangoni force pointing away from the drum resulting in a relaxation of the heavily deformed air-liquid interface and therefore to a raise of the three-phase contact line. This raise can be supported by the decreased surface tension as well as by the through adsorbed surfactant molecules slightly hydrophilized drum surface. Additionally, a further effect influencing the advancing contact angle can be assumed: The free air-liquid interface is stretched due to the hydrodynamic flow and the downwards pushing of the three-phase contact

line, probably leading to a weak surface tension gradient. The stretching as well as the accumulation effects described above, can be considered to have only a weak influence on the advancing contact angles. This is in agreement with the measured advancing contact angles (e. g. Figure 3.5) only showing a weak dependency on rotation velocity and surfactant concentration.

#### 3.2.2.2 Flow profile in the liquid

On the advancing side, the liquid flowed from the bulk-phase (along the air-liquid interface) in direction of the drum and then along the solid-liquid interface (Figure 3.20 A). This sketched flow held true for pure water as well as for CTAB solutions. The flow at the air-liquid interface is assumed to change when Marangoni forces are present and not to be negligible because the forces should either counteract or enhance the flow, i. e. the flow velocity should change with Marangoni forces being present. But the flow velocities, measured via particle tracking, did not change significantly when CTAB was added to the system - only about $\pm 5\,\%$, leading to the assumption of negligible Marangoni forces in case of advancing contact angles.

On the receding side, the liquid was transported along the solid-liquid interface upwards to the air-liquid interface and then flowed in direction of the bulk phase (Figure 3.20 B). This sketched flow profile was true for a pure liquid like water, but could change in presence of surfactants. Surfactant molecules can adsorb at the interface leading to a surface tension gradient and therewith to a Marangoni force at the air-liquid interface towards the drum. This means that in presence of surfactant molecules two effects counteract each other - the Marangoni flow and the initial flow away from the drum. How can the counteracting flows affect the total flow profile?

To visualize the flow profile inside the liquid, silica tracer particles were added to the liquid, which were large enough to be visible ($\varnothing \approx 10\,\mu m$), but did not sediment. They reflected the light and appeared as white spots in the dark liquid (Figure 3.24).

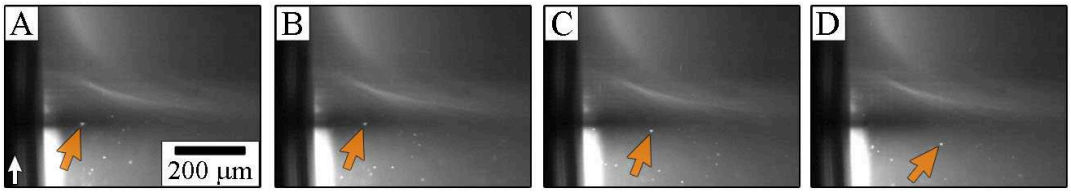


**Figure 3.24:** Sequence to illustrate the flow in a 20 % cmc CTAB solution at 6 mm/s. Images were taken every 20 ms. Orange arrows illustrate the position of particles following the flow close to the air-liquid interface and further away, while the white arrow indicates the rotation direction of the drum.

A visualization of the flow was possible, except of the regions close to the three-phase contact line ($\approx 200\,\mu m$ from the drum) and the air-liquid interface ($\approx 100\,\mu m$). These regions did not allow for an observation of the scattered light due to reflections at the interfaces.

For pure water, the observed flow corresponded to the sketched flow profile (Figure 3.20) - close to the drum the particles were transported upwards, while further apart they flowed downwards again. The velocity of the particles depended on the rotation velocity of the drum, but in general it could be said, the further the particles were away from the three-phase contact line, the faster they moved.

In the presence of CTAB, the flow at the receding side could change significantly - when Marangoni tensions at the air-liquid interface were considered (Figure 3.25):

(1) Particles close to the drum ($< 200\,\mu m$) were transported upwards in direction of the three-phase contact line (yellow arrow), while the velocity decreased the further the particles were transported upwards.

(2) Close to the air-liquid interface - as far as observable - the particles were slowed down or moved in direction of the three-phase contact line for high rotation velocities (red arrow, $U > 40\,mm/s$).

(3) Further apart from the interfaces, the particles were transported in direction of the bulk phase (orange arrow). The velocity increased with increasing distance to the three-phase contact line.

(4) The flow in the region close to the three-phase contact line could not be determined. This region covered the updrawn liquid in a distance about $200\,\mu m$ from the drum.

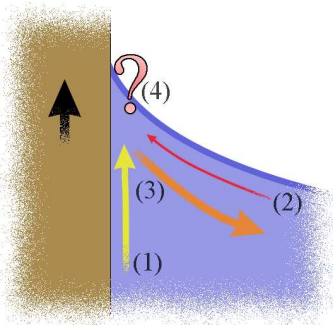


**Figure 3.25:** Sketch of the flow profile in the presence of surfactant. Liquid flowed at the air-liquid interface due to the Marangoni flow in direction of the drum ((2), red arrow), while the liquid close to the drum flows upwards ((1), yellow arrow). The liquid was transported away from the drum in the middle of the liquid ((3), orange arrow). The flow behavior close to the three-phase contact line is not known (4).

The situation when particles close to the air-liquid interface flowed in direction of the drum, was only observed for high velocities ($U > 40\,mm/s$). At lower velocities, the flow profile of CTAB solutions looked more like the one for pure water - particles close to the drum were transported upwards and then flowed downwards in direction of the bulk phase (Figure 3.26). For tracking the particles[6], the recorded video was divided

[6] by Marcel Weirich

into three parts to ensure that the particles did not get lost while thresholding the video, leading to intenser trajectories at the left side of each video part. Further, the velocity of the particles close to the drum was higher than the velocity of the particles closer to the bulk phase (Figure 3.26, red versus orange color).

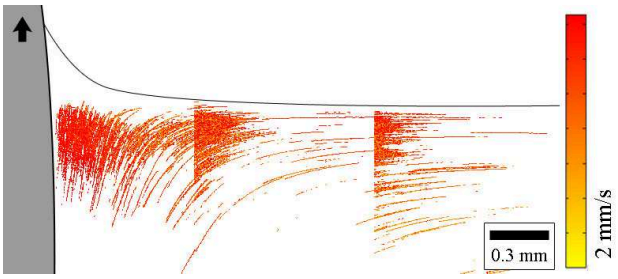


**Figure 3.26:** Visualization of the silica particle trajectories following the flow in a 10 % cmc CTAB solution at a rotation velocity of 6 mm/s.

This visualization of the flow at the receding side shows that there is no significant difference whether CTAB is present in the solution or not, i. e. the flow profile does not change significantly and therefore it does not contradict my hypothesis about Marangoni flow. When the surface would flow in direction of the three-phase contact line, the surface at the three-phase contact line would not be fresh, i. e. Marangoni tensions should not longer exist.

Following, I will estimate the critical velocity of Marangoni tensions influencing the wetting/dewetting and therewith gain an estimate of the dimension of the high surface tension region close to the three-phase contact line.

#### 3.2.2.3 Estimation of the critical velocity

A calculation of the surface tension gradient at the air-liquid interface is difficult because different processes occur on comparable length and time scales. One would need to take the diffusion of individual surfactant molecules, hydrodynamic flow, and the kinetics of adsorption into account. To at least estimate the length scale, a simple diffusion model is applied, neglecting hydrodynamic flow effects. On the receding side, a fresh liquid surface is created. For simplicity, I assume that initially a liquid wedge with a low contact angle is created at the three-phase contact line (Figure 3.27 A).

The coordinate parallel to the solid surface starting at the three-phase contact line is $x$. The initial surfactant concentration $c_i$ is homogeneously distributed in the liquid. At the three-phase contact line, a fresh liquid surface is continuously created that is supposed to be free of surfactant. Then surfactant diffuses to the surface until equilibrium is established between interface and bulk phase. A slice at a certain distance $x$ is considered, where the film has a thickness of $h = x \tan\theta$. In the first step, only diffusion in the vertical direction is allowed. Diffusion in one direction over a distance $h$ takes a characteristic time of $\tau_h = h^2/(2D)$, where $D$ is

the diffusion coefficient. Because $h = x \tan\theta$, the diffusion time between the contact line and the slice under consideration is always a factor of $1/\tan^2\theta$ larger. For angles smaller than approximately 20°, there is at least one order of magnitude difference between the time scales of the diffusion along and across the liquid wedge. For this reason, a decoupling of both diffusion processes seems to be justified.

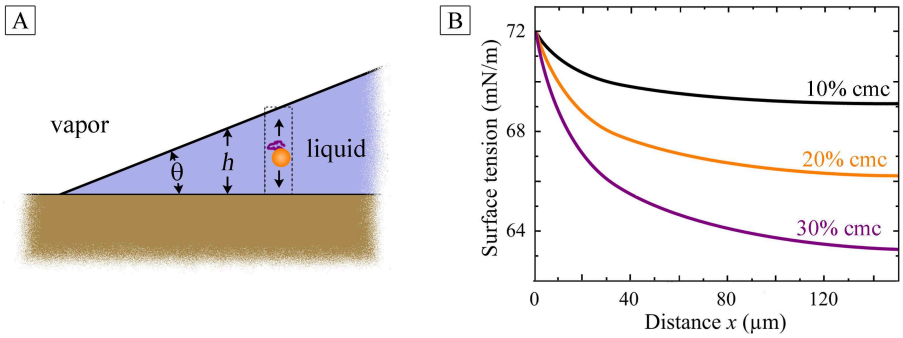


**Figure 3.27:** (A) The schematic shows the parameters used for calculating the surface tension $\gamma$ according to Equation (3.4). (B) Calculated surface tension with $\gamma_0 = 72\,\mathrm{mN/m}$, film thickness $h = x\tan\theta$, $\theta = 20°$, $\alpha = 6.6\,\mu\mathrm{m}$, and initial concentrations of 10 %, 20 %, and 30 % cmc. Adapted from [86].

To take adsorption into account, a linear adsorption isotherm is assumed: $\Gamma = \alpha c$ for $c \leq$ cmc and $\Gamma = \Gamma_0$ for $c >$ cmc. Here, $\Gamma$ is the surface excess of surfactant at the air-liquid interface in mol/m$^2$. Using the Gibb's adsorption isotherm for CTAB results in

$$\Gamma = -\frac{c}{2RT}\frac{d\gamma}{dc}. \tag{3.2}$$

Inserting $\alpha c$ for $\Gamma$ and integrating obtains:

$$\gamma_0 - \gamma = 2RT\alpha c. \tag{3.3}$$

Here, $\gamma_0$ is the surface tension of pure water and $R$ is the gas constant. The factor of 2 was added to take the ions into account, which dissociate from CTAB. For high concentrations ($c >$ cmc), $\gamma_0 - \gamma = 33\,\mathrm{mN/m}$. With cmc = 1 mM, I obtain $\alpha = 6.6\,\mu\mathrm{m}$.

Once equilibrium is established, the initial concentration $c_i$ in the vertical slice and the new concentration $c$ are related by $c_i h = ch + \Gamma$ for $c_i \leq$ cmc, leading to

$$c = \frac{c_i h}{h+\alpha} \qquad \text{and} \qquad \gamma_0 - \gamma = \frac{h(\gamma_0 - \gamma)}{h+\alpha}. \tag{3.4}$$

Here, $\gamma_0 - \gamma = 2RT\alpha c_i$. Equation (3.4) shows the physical significance of $\alpha$: For $h = \alpha$, the bulk concentration drops by a factor of 2 due to adsorption. Further, there is a characteristic film thickness necessary for the film pressure to increase by half of its maximal value. For thicker films, the film pressure is higher, and for thinner films, the film pressure is less than half of the final value. Figure 3.27 B shows the surface tension of an aqueous solution of CTAB with a contact angle of 20° once CTAB was allowed to diffuse in a vertical direction and to establish equilibrium with the surface. For concentrations below cmc, the shape of the curve is independent of the actual concentration. A gradient in the surface tension in the horizontal direction extends to a distance of several tens of micrometers.

In the second step, I estimate how long it would take to equilibrate this horizontal gradient in surface tension. The film has reached a thickness of $h = \alpha$ at $x = \alpha/\tan\theta$. In the used example, this is at 18.1 µm. With a diffusion coefficient for CTAB molecules of $D = 5.5 \cdot 10^{-10}$ m$^2$/s [88], the time required for a horizontal CTAB gradient to equilibrate is roughly $\tau_x = \alpha^2/(2D\tan^2\theta) = 0.3$ s. If the horizontal distance $x$ is divided by this relaxation time, a critical velocity of $U_c = 2D\tan\theta/\alpha = 0.06$ mm/s is obtained. For velocities above $U_c$, the Marangoni effect is expected to hinder dewetting. For velocities much below $U_c$, Marangoni effects should be negligible. Considering that hydrodynamic flow will accelerate equilibration, this rough estimate leads to the right order of magnitude of the critical velocity [86].

Here, the region close to the three-phase contact line is estimated, where Marangoni forces arise. This region is in the order of 20 µm and therefore with my optics not resolvable, even if I could resolve the region close to the three-phase contact line. The flow sketched in Figure 3.25 may be even more complex close to the three-phase contact line. To further test the hypothesis about Marangoni tensions influencing the dynamic contact angles, the surfactant properties were varied.

## 3.3 Testing the Marangoni effect hypothesis

The above described decreasing of the receding contact angle due to local surface tension gradients and therewith due to Marangoni tension, is further referred to as **Marangoni effect hypothesis**. To test this hypothesis, let us think about what happens when the surfactant concentration in the solution is increased or the surfactant strength is varied.

### 3.3.1 Increasing the surfactant concentration

The decrease of the receding contact angle for surfactant solutions compared to pure water can be explained with the Marangoni effect hypothesis. But why do the contact angles decrease with increasing surfactant concentration?

The surfactant concentrations were well below the cmc, i. e. when increasing the surfactant concentration further, the molecules tent to adsorb at the air-liquid interface and decrease the surface tension. The higher the surfactant concentration (but always below cmc), the higher the surface coverage what could result in larger surface tension gradients. Furthermore, the updrawing of the three-phase contact line is simplified with increasing surfactant concentration (Figure 3.22). The combination of an increased Marangoni tension and a simplified updrawing of the three-phase contact line due to lower surface tensions leads to decreasing contact angles with increasing surfactant concentration.

With further increasing the surfactant concentrations, the contact angle decrease continued. For a concentration above 50 % cmc, the receding contact angles were no longer measureable ($< 5°$), also for velocities below 1 mm/s. Even the advancing contact angles decreased to values below 90°, while the critical velocity was below 1 mm/s.

### 3.3.2 Variation of the surfactant strength

The Marangoni flow hypothesis is based on the formation of a surface tension gradient. The stronger the surface tension gradient, the larger the flow in direction of the freshly created surface leading to a decrease of the receding contact angle. The strength of this gradient is not only influenced by the maximal difference in surface tension between a pure air-liquid interface and the equilibrium interface, but also by the adsorption efficiency of surfactant molecules to the air-liquid interface leading to a equilibration of the gradient. The question about a possible influence of the surfactant strength on the surface tension gradient is discussed below.

Independent of the surfactant strength, a surface tension gradient should be formed, because surfactant molecules adsorb at the surface. The velocity with which the surface tension gradient is reduced depends on the number of surfactant molecules present in the solution. The more molecules are freely dissolved in the solution, the higher the probability of surfactant molecules adsorbing at the air-liquid interface, at concentrations well below cmc. Diffusion and hydrodynamic flow can more efficiently transport these molecules to the air-liquid interface, where they can adsorb at the interface and thus decrease the local surface tension gradient.

When the number of surfactant molecules influences the contact angle decrease, a faster contact angle decrease is expected for strong surfactants (low cmc) than for

weak surfactants. This is due to a more efficient diffusion of surfactant molecules to the air-liquid interface to reduce the surface tension gradient when more surfactant molecules are present (high cmc). The nonionic alkyl glycole surfactants $C_4E_1$, $C_8E_3$, and $C_{12}E_5$, which cover 5 orders of magnitude of cmc (Table 3.1), were used to test this hypothesis. The number of surfactant molecules present in solution decreases with increasing surfactant strength (when the concentration is given in % cmc).

| surfactant | cmc / mM | $\gamma^*$ / mN/m | number of molecules* |
|---|---|---|---|
| $C_4E_1$ | 500 | 66 | $2.7 \cdot 10^{22}$ |
| $C_8E_3$ | 7.5 | 61 | $4.1 \cdot 10^{20}$ |
| $C_{12}E_5$ | 0.07 | 59 | $3.4 \cdot 10^{18}$ |

* at 10 % cmc

**Table 3.1:** Summary of the measured cmc and surface tension at 10 % cmc of the nonionic surfactants $C_4E_1$, $C_8E_3$, and $C_{12}E_5$.

Each surfactant taken by itself, shows decreasing contact angles with increasing surfactant concentration as described in Section 3.1 for CTAB. A comparison of the nonionic surfactants at 10 % cmc shows decreasing receding contact angles with increasing surfactant strength (from $C_4E_1$ to $C_{12}E_5$), while the advancing contact angles were almost constant (Figure 3.28 A). This behavior was observed for all measured concentrations (Figure 3.28 B). The fact that the advancing contact angles were only weakly influenced by surfactant strength, implies that surface tension gradients are not the main reason for a reduction of the advancing contact angles.

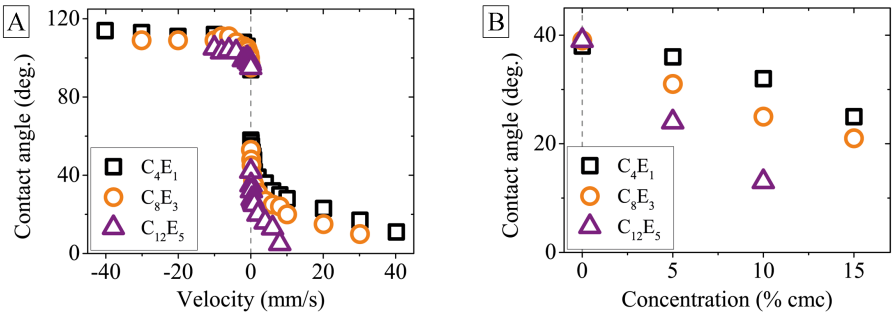


**Figure 3.28:** Comparison of the nonionic surfactants $C_4E_1$, $C_8E_3$, and $C_{12}E_5$ at (A) 10 % cmc and (B) 6 mm/s shows that the receding contact angles decreased with increasing (A) surfactant strength and (B) concentration.

The systematic variation of cmc and therewith of the number of surfactant molecules per volume in the solution leads to a variation of the diffusion time. For weak surfactants more molecules are in the solution (at concentrations in % cmc), leading to lower diffusion times. Further, the diffusion coefficient decreases with increasing surfactant strength - for the here investigated surfactants $C_4E_1$, $C_8E_3$, and $C_{12}E_5$ [89]. These low diffusion coefficients respectively high diffusion times for strong surfactants lead to more distinct surface tension gradients and therewith to a stronger decrease of the receding contact angle for strong than for weak surfactants. The hypothesis of Marangoni tensions being responsible for the decreasing receding contact angles is supported by the results of increasing surfactant strength as well as increasing surfactant concentration.

## 3.4 Comparison with theory

The existing theories, including the hydrodynamic and molecular kinetic theories, do not take surface tension gradients into account which I suggested to be the cause of the observed wetting/dewetting of the surfactant solutions. Further, the theories have a lot of free fitting parameters which allow for fitting the observed wetting/dewetting of one-component liquids as well as of more complex liquids like surfactant solutions. This means, the wetting/dewetting of the surfactant solutions could be fitted, but due to the number of fitting parameters the physical significance of the fitted parameters, e. g. macroscopic and microscopic length or three-phase contact line friction, is not implicitly given. For the reasons of the neglected surface tension gradients and the number of free fitting parameters, I did not use the existing theories to fit my results for the wetting/dewetting of the surfactant solutions.

Further, I refrained from comparing the wetting/dewetting results of the surfactant solutions obtained by the rotating drum setup with the Landau Levich Derjaguin-theory. The Landau Levich Derjaguin-theory deals with velocities above the critical velocity, the velocities where I stopped my measurements with the rotating drum setup. This means that not only different velocity ranges are considered, but also the presence of the three-phase contact line and its influence on the wetting/dewetting varied: In case of the Landau Levich Derjaguin-theory, the three-phase contact line does not exist (it is too far away from the bulk liquid, about several cm) in contrast to the rotating drum setup where the three-phase contact line is present in the observation range (distance was maximal a few cm). This means that the Landau Levich Derjaguin-theory misses one central part of my experiments. Further, the differing position of the three-phase contact line led to different flow profiles - in case of velocities above the critical velocity liquid close to the air-liquid interface (up to a distance of 2 mm) flowed in direction of the three-phase contact line [90, 91].

## 3.5 Conclusions

The developed rotating drum setup was most suitable to investigate the wetting/dewetting processes involved in the gravure printing technique as well as structural and geometrical influences of the setup at a geometry similar to the one used in real processes. This allowed to have a closer look at the wetting/dewetting of surfactant solutions and showed that they did not follow the Cox-Voinov relation as simple liquids did.

Here, I showed that the wetting/dewetting properties of a liquid could be significantly changed by adding surfactant. All investigated surfactant solutions - $C_4E_1$, SDS, $C_8E_3$, CTAB and $C_{12}E_5$ - showed one common behavior: The receding contact angles decreased with increasing velocity as well as with increasing surfactant concentration. The advancing contact angles slightly increased with increasing velocity, but decreased with increasing surfactant concentration. Electrostatic repulsion seemed to have no significant influence on the wetting/dewetting of ionic surfactant solutions. In case it affected the wetting/dewetting, it had a minor contribution. The main contribution was the formation of a surface tension gradient close to the three-phase contact line and therewith a Marangoni tension. This tension was independent of surfactant type, but depended on surfactant strength - the stronger the surfactant, the stronger the reduction of the receding contact angles. Surfactant strength can be seen as an equivalent to the number of surfactant molecules available in the liquid to reduce the surface tension gradient.

A comparison of all surfactants at 10 % cmc - independent of surfactant type and surfactant strength - showed that the advancing contact angles were almost not influenced by the different types and strengths (Figure 3.29 A). The reduction of the receding contact angles resembled the surfactant strength - similar cmc led to similar contact angles independent of the different surfactant types (SDS and $C_8E_3$).

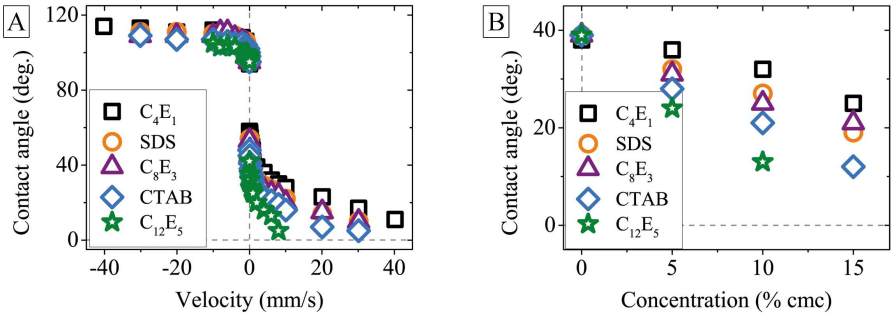


**Figure 3.29:** Comparison of all measured surfactants - $C_4E_1$, SDS, $C_8E_3$, CTAB, and $C_{12}E_5$ in order of increasing strength - at (A) 10 % cmc and (B) 6 mm/s.

Compared to Chaudhuri and Paria [85], I was able to go to higher velocities (up to several cm/s). They observed almost constant receding and slightly decreasing advancing contact angles with increasing velocity - completely contrary to my results. One major difference between their and my measurement was the substrate: They used PTFE while I used a polystyrene surface. The comparison with their work showed that the interaction between surfactant and substrate (PTFE or polystyrene) should play a role. The PTFE surface has only little interaction with the surfactant molecules, as can be seen from relatively high contact angles of long chain alkanes on PTFE. CTAB molecules should not adsorb at the highly fluorinated PTFE surface (hexadecane on PTFE: 46° [92]) as strongly as they do at the polystyrene surface (hexadecane on polystyrene: $< 5°$ [93]). This difference in adsorption could lead to different dynamic contact angles with increasing velocity - in case of PTFE to constant and in case of polystyrene to decreasing receding contact angles. A further difference between their and my experiments was the method which was used to obtain the dynamic contact angles. I determined them optically while Chaudhuri and Paria derived them from tensiometer measurements, which could also influence the contact angle values - an almost continuous motion in case of the rotating drum setup versus a stepping motion in case of the tensiometer measurements.

I have shown that surfactants influence the wetting/dewetting of aqueous solutions at concentrations well below cmc. Thus not only the surfactant concentration is important, but also the surfactant strength and the surface energy of the substrate. Further, I developed a theory about local surface tension gradients (close to the three-phase contact line) to significantly influence and therefore change the wetting/dewetting of surfactant solutions.

## 3.6 Experimental details

### Drum preparation

The barrel-shaped drum was cleaned with acetone (fisher scientific) and then coated with polystyrene[7] ($M_w \approx 300\,\mathrm{kg/mol}$) in THF (0.8 wt %, Section 2.3.3.5). After a first drying at room temperature, the drum was dried for 16 hours at 60 °C and then inserted into the bath.

### Contact angle measurement

The bath was half filled with Milli-Q water (purified by a Sartorius Arium 611 at a resistivity of $18.2\,\mathrm{M\Omega \times cm}$) and then closed with parafilm (Bemis). To ensure a

[7] anionically polymerized by Thomas Wagner

saturated atmosphere inside the bath from beginning, the drum was allowed for rotating at a high velocity (about 10 cm/s) for at least 20 minutes before measurements started. Contact angles were observed in side view using the Photron high-speed camera with the Navitar tubus ($12\times$ magnification) at a frame rate of 500 Hz with back lighting.

The concentration of the used surfactants/salt was steadily increased by adding pure surfactant/salt to the liquid and stirring the solution for at least 20 minutes at $\approx 10$ cm/s. After completion of the measurement series, the bath was cleaned until pure water measurements resulted in the same behavior as at the beginning of the measurement.

### Surfactant and salt solutions

As surfactants the ionic surfactants SDS (Acros Organics) and CTAB (Sigma-Aldrich) as well as the nonionic surfactants $C_4E_1$ (Fluka), $C_8E_3$ (Bachem), and $C_{12}E_5$ (Bachem) were used (details in Table 2.1). The measured concentrations were 0 %, 5 %, 10 %, and 15 % of the cmc.

NaCl (Sigma-Aldrich) was used to decrease the electrostatic repulsion between the charged surfactant molecules at concentrations of 5 and 25 mM.

### Visualization of the flow profile

A small amount of silica particles (Kromasil 100, $\varnothing = 10 \pm 2\,\mu$m, Analysentechnik, Mainz, Germany) was added as tracer particles to the liquid - either pure water or a CTAB solution (10 % or 20 % cmc). The flow was followed in side view with back lighting using the Photron high-speed camera at a frame rate of 1000 Hz at $6\times$ magnification (zoom objective). For analyzing the flow profile, the video was divided into three parts to allow also a visualization of the particles further away from the drum. The particles have been followed resulting in trajectories reflecting the actual flow profile.

### SFM measurements

The polystyrene coated drum was analyzed with the NanoWizard$^{TM}$ atomic force microscope by JPK instruments in tapping mode, equipped with Si cantilevers (Olympus OMCL-AC240TS, spring constant of 2 N/m, resonance frequency of 70 kHz). The scanning size was typically $50 \times 50\,\mu$m$^2$.

# 4 Influence of the setup geometry on dynamic wetting/dewetting[8]

In the absence of rotation, the drum surface and the liquid-air interface are covered by a surfactant layer whose concentration is in equilibrium with the bulk surfactant concentration. Since all experiments are carried out at concentrations well below cmc, I assume that the surface surfactant concentrations at the drum as well as at the air-liquid interface depend on the bulk concentration. Upon drum rotation, the surface surfactant concentration changes leading to surface tension gradients: On the receding side, fresh surface is created that is not immediately covered with surfactant molecules. This inhomogeneous covering of the air-liquid interface leads to a local surface tension gradient close to the three-phase contact line. On the advancing side, during rotation the air-liquid interface is transferred onto the drum and thereby surfactant molecules are pushed into the bulk, also resulting in a small local surface tension gradient. These local surface tension gradients are the reason for a contact angle reduction in presence of surfactants as I discussed in Chapter 3. Beside the discussed local surface tension gradients, also a non-local surface tension gradient ranging over the complete bath could exist.

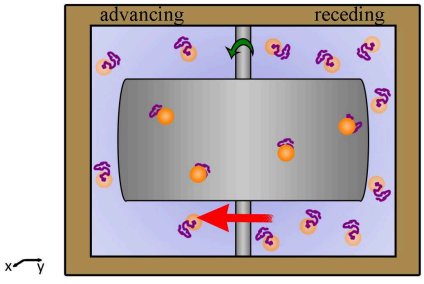


**Figure 4.1:** Creation of new surface at the receding side leads to a higher surface surfactant concentration at this side than at the depleted advancing side. This imbalanced surfactant distribution results in a surfactant flux from the receding to the advancing side (red arrow).

As already discussed, new surface is created at the receding side. This freshly created surface has to be covered with surfactant molecules what leads to a surfactant molecule's enrichment at this side. At the same time on the advancing side: Surface is destroyed and therefore depleted of surfactant molecules leading to an imbalanced

[8]This chapter is based on "D. Fell, N. Pawanrat, E. Bonaccurso, H.-J. Butt, G.K. Auernhammer, *Influence of surfactant transport suppression on dynamic contact angle hysteresis*, Colloid and Polymer Science, **291** (2012) 361".

distribution of surfactant molecules at the air-liquid interface - high concentration at the receding side, low concentration at the advancing side (Figure 4.1). This non-local concentration gradient has to be balanced by surfactant molecules transported from the receding to the advancing side, resulting in a surfactant flux.

### Surfactant transport

The surfactant fluxes to and from the air-liquid interface at the advancing and receding side of the drum can be replenished either by transport of surfactant into the bulk or along the surface. Along the surface, surfactant molecules can either diffuse due to a concentration gradient or be advected by bulk flow involving surface motion. Any transport along the surface would lead to an equilibration of the surface surfactant concentration between the advancing and the receding side. A second possibility is the equilibration of the surface concentration with the bulk phase underneath. Subsequently, the equilibration between the advancing and receding side is achieved by advection with the hydrodynamic flow or diffusion in the bulk phase. Relative importance of these two possible transport mechanisms strongly depend on the characteristic time scale of the surfactant adsorption to and desorption from the air-liquid interface. Fast equilibration of the surface concentration with the bulk phase favors bulk transport, while a slow equilibration favors surface transport.

In this chapter, I discuss the influence of non-local surface tension gradients on the wetting/dewetting of surfactant solutions, using the example of CTAB. Therefore I measured dynamic contact angles at different setup geometries to investigate the importance of different equilibration mechanisms (Figure 4.2).

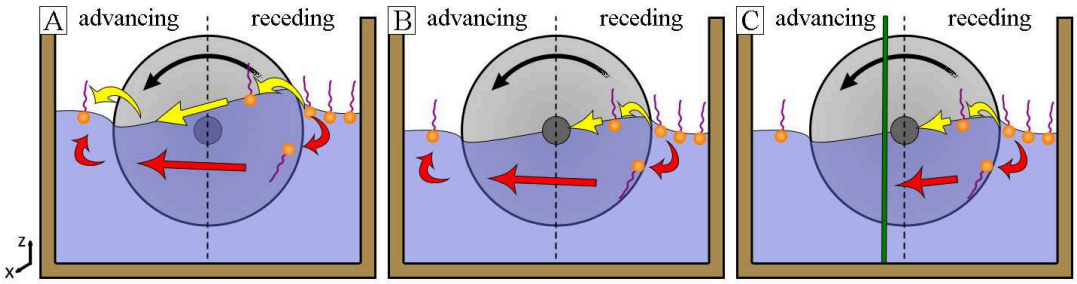


**Figure 4.2:** Illustration of the possible surfactant transport mechanisms. (A) Surface as well as bulk transport is possible, when the liquid level is above the axis. (B) Only bulk transport is allowed, when the axis divides the air-liquid interface. (C) Maximal hindrance in case of a half-filled bath with an external barrier added that divided the bulk. The yellow arrows symbolize the surface transport, the red ones the bulk transport. The green vertical line illustrates the external barrier.

To this end, transport along the surface and in the bulk of the water bath was successful hindered (Figure 4.2) by allowing for advection and diffusion at the surface and in the bulk (A), only in the bulk (B) or with maximal hindrance (C):

(A) The axis holding the drum is completely immersed in the liquid allowing for surface as well as for bulk transport.

(B) The axis, half immersed in the liquid, divides the surface of the advancing and receding side and therefore allows only for bulk transport.

(C) An external barrier divides the surface as well as the bulk into advancing and receding side and therefore allows for maximal hindrance.

In the rotating drum setup the barrel-shaped drum was used. It was coated with polystyrene resulting in an average film roughness of $120 \pm 20$ nm and a static contact angle for water of 79°.

## 4.1 Influence of transport limitations

The case of hindered surface transport (Figure 4.2 B) has already been discussed in Chapter 3, when the CTAB solution was filled up to the axis of a polystyrene coated drum with an average roughness of 140 nm. The contact angles decreased with increasing velocity and surfactant concentration (Figure 3.5). The same wetting behavior was observed for a different, but comparable polystyrene coating (roughness of 120 nm) that allowed for contact angle measurements up to CTAB concentrations of 40 % cmc (Figure 4.3).

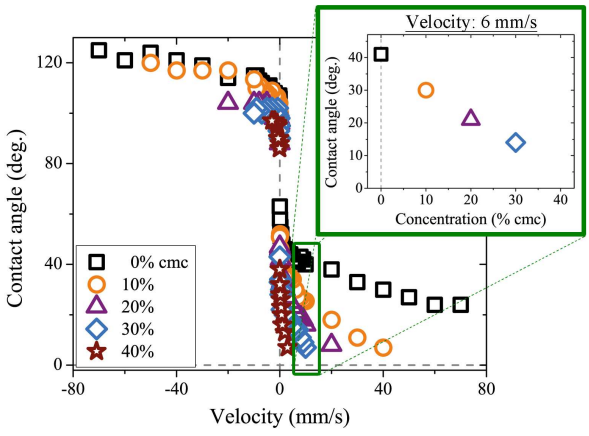


**Figure 4.3:** $\theta - U-$plots for CTAB solutions when only advection and diffusion through the bulk were allowed to equilibrate the surfactant concentration gradient in the liquid. The contact angle decrease at 6 mm/s is shown in the $\theta - c-$plot (blow up).

The wetting/dewetting of a CTAB solution changed slightly with coating quality including roughness and homogeneity. Absolute values differed, but altogether the overall trend of decreasing contact angles with increasing surfactant concentration

was preserved. The receding contact angles decreased significantly with increasing velocity as well as with increasing surfactant concentration, while the advancing contact angles were less influenced. Furthermore, the advancing as well as the receding contact angles showed again two different slopes - a higher one below 2 mm/s and a lower one at higher velocities. A possible origin of the different slopes is discussed in Section 5.3.

For a better visibility of the CTAB concentrations, the $\theta - U-$plots below will be limited to velocities between -10 and 10 mm/s. These plots provide the same information about the contact angle dependency than the ones covering the complete velocity-range (due to the constant second slope) except of the critical velocity. But the critical velocities decreased with increasing CTAB concentration - from about 100 mm/s for pure water to below 7 mm/s for a 40 % cmc CTAB solution (Figure 4.4).

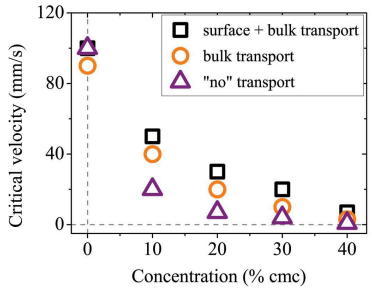


**Figure 4.4:** Critical velocities decrease with increasing CTAB concentration and increasing limitations of the surfactant transport.

Figure 4.5 shows the $\theta - U-$plot in case of limited CTAB surface transport from the receding to the advancing side for limited velocities. CTAB molecules could only diffuse/advect to the advancing side through the bulk liquid (Figure 4.2 B).

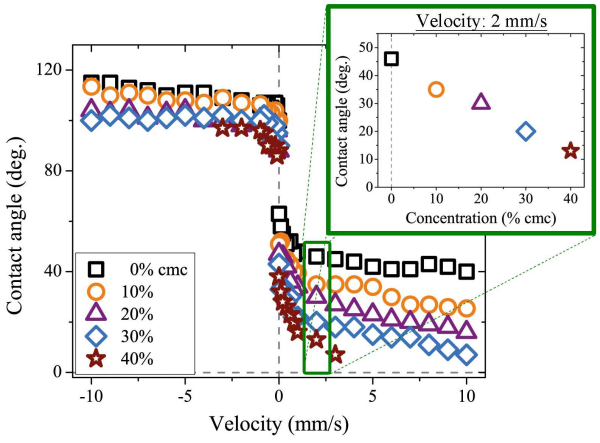


**Figure 4.5:** Replot of Figure 4.3 in the velocity range of -10 mm/s to 10 mm/s. Only advection and diffusion through the bulk is allowed for surfactant equilibration. The blow up shows a $\theta - c-$plot at 2 mm/s.

The data compared so far, represented the case, when only bulk transport was allowed. How does the wetting/dewetting change for allowed surface as well as bulk transport or no allowed transport at all?

### 4.1.1 Transport limitations

In case of a fast equilibration of the concentration gradient between the advancing and receding side, I expect slower decreasing contact angles on the receding side. In contrast to this, a faster contact angle reduction, i. e. lower contact angles, is expected for a slow or almost absent equilibration of the concentration gradient.

The concentration gradient should equilibrate slower with increasing transport limitations, i. e. the larger the transport limitations, the lower the expected receding contact angles. This means, the stronger the concentration gradient and thereby the surface tension gradient, the larger should be the contact angle reduction.

#### 4.1.1.1 Surface as well as bulk transportation

When surface as well as bulk transport is allowed during drum rotation (axis is immersed in the liquid), the equilibration of the CTAB concentration gradient along the surface should be fast, compared to the case of hindered surface transport. Surfactant molecules can either diffuse along the air-liquid interface or be transported by advection or diffusion through the bulk from the receding to the advancing side (Figure 4.2 A).

Analog to the case of limited surface transport, the contact angles decreased with increasing CTAB concentration in case of unlimited transportation (surface as well as bulk transport were allowed). Again, the receding contact angles showed a stronger dependence on CTAB concentration than the advancing contact angles (Figure 4.6). As expected, the unlimited case showed higher contact angles (at a constant velocity of 2 mm/s: 20° compared to 10°) than the limited case when only bulk transport was allowed (Figure 4.6 compared to Figure 4.5). Also the critical velocities were higher for the unlimited case (Figure 4.4).

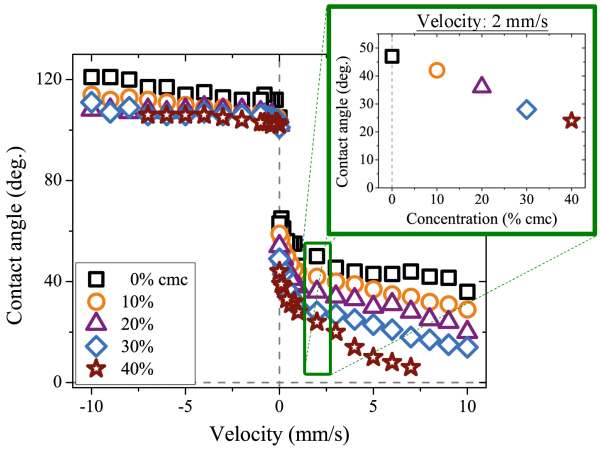


**Figure 4.6:** $\theta - U-$plots for CTAB solutions in case of unlimited surfactant transport. The blow up shows a $\theta - c-$plot at 2 mm/s.

#### 4.1.1.2 "No" transportation

A similar behavior could be observed, when neither surface nor bulk transport was allowed: The contact angles decreased with increasing surfactant concentration, whereby again the advancing contact angles did not decrease as significantly as the receding ones (Figure 4.7). The external barrier allowed for blocking most of the surfactant transport, but small gaps between barrier and drum/bath walls, which were in the order of $\approx 1\,\mathrm{mm}$, could not hinder surfactant transport completely.

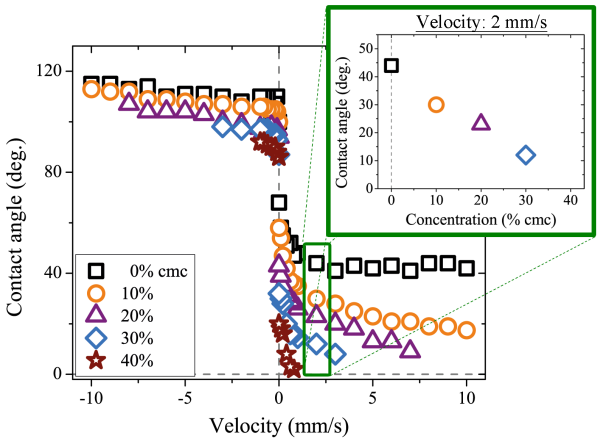


**Figure 4.7:** $\theta - U-$plots for CTAB solutions in case of totally limited surfactant transport. Surface as well as bulk transport was hindered. The blow up shows a $\theta - c-$plot at $2\,\mathrm{mm/s}$.

Compared to the geometries where surfactant transport was limited - allowed surface and bulk transport as well as only allowed bulk transport - the case of completely limited surfactant transport showed the lowest critical velocities (Figure 4.4) and lowest contact angles at $2\,\mathrm{mm/s}$ ($\approx 0°$ compared to 20° respectively 10°, Figure 4.7 compared to Figures 4.5 and 4.6).

So far it seemed that the contact angles decreased with increasing limitations of the surfactant transport from one side of the bath to the other side. In case of fast equilibration (surface as well as bulk transport were allowed), higher contact angles were observed than for the cases of slower equilibration.

### 4.1.2 Comparison of the different setup geometries

The wetting/dewetting of the surfactant solutions was similar, independent of the different setup geometries, but varied in the absolute contact angle values: The contact angles decreased with increasing CTAB concentration. The receding contact angles decreased faster in case of maximal hindrance than for the less hindered cases. Before I further compare these contact angle measurements, one important question has to be answered: Are the achieved $\theta - U-$plots comparable in respect of the absolute contact angle values, independent of the differing setup geometries?

#### 4.1.2.1 Pure water

As discussed above, the different setup geometries should influence the wetting/ dewetting of surfactant solutions due to the varying limitations of the surfactant molecules diffusing from the receding to the advancing side. But due to the differing filling height and barrier added to the bath, the initial flow profiles could differ. This could lead to hardly comparable $\theta - U-$plots with respect to the absolute contact angles. Because of that, the three geometries are compared for a one-component liquid, where concentration gradients do not exist. Therefore, I used pure water to test the influence of the flow profile - in absence of concentration gradients - on the wetting/dewetting of the different setup geometries.

Independent of the setup geometry, the dynamic contact angles of pure water behaved identical (Figure 4.8). This means that the flow profile of the three different geometries did not vary for a one-component liquid and therefore a comparison of the different geometries should be possible for the more complex CTAB solutions.

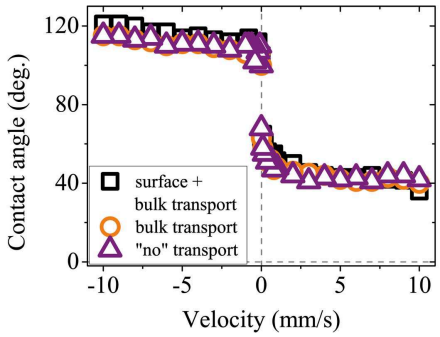


**Figure 4.8:** Comparison of the wetting behavior of pure water for the different setup geometries - filling height and presence of external barrier.

In contrast to the observed dynamic contact angles of pure water, I expect differences in case of CTAB solutions, as mentioned above: The stronger the transport limitations, the lower the expected dynamic contact angles.

#### 4.1.2.2 CTAB solutions

The general shape of the $\theta - U-$plots was similar in all experiments, independent of surfactant concentration and transport limitation (Section 4.1.1). At any given rotation velocity and limitation of surfactant transport, the overall dependence on surfactant concentration did not change. The receding contact angles decreased with increasing velocity while the advancing contact angles increased.

A comparison of the different geometries at a CTAB concentration of 10 % cmc showed that the advancing contact angles were within the experimental uncertainty, while the receding contact angles differed depending on the degree of transport limitation (Figure 4.9 A). The case without any limitation (surface as well as bulk transport was allowed) shows the highest contact angles while with increasing limitations

the receding contact angles decreased. The differences were not really significant, but clearly beyond the experimental uncertainty.

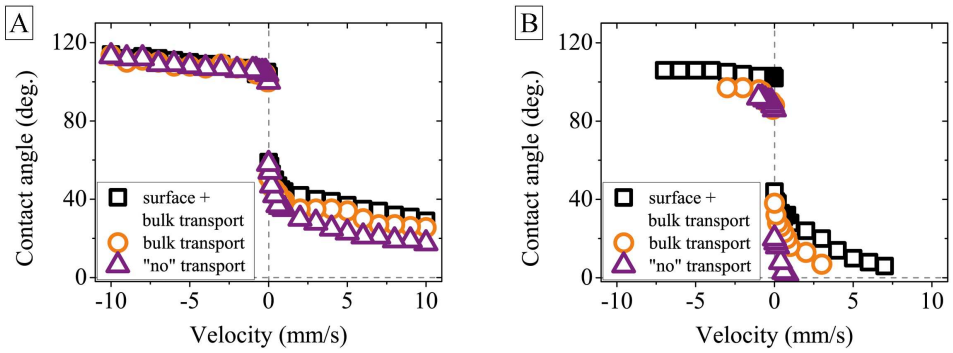


**Figure 4.9:** Comparison of $\theta - U-$plots for different setup geometries at (A) 10 % and (B) 40 % cmc of CTAB. The contact angle difference increased with increasing transport limitations.

With increasing CTAB concentration, this difference in the decreasing receding contact angles with increasing transport limitations got more and more pronounced. At 40 % cmc, the difference was two times higher than for 10 % cmc (at a velocity of 2 mm/s). In all experiments the difference in the receding contact angles was more sensitive to surfactant concentration and transport limitation of surfactant transport than the difference in the advancing contact angles.

Altogether, the contact angles decreased with increasing limitation of surfactant transport from one side of the bath to the other. This effect was more pronounced for comparable high CTAB concentrations than for low concentrations. But why did the dependency of the receding contact angles on the surfactant transport limitation also depend on the surfactant concentration?

## 4.2 Reasons for the contact angle reduction

Independent of the limitations, the wetting/dewetting of surfactant solutions was similar: The advancing contact angles were more or less constant while the receding contact angles decreased with increasing velocity. Further, with increasing the surfactant concentration, the receding contact angles decreased significantly while the decrease of the advancing contact angles was less pronounced. This behavior can be described by my Marangoni effect hypothesis discussed in Chapter 3. Due to the creation/destruction of the air-liquid interface close to the three-phase contact line, local surface tension gradients arise and induce a Marangoni tension leading to

a reduction of the dynamic contact angles with increasing surfactant concentration. This argument considered only the local situation close to the three-phase contact line at length scales of the order of the capillary length or smaller. Therefore it is possible to apply this model for all three cases - allowing for surface as well as bulk, only bulk, or "no" surfactant transport at all.

To minimize the influence on local processes close to the three-phase contact line, the surfactant transport limitations were placed far away (on the length scale of the capillary length) from the contact line. Still, clear differences with and without limitations were measured. With increasing limitations the contact angles decreased (Figure 4.10), i. e. non-local processes (large scale transport processes between the receding and advancing side of the drum) had a strong influence on the wetting/dewetting of the surfactant solutions.

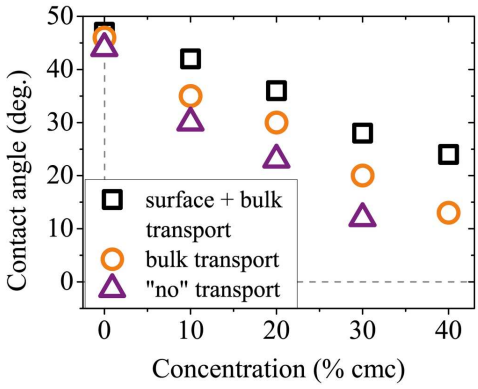


**Figure 4.10:** Comparison of the $\theta - c-$plots for the three different setup geometries at 2 mm/s. The receding contact angles decreased with increasing limitations - the case of allowed surface and bulk transport showed the highest contact angles, the case with hindered surface and bulk transport showed the lowest contact angles.

In case of unlimited surfactant transport (surface as well as bulk transport was allowed), surfactant molecules were transported faster from the receding to the advancing side as in the cases of limited surfactant transport. The faster transport led to a faster equilibration of the surface tension gradient and therefore to a slower decrease of the receding contact angles, compared to slow transport, i. e. limited surface transport.

## 4.3 Conclusions

As discussed earlier, the changes in contact angles did not depend on the absolute surfactant concentration, but rather on a "normalized" concentration (i. e. in % cmc). I argued, that adsorption or desorption kinetics were not the limiting factor in the relaxation of the surface surfactant concentration (and the surface tension) towards its local equilibrium value that was given by the bulk concentration. Instead, I proposed non-local surfactant transport processes, like diffusion of the surfactant molecules to the surface, to be relevant for the relaxation of the surface surfactant

concentration. By successively hindering surfactant transport from the receding (surfactant-rich surface) to the advancing side (surfactant-poor surface), I observed decreasing contact angles and therefore was able to show the importance of large scale transport processes: These consequential non-local surface tension gradients add to the local surface tension gradient and enhance the contact angle decrease - at constant surfactant concentration and rotation velocity.

The wetting/dewetting and therefore the dynamic contact angle of a surfactant solution is influenced by transport processes on different length scales. Short-range effects close to the three-phase contact line (on the length scale of the capillary length) generate local surface tension gradients and induce a strong dependence of the dynamic contact angles on surfactant concentration [86] (Chapter 3). Further, long-range effects affected the dynamic contact angles for any non-zero surfactant concentration. The more efficient the transport mechanisms are between the region close to the receding and the advancing contact line, the larger are the contact angles.

In case of CTAB, both, surfactant transport along the air-liquid interface as well as through the bulk (e. g. by diffusion and advection) played a role. I showed this by successively hindering these transport mechanisms with selective barriers.

## 4.4 Experimental details

### Drum preparation

The barrel-shaped drum was cleaned with acetone (fisher scientific) and then coated with polystyrene[9] ($M_w \approx 300\,\mathrm{kg/mol}$) in THF (0.8 wt%, Section 2.3.3.5). After a first drying at ambient conditions, the drum was annealed for 16 hours at 60 °C and then inserted into the bath.

### Bath geometry

Depending on the surfactant transport suppression type, three different geometries were used (Figure 2.23):

- A bath filling above the axis allowed for surface as well as bulk transport during drum rotation.
- Liquid filled up to the axis hindered surface transport.

[9] anionically polymerized by Thomas Wagner

- The external barrier added to the bath hindered surface as well as bulk transport, but could not completely suppress it. Small gaps ($\approx 1\,\mathrm{mm}$) between barrier and drum/bath walls allowed for a minimal surfactant transport.

### Contact angle measurement

Contact angles were measured in side view using a Photron high-speed camera with a Navitar tubus ($12\times$ magnification) at a frame rate of 500 Hz with back lighting. The bath was closed with parafilm (Bemis) and to ensure a saturated atmosphere inside the bath, the drum was allowed to rotate for at least 20 minutes before measurements started.

The CTAB concentration was subsequently increased by adding pure surfactant to the liquid and the solution was stirred for at least 20 minutes at a high rotation velocity. After a measurement series, the bath was cleaned until pure water measurements showed the same results as before the first CTAB addition. Milli-Q water purified by a Sartorius Arium 611 was used for all experiments. CTAB was purchased from Sigma-Aldrich and used without further purifications.

# 5 Influence of surface properties on dynamic wetting/dewetting

Not only liquid properties, but also substrate properties, including roughness, wettability, and homogeneity, may influence the wetting/dewetting of aqueous surfactant solutions. Many studies dealt with the influence of surface roughness on contact angles and spontaneous spreading [94–97], but neglected the influence on forced wetting/dewetting. The wetting/dewetting of a surface can be altered by changing surface roughness, chemical homogeneity, etc. The link between surface roughness and the measured contact angle is given by the Wenzel equation

$$\cos\theta_{ap} = r\cos\theta \tag{5.1}$$

with the average roughness ratio $r$, given as the factor with which the solid-liquid interface is increased due to roughness [98–100]. $\theta$ is the contact angle as defined for ideal smooth surfaces in the Young equation (Section 2.2). Roughness increases the surface characteristics, i. e. hydrophilic surfaces appear more hydrophilic, while hydrophobic surfaces appear more hydrophobic for rough surfaces than for smooth surfaces [101]. This effect is used for developing e. g. superhydrophobic surfaces by introducing an additional roughness to hydrophobic materials [100, 102, 103].

## 5.1 Variation of the drum's surface properties

For studying the influence of drum roughness, wettability, and homogeneity on the wetting/dewetting of aqueous surfactant solutions, three different drum coatings were tested: A polystyrene coating, a sealing treatment, and a hydrophobized glass slide. Sealing treatment refers to a polishing step with a commercial, polymer-based sealant containing nanoparticles, usually used for protecting metal parts on cars. In case of the polystyrene coating and the sealing treatment, the barrel-shaped steel drum was used, while the planar drum was used in case of the hydrophobized glass slide. The different coatings provide different average roughnesses ranging from $\approx 150\,\mathrm{nm}$ for the sealant-treated drum to $\approx 1\,\mathrm{nm}$ for the hydrophobized glass slide. The wettability of all these surfaces is comparable in their static contact angles of pure water ranging from $\approx 80°$ for the polystyrene-coated and sealant-treated drum

surface to ≈65° for the hydrophobized glass surface. The properties of the coatings as well as the surfactant solutions tested are summarized in Table 5.1.

| coating | roughness | $\theta_s$ | CTAB | SDS | $C_4E_1$ | $C_8E_3$ | $C_{12}E_5$ |
|---|---|---|---|---|---|---|---|
| polystyrene | ≈140 nm | ≈80° | • | • | • | • | • |
| sealant | ≈150 nm | ≈80° | • | | | | |
| hydrophobized glass | ≈1 nm | ≈65° | • | • | | • | |

**Table 5.1:** Summary of the properties of the drum coatings and the tested surfactant solutions.

### 5.1.1 Polystyrene-coated steel drum - already known

The wetting/dewetting of various aqueous surfactant solutions on the polystyrene-coated steel surface has been described in detail in Chapters 3 and 4: The contact angles decreased with increasing surfactant concentration at a constant rotation velocity, exemplarily shown for aqueous CTAB solutions in Figure 5.1 (redrawn from Chapter 3). All tested surfactants showed an identical behavior of decreasing contact angles with increasing surfactant concentration.

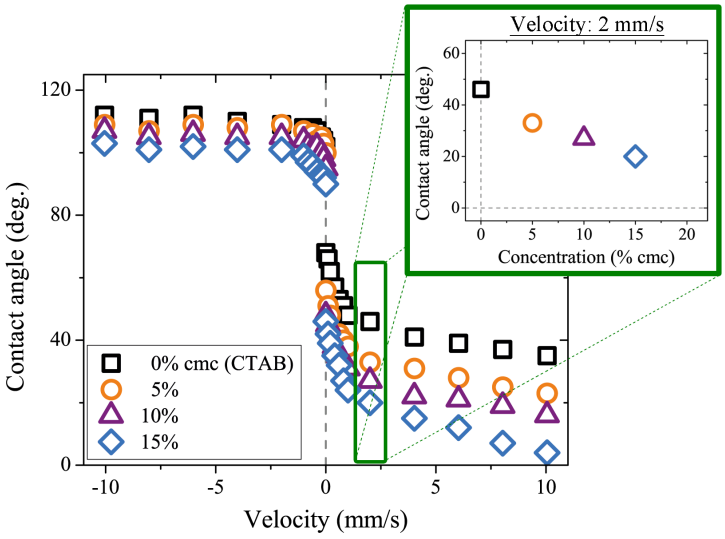


**Figure 5.1:** $\theta - U-$plot of aqueous CTAB solutions wetting/dewetting a polystyrene-coated drum with an average roughness of ≈140 nm. A $\theta - c-$plot at 2 mm/s is shown in the blow-up.

Applying a polystyrene coating to the steel drum resulted in an average roughness about 140 nm, as determined from SFM topography images (Figure 3.2 A). The

polystyrene coating seemed to be homogeneously applied onto the steel surface, as can be seen from the homogeneous phase image (Figure 3.2 B). The static contact angle of water on the polystyrene surface was about 80°.

### 5.1.2 Sealant-treated steel drum - comparable roughness

After applying the sealing to the steel drum, the drum had a static contact angle of $\approx 80°$ and an average roughness about 150 nm (as measured from the SFM topography image (Figure 5.2 A)). These values are comparable to those reported for the polystyrene-coated surface. But by comparing the phase information given by the phase images (Figures 3.2 B and 5.2 B), one difference gets obvious: The phase contrast increased significantly from 10° for the polystyrene-coated drum to 100° for the sealant-treated drum. This hints to an inhomogeneous coating of the sealant-treated drum. The sealant seemed to partially dewet the drum surface, i. e. parts of the drum were sealant-coated while other parts were pure steel. This could lead to pinning sites and therefore to a changed wetting/dewetting in comparison to the polystyrene-coated drum, which showed a more homogeneous coating (Figure 3.2).

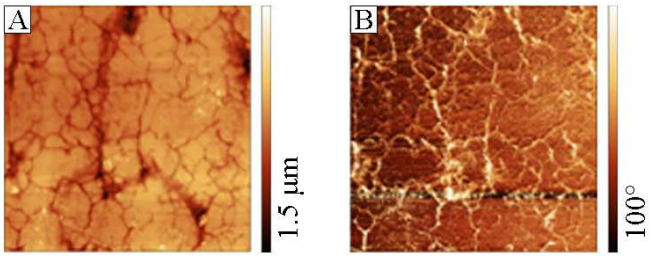


**Figure 5.2:** SFM images of the sealant-treated barrel-shaped steel drum. (A) Topography image: roughness about 150 nm; (B) phase image: inhomogeneous coating.

For pure water the general trend of the advancing and receding contact angles on a sealant-treated drum surface is similar to the one obtained for a polystyrene-coated drum: The advancing contact angles increased with increasing velocity while the receding contact angles decreased (Figure 5.3, black squares). But there is one difference obvious between these to drum coatings: In case of the advancing contact angles a steady increase could be observed, no levelling off at a specific contact angle value like it was observed for the polystyrene-coated drum (Figure 5.1). Further, the advancing as well as the receding contact angles seem to follow a linear trend, not the two-slope-behavior observed for the polystyrene-coated drum with a strong increase/decrease at low velocities ($U < |2|$ mm/s) followed by a less pronounced increase/decrease at higher velocities as described in Section 3.1.

Further, when CTAB was added to the water, the contact angles decreased slightly with apart from that a similar wetting/dewetting behavior as described for pure water: The advancing contact angles did not level off and the $\theta - U-$plots showed an almost linear trend (Figure 5.3). The advancing contact angles were similar to those of pure water, but decreased about 5°, while the receding contact angles showed a larger decrease when CTAB was added - about 15° to 20°. In contrast to the homogeneously coated steel surface, the receding contact angles measured for the inhomogeneously coated drum showed no significant contact angle decrease with increasing CTAB concentration, i. e. the receding contact angles do not decrease significantly when CTAB is present in the solution (Figure 5.3 compared to Figure 5.1). Figure 5.3 B shows the steady decrease of the receding contact angles with increasing CTAB concentration.

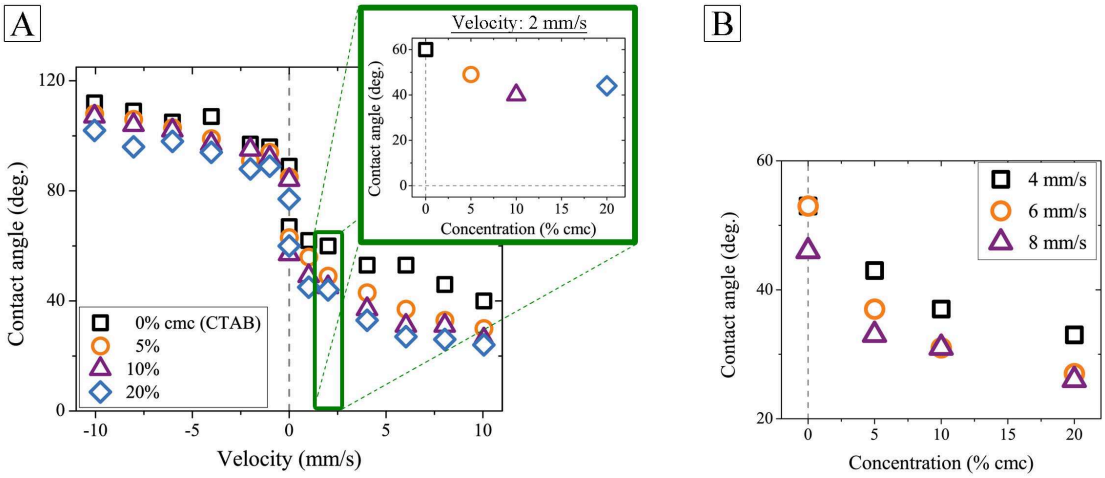


**Figure 5.3:** (A) $\theta - U-$plot of CTAB solutions showing the surfactant influence on the wetting/dewetting of a sealant-treated steel drum with a roughness about 150 nm. The blow-up shows a $\theta - c-$plot at 2 mm/s. (B) $\theta - c-$plot for constant velocities of 4, 6, and 8 mm/s.

The velocity-dependent contact angles measured on the sealant-treated drum surface showed a stronger scattering than the ones measured on the polystyrene-coated surface. This was also reflected by a greater instability of the three-phase contact line in case of the sealant-treated drum surface. The contact line was pinned more often due to the inhomogeneous surface coating, leading to a stronger variation of the measured contact angles and therefore to an uncertainty about 8° in case of the sealant-treated surface compared to an uncertainty about 5° in case of the polystyrene-coated surface.

The observation of only one slope being present and no levelling off of the advancing contact angle for the sealant-treated drum surface rises the question about

the reason causing these differences. The surface homogeneity - as the major difference between these two coatings - and its influence on the wetting/dewetting will be discussed in Section 5.2.2.

### 5.1.3 Hydrophobized glass - smooth surface

The roughness of the glass cover slide glued around the steel drum was about 1 nm after hydrophobizing the glass with HMDS, as measured from the SFM topography image (Figure 5.4 A). The phase image revealed a homogeneously hydrophobized glass surface (Figure 5.4 B, low phase contrast) with a static contact angle of pure water about 65°.

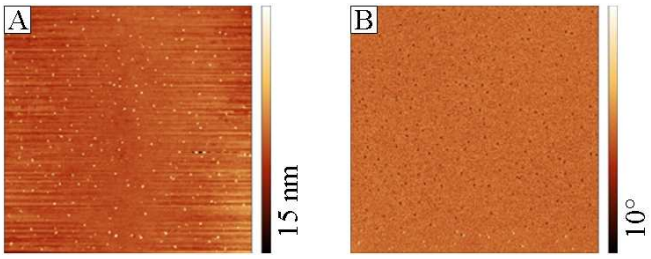


**Figure 5.4:** SFM images of hydrophobized glass slides glued around the planar drum. (A) Topography image: roughness about 1 nm; (B) phase image: homogeneous coating.

The wetting/dewetting of the smooth surface is similar to that of the rough polystyrene-coated surface - the advancing as well as the receding contact angles showed two different slopes and the advancing contact angle levelled off (Figure 5.5).

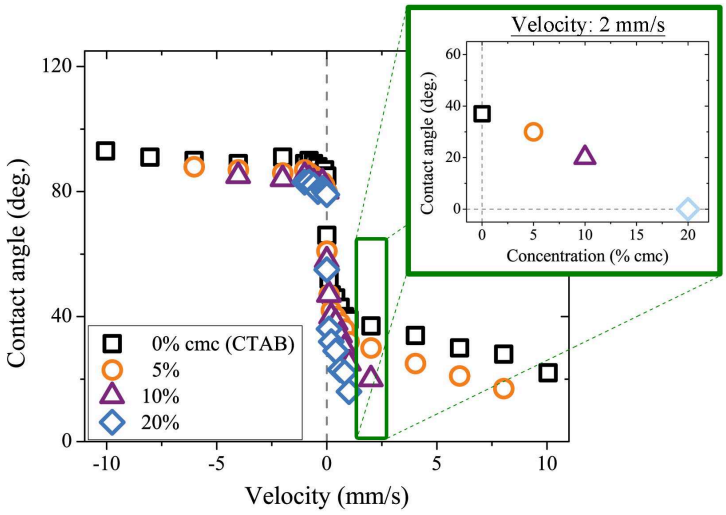


**Figure 5.5:** $\theta - U-$plot of aqueous CTAB solutions wetting/dewetting a hydrophobized glass surface with an average roughness about 1 nm. A $\theta - c-$plot with an extrapolated contact angle value for 20 % cmc is shown in the blow-up.

Further, by adding surfactant, e. g. CTAB, to the liquid, the dynamic contact angles decreased. With increasing the CTAB concentration, the receding contact angles decreased steadily, while the advancing contact angles showed a less pronounced decrease. The uncertainty of the contact angle determination was about 3°, due to the more "static-like" three-phase contact line compared to the rougher surfaces resulting in less variations in the measured contact angles.

Similar to the rough polystyrene-coated surface, the wetting/dewetting on the smooth hydrophobized glass surface was independent of the surfactant type: The addition of SDS and $C_8E_3$ showed the same effect as CTAB - the contact angles decreased with increasing surfactant concentration (Figure 5.6 A and B). The observations described in Chapters 3 and 4 for a rough surface - the stronger the added surfactant, the stronger the contact angle decrease - holds true for the smooth surface: The contact angles in case of the stronger surfactant CTAB were lower than the contact angles for SDS and $C_8E_3$ - two surfactants of similar cmc - which showed similar contact angle values (Figure 5.6 C).

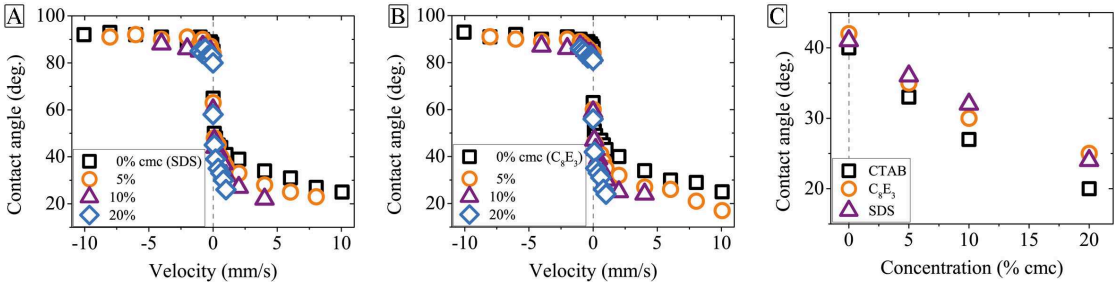


**Figure 5.6:** Influence of (A) SDS and (B) $C_8E_3$ on the wetting/dewetting of aqueous solutions on a hydrophobized glass surface with an average roughness about 1 nm. (C) $\theta - c$–plot for the different surfactants CTAB, $C_8E_3$, and SDS - in the order of increasing cmc - at a constant velocity of 2 mm/s.

## 5.2 Different properties - same wetting behavior?

In case of differing surface properties of the substrates, a different wetting/dewetting behavior could be expected. A rougher surface, independent if caused by topology or inhomogeneity, could allow for more pinning sites. Pinning sites hinder the three-phase contact line in its motion due to a higher depinning energy leading to a further pulling up of the three-phase contact line until the energy barrier of depinning is overcome and the three-phase contact line flows down to its initial position. At the same time, increased roughness can enhance the hydrophobic character of the samples, according to the Wenzel equation [98–100] leading to higher contact angles.

Not only a rough surface, but also an inhomogeneous surface with its different chemical properties leads to an increased number of pinning sites.

The investigated surfaces - polystyrene-coated steel, sealant-treated steel and hydrophobized glass - showed different properties regarding roughness and chemical homogeneity, as summarized in Table 5.2. The different surface properties allow for a different number of pinning sites. The polystyrene-coated surface was rough but chemically homogeneous, while the sealant-treated surface offered a comparable roughness while being chemically inhomogeneous due to the partially dewetted steel surface. The hydrophobized glass surface was smooth and chemically homogeneous.

| surface | polystyrene-coated steel | sealant-treated steel | hydrophobized glass |
|---|---|---|---|
| topological roughness | $\approx 140\,\mathrm{nm}$ | $\approx 150\,\mathrm{nm}$ | $\approx 1\,\mathrm{nm}$ |
| chemical homogeneity | • | - (partially dewetted) | • |

**Table 5.2:** Summary of the surface properties of the different drum coatings regarding topological roughness and chemical homogeneity.

### 5.2.1 Influence of roughness on the wetting behavior

Topological roughness leads to an increased number of pinning sites [4, 100, 104], i. e. a chemical homogeneous, but rough surface offers additional pinning sites compared to a chemical homogeneous and smooth surface. The increased number of pinning sites should lead to a simplified upwards-pulling of the liquid on the receding side resulting in lower receding contact angles at a constant velocity and surfactant concentration. In order to verify this expectation, the wetting/dewetting of CTAB solutions at different concentrations and different surface roughnesses, but chemical homogeneous surfaces was compared: The polystyrene-coated steel surface with its roughness about 140 nm was compared to the hydrophobized glass surface with a roughness about 1 nm.

The wetting/dewetting of surfactant solutions wetting/dewetting the polystyrene-coated steel surface was already discussed in detail in Chapters 3 and 4: In the presence of surfactants, local as well as non-local surface tension gradients caused the dynamic contact angles to decrease. As shown earlier (Section 5.1.3), the wetting behavior of surfactant solutions wetting the smooth glass surface was similar to that of the wetted polystyrene surface, i. e. also my explanation of local surface tension

gradients (Marangoni tension) causing the contact angles to decrease fitted to the smooth surface experiments.

A comparison of the two different surfaces wetted by aqueous CTAB solutions showed that the velocity-dependent contact angle behavior was similar - in the overall shape and the strength of the contact angle decrease. Both surfaces showed an identical trend of velocity-dependent contact angle curves (Figure 5.7), but the curves were shifted due to the difference in the static contact angles about 15°. In case of the smooth surface (orange circles), the advancing contact angles were shifted to lower values, while the receding contact angles were almost identical.

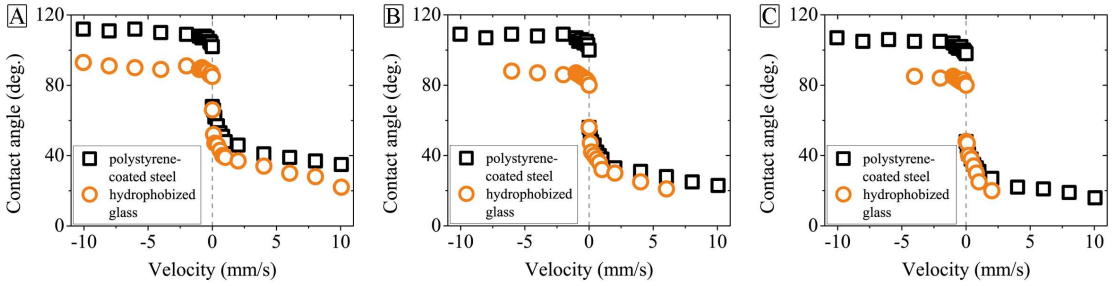


**Figure 5.7:** Comparison of $\theta - U-$plots of CTAB solutions wetting a polystyrene-coated steel or a hydrophobized glass surface at a CTAB concentration of (A) 0 %, (B) 5 %, and (C) 10 % cmc.

Beside these velocity-dependent similarities of the wetting/dewetting on smooth and rough surfaces, the rate with which the contact angles decreased with increasing CTAB concentration was independent of the surface roughness. The slopes given by the $\theta - c-$plots of rough and smooth surfaces at 1 respectively 2 mm/s were almost identical (Figure 5.8).

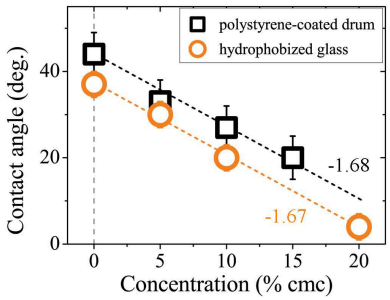


**Figure 5.8:** Comparison of the $\theta - c-$plots for the polystyrene-coated steel and the hydrophobized glass surface at a rotation velocity of 2 mm/s.

This almost identical wetting/dewetting shown for rough and smooth surfaces that was independent of velocity and CTAB concentration, led to the assumption of surface roughness having no significant influence on the wetting/dewetting.

However, the critical velocity varied depending on the surface roughness: The smooth surface showed lower critical velocities than the rough surface (Figure 5.7) what is in contrast to the earlier mentioned influence of an increased number of pinning sites. In case of an increased number of pinning sites (as given for rougher surfaces), the upwards drawing of the liquid should be facilitated resulting in a lower critical velocity, but a different behavior was observed. Possible reasons explaining this unexpected behavior are discussed below.

### Normalization of the $\theta - U-$plots

Due to different surface coatings and therefore different static contact angles, a direct comparison of the velocity-dependent contact angles was hardly possible. To allow for a direct comparison, a normalization of the contact angles was used, i. e. the actual contact angles were reduced by the according zero-velocity contact angle $(\theta - \theta_0)$. $\theta_0$ was measured depending on the wetting/dewetting history: 30 seconds after the drum was stopped, $\theta_0$ was measured either for the receding or the advancing contact angles. The normalization of the $\theta - U-$curves led to similar curves for both chemical homogeneously coated surfaces (Figure 5.9). The advancing contact angles were similar for both roughnesses, while the receding contact angles slightly differed. The receding contact angles in case of the smooth hydrophobized glass surface were lower than the ones of the rougher polystyrene-coated steel surface. This behavior was observed for all CTAB concentrations.

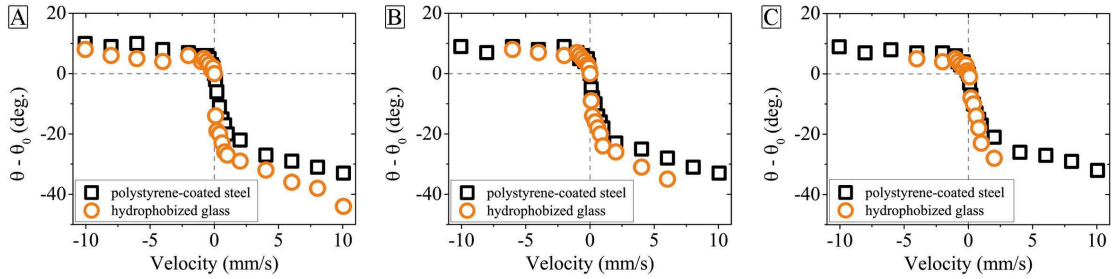


**Figure 5.9:** Plots of $(\theta$ - $\theta_0)$ versus velocity $U$ allow for comparing the wetting/dewetting of the polystyrene-coated steel surface with the hydrophobized glass surface at different CTAB concentrations: (A) 0 %, (B) 5 %, and (C) 10 % cmc.

The increased number of pinning sites in case of the rough surface would suggest a faster pulling up of the three-phase contact line leading to lower critical velocities and lower receding contact angles compared to the smooth surface. However, not only the critical velocity (Figure 5.7), but also the receding contact angles (Figure 5.9, orange circles) were lower in case of the smooth surface compared to the rough surface - in contrast to the suggestion of an increased number of pinning sites.

**Less pinning sites - lower contact angles and critical velocities?**

The identical decreasing rate of the receding contact angles with increasing CTAB concentration (Figure 5.8) as well as the similar $\theta - U-$plots for the different surfaces (Figure 5.7) suggested roughness having no significant influence on the wetting/dewetting on the examined polystyrene-coated steel and hydrophobized glass surfaces. When the number of pinning sites present at the surface would influence the wetting/dewetting, lower receding contact angles and lower critical velocities would be expected for the surface with a larger amount of pinning sites, i. e. for the rougher surface. But the differences shown in the normalized $\theta - U-$plots (Figure 5.9), revealed an opposite behavior - the smoother surface, i. e. less pinning sites, showed lower receding contact angles as well as lower critical velocities.

Thus, what is the reason for the smoother surface showing lower critical velocities and lower receding contact angles than the rough surface? The investigated surfaces showed one major difference beside the topological roughness - one was made of polystyrene, the other one was slightly silanated. Due to these different surfaces, different interaction strengths between the CTAB solution and the hydrophobized glass respectively polystyrene-coated steel surface could be possible, resulting in differing critical velocities. The stronger the interaction between the liquid and the drum surface, the easier the liquid would be drawn upwards resulting in lower receding contact angles and critical velocities. Here, the hydrophobized glass surface showed a stronger solid-liquid interaction and therefore lower contact angles as well as lower critical velocities.

This explanation should be independent of the surface roughness, but depend on the interaction between drum and CTAB solution. Different surfaces, e. g. structured, but chemically homogeneous polymer surfaces, would be necessary to test the influence of interaction strength as well as to determine the influence of roughness on chemical homogeneous surfaces.

### 5.2.2 Influence of homogeneity on the wetting behavior

Two surfaces of similar roughness should show a comparable number of pinning sites at similar liquid-solid interactions. When a chemical inhomogeneity is added to one of the surfaces, the number of pinning sites should be changed because of altered liquid-solid interactions. To study the influence of surface homogeneity, two surfaces of similar surface roughness, about 140 to 150 nm, but differing surface homogeneity were examined. The polystyrene-coated as well as the sealant-treated steel surface showed static contact angles about 80°. In case of the inhomogeneous sealant-treated surface, this is an average value due to drum parts covered with the sealant ($\theta_s > 80°$), while other parts were pure steel ($\theta_s \approx 40°$).

CTAB solutions wetting the inhomogeneous sealant-treated steel surface showed in contrast to the homogeneous polystyrene-coated steel surface only one slope in the $\theta - U -$plots (Figure 5.10). This slope was more comparable to the high velocity part ($U > |2|$ mm/s) of the homogeneous surface than to the low velocity part. Further, in case of the inhomogeneously coated surface the advancing contact angles did not level off at a certain value, as they did in case of the homogeneous surface coatings.

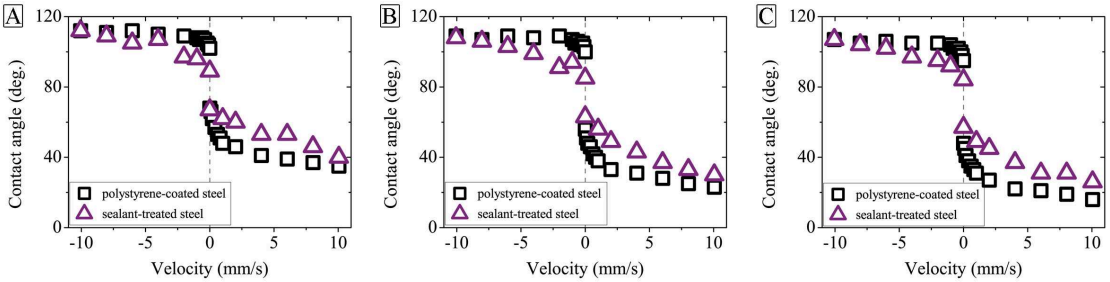


**Figure 5.10:** Comparison of the $\theta - U -$plots of a CTAB solution wetting/dewetting a homogeneously coated polystyrene surface or an inhomogeneous sealant-treated surface at (A) 0 %, (B) 5 %, and (C) 10 % cmc CTAB.

### Critical velocity

The critical velocities of the aqueous solutions dewetting the polystyrene-coated and the sealant-treated surface differed. The homogeneous polystyrene-coated surface showed higher critical velocities - about 60 mm/s compared to 30 mm/s for the sealant-treated surface (at a CTAB concentration of 5 % cmc). In addition to the argument of different liquid-solid interactions resulting in different critical velocities, the inhomogeneous surface itself could help to explain the lower critical velocity of the inhomogeneous sealant-treated steel surface compared to the homogeneous polystyrene-coated steel surface. The inhomogeneous surface consisted of regions of sealant with high contact angles ($> 80°$) and regions of steel with low contact angles ($\approx 40°$) leading to an easier wetting of the steel regions. This could support the drawing up of the liquid and result in lower critical velocities.

### Decreasing rate of the receding contact angles

The slope with which the receding contact angles decreased with increasing CTAB concentration differed in case of the homogeneous polystyrene-coated surface and the inhomogeneous sealant-treated surface (Figure 5.11). The inhomogeneous sealant-treated surface showed a lower slope than the homogeneous polystyrene-coated surface. The untreated steel parts of the sealant-treated drum seemed to influence

the dewetting of the drum, although the decrease of the receding contact angles was slowed down, not accelerated as one would expect for the more hydrophilic steel parts. One possible explanation for the slower decrease in case of the inhomogeneous surface coating could be the adsorption of surfactant molecules at the untreated hydrophilic steel parts leading to a hydrophobization of those and therefore to a slower decrease of the receding contact angles.

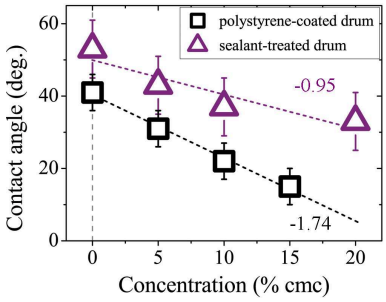


**Figure 5.11:** Comparison of the $\theta - c-$plots for the polystyrene-coated and the sealant-treated drum at 4 mm/s.

### Normalization of the $\theta - U-$plots

In order to allow for comparing the two different surfaces, again a normalization of the contact angles was used ($\theta - \theta_0$ versus $U$, Figure 5.12). This led not only to a visualization of differences between the two different surfaces, but also between the liquids either being pure water (A) or containing CTAB (B and C).

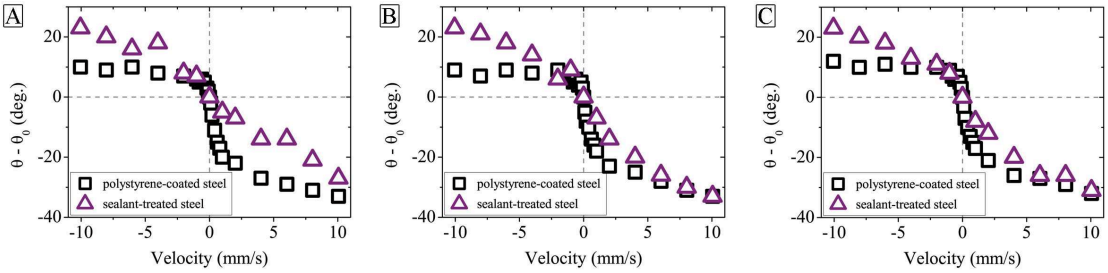


**Figure 5.12:** $(\theta$ - $\theta_0)-U-$plots allow for comparing the wetting/dewetting of the homogeneous polystyrene-coated with the inhomogeneous sealant-treated steel surface for CTAB solutions of (A) 0 %, (B) 5 %, and (C) 10 % cmc.

In case of pure water, the inhomogeneous sealant-treated surface showed an almost linear contact angle decrease with velocity, while for homogeneous coatings, here a polystyrene coating, different slopes were observed (Figure 5.12 A). But when CTAB was added to the pure water (Figure 5.12 B and C), this linear decrease was brought more into line with the contact angle behavior in case of a homogeneous surface,

i. e. two different slopes were observable although there was no significant difference. Further, the slope of the inhomogeneous coating for $U > |2|$ mm/s got more and more similar to the slope of the homogeneous polystyrene coating with increasing CTAB concentration. But still, the slopes of the receding contact angles for $U < |2|$ mm/s showed a significant difference. Independent of the examined liquids, the advancing contact angles in case of the inhomogeneous coating did not level off, but steadily increased with increasing velocity.

The fact, that the contact angles of the CTAB solution wetting/dewetting an inhomogeneous surface came closer to the contact angle behavior in case of a homogeneous surface, led to the idea that surfactant molecules adsorbed at the surface and made it therewith more homogeneous. This idea was supported by the slight change of the contact angles to a two slope contact angle behavior in case of the 5 % and 10 % cmc CTAB solution (Figure 5.12 C).

## 5.3 Different slopes offering surface information?

As described earlier, the homogeneous coatings, independent of their topological roughness, offered two different slopes in the $\theta - U-$plots for the advancing as well as the receding region (Figure 5.7, Section 5.2.1). The inhomogeneous sealant-treated surface showed in contrast to those surfaces, only one slope for low surfactant concentrations that was closer to the high velocity slope in case of the homogeneous coatings ($U > |2|$ mm/s, Figure 5.10 A). Due to the missing first slope (for $U < |2|$ mm/s) in case of the inhomogeneous sealant-treated surface compared to the homogeneous polystyrene-coated surface of similar roughness and static contact angle, the idea of an influence of the chemical homogeneity on the wetting/dewetting came to ones mind. This idea was supported by the fact, that the "one-slope-behavior" of the inhomogeneous coating changed to a slight "two-slope-behavior" with increasing CTAB concentration (Figure 5.10 B and C). A more homogeneous coating could be obtained due to CTAB molecules adsorbing at the inhomogeneous surface.

The idea, the second slope could depend on surface homogeneity ($U < |2|$ mm/s) was supported by Slavchov et al., who proposed a step mechanism for the three-phase contact line motion [105]. There, surface energy fluctuations, given by surface roughness or surface inhomogeneity [106, 107], served as an energy barrier for the spreading process. They were able to model a "two-slope-behavior" by applying their theory including roughness and inhomogeneity aspects.

To further study the influence of chemical homogeneity and topological roughness, identical surfaces should be compared, which are chemically altered - not two completely different surfaces, since the differences could also result from or be enhanced by different solid-liquid interactions.

## 5.4 Conclusion

Additionally to the liquid and setup properties influencing the wetting/dewetting of surfactant solutions as discussed in Chapters 3 and 4, the surface properties of the drum had a significant effect on the wetting/dewetting of surfactant solutions: Not only the hydrophobicity of the surface, but especially the surface inhomogeneity influenced the wetting/dewetting by just altering pinning and dewetting properties of the different surface materials. In case of chemically homogeneous surfaces (polystyrene-coated steel or hydrophobized glass), two different slopes in the $\theta - U-$plots for either the advancing and the receding side were observable while for chemically inhomogeneous surfaces (sealant-treated steel) only one slope could be observed. The absence of the second slope, pointed towards the chemically homogeneity influencing the low velocity regime (up to $|2|$ mm/s).

I showed that the wetting/dewetting of an inhomogeneous surface came closer to a homogeneous one when surfactant was added to the liquid. The surfactant molecules can adsorb at the inhomogeneous surface and thus make it more homogeneous by providing a chemically homogeneous surface. So far, surface roughness did not seem to have any significant influence on the wetting/dewetting. But to verify these first observations, further studies of chemically more identical surfaces are necessary, e. g. a CTAB solution wetting/dewetting a smooth polystyrene surface as well as a chemically modified/roughened polystyrene surface.

## 5.5 Outlook

The rotating drum setup is a fairly good technique to observe the wetting/dewetting behavior of rotating drums, but is best suitable for slightly convex drums. Since the engraved cylinders used during gravure printing are planar, a further development of the technique is necessary. Eibach et al. used the basic idea of the existing rotating drum technique, but developed a different way of analyzing the contact angles based on a reflected laser beam [108, 109]. This method allows for determining receding contact angles on planar surfaces at a high roughness-sensitivity due to the reflected beam (Figure 5.13). In case of the analyses via the reflected laser beam, the error bar is a measure of the surface roughness - the rougher the surface, the larger the contact angle variation and therefore the larger the error bar.

As shown above, the optical analysis method used in this work as well as the reflected laser beam method described by Eibach et al. allow for determining the contact angles. But with the help of the reflected laser beam an in situ characterization of the wetting/dewetting behavior of a working gravur printing drum could be possible due to the scalability of this method. This further combination should

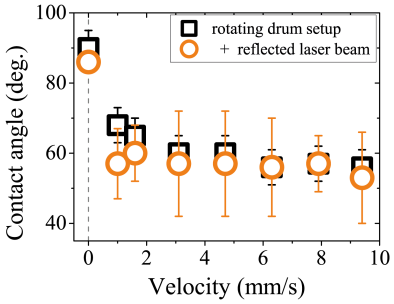


**Figure 5.13:** Comparison of the $\theta-U-$plot of the conventional rotating drum setup (black squares) and the analyses via a reflected laser beam (orange circles). The error bars are a measure of surface roughness in case of the reflected laser beam. The results are shown for pure water on the planar polystyrene-coated steel drum.

allow for getting more information about the wetting/dewetting behavior during a real printing process.

Since the determination of contact angles and therefore the wetting/dewetting of liquids on a "simple" surface is possible, the study of a real printing plate (called Ballard skin) with its structured surface is one of the next steps. The structures of the Ballard skin are in the range up to $150 \times 150\,\mu m^2$ with a depth to $45\,\mu m$, depending on the printing results. Large areas require larger cavities than small structures. In paper printing, small structures allow for light colors while large cavity structures are used for strong color results.

A reflection image[10] of a Ballard skin as used in paper printing is shown in Figure 5.14 with three different structures shown - a smooth surface as well as small and large cavities. The roughness of the smooth surface is about 110 nm, while the cavity structure varies between $70 \times 40\,\mu m^2$ for the small cavities and $130 \times 115\,\mu m^2$ for the large cavities. The depth of the cavities can range up to $45\,\mu m$.

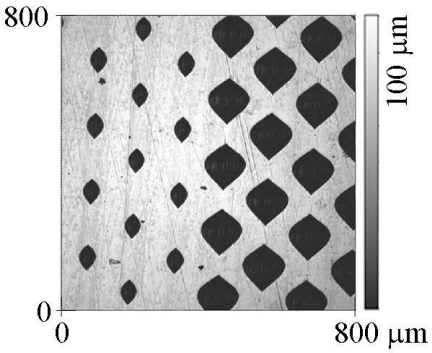


**Figure 5.14:** Reflection image of a Ballard skin used for paper printing measured with a NanoFocus microscope showing three different structures - smooth surface (roughness about 100 nm), small cavities ($70 \times 40\,\mu m^2$, depth about $25\,\mu m$), and large cavities ($130 \times 115\,\mu m^2$, depth about $45\,\mu m$).

Due to the defined structures of the Ballard skin a direct comparison of a rough and smooth surface is possible. A first measurement[11] showed that increasing roughness led to a stronger pinning and therefore a higher pulling up of the three-phase contact line (Figure 5.15 A, purple arrow). With increasing the rotation velocity, the height

[10] measured by Emmanouil Anyfantakis with a NanoFocus microscope

[11] by Pabhavi "Gam" Navasiri

difference of the three-phase contact line between structured and unstructured surface also increased (Figure 5.15 B).

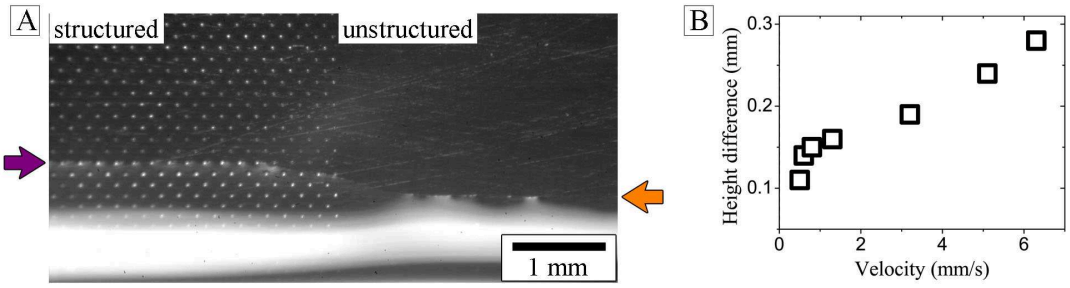


**Figure 5.15:** Pure water dewetting a Ballard skin shows different pull-up heights for a structured and an unstructured surface. (A) About 0.3 mm difference at a rotation velocity of 6.7 mm/s. (B) The difference increases with increasing rotation velocity.

Further, the printing thickness should depend on the amount of ink transferred from the ink tray to the Ballard skin and then to the substrate. But the amount of liquid filling the cavities is not known, i. e. it is not known if the cavities are filled completely or only partially, or if the filling amount varies. Additionally, the question about the completeness of the single wetting and dewetting steps is not known - is the complete amount of liquid in the tray completely transferred onto the substrate? These questions and the study of the wetting/dewetting of such a Ballard skin are some of the next steps.

## 5.6 Experimental details

### Sealant-treated steel - rough surface

A polymer-based sealant containing nanoparticles (NanoTec Felgenversiegelung, NIGRIN) was evenly applied to the barrel-shaped drum surface before polishing it with a soft linen (Section 2.3.3.5). This sealant slightly hydrophobized the steel surface (static contact angle $\approx 80°$).

### Hydrophobized glass - smooth surface

With the help of two components glue (Uhu), a thin glass side (Menzel, cover slide # 00) was glued around half of the planar drum. After cleaning the glass surface with ethanol (Sigma-Aldrich), THF (Sigma-Aldrich), and acetone (fisher scientific), it was hydrophobized with HMDS (Aldrich, Section 2.3.3.5) by rotating the drum

for 7 hours through a 2.5 wt % solution of HMDS in toluene. After a drying time of at least 3 hours at 50 °C, the coating resulted in a static contact angle of 65°.

### Contact angle measurement

The bath was half filled with Milli-Q water (purified by a Sartorius Arium 611) and then closed with parafilm (Bemis). To ensure a saturated atmosphere inside the bath from beginning, the drum was allowed for rotating at a high velocity (about 10 cm/s) for at least 20 minutes before measurements started. Contact angles were observed in side view using the Olympus high-speed camera with the Navitar tubus ($12\times$ magnification) at a frame rate of 500 Hz with back lighting.

The concentration of the used surfactant was steadily increased by adding pure surfactant to the liquid and stirring the solution for at least 20 minutes at a high rotation velocity. After completion of the measurement series, the bath was cleaned until pure water measurements resulted in the same wetting behavior as they did at the beginning of the measurement.

### Surfactant solutions

As surfactants the ionic surfactants SDS (Acros Organics) and CTAB (Sigma-Aldrich) as well as the nonionic surfactant $C_8E_3$ (Bachem) were used (details in Table 2.1). The measured concentrations were 0 %, 5 %, 10 %, and 20 % of the surfactants cmc.

### SFM measurements

The differently coated drums were analyzed with the NanoWizard$^{TM}$ atomic force microscope by JPK instruments in tapping mode, equipped with Si cantilevers (Olympus OMCL-AC240TS, a spring constant of 2 N/m, and a resonance frequency of 70 kHz). The scanning size was typically $50\times 50\,\mu m^2$.

### Ballard skin glued around the drum

The Ballard skin (5 cm × 15 cm) was glued around the planar drum with the help of tesa Powerstrips® at each side. The Powerstrips® allowed for easily gluing the Ballard skin around the drum as well as removing it again. After the Ballard skin was glued around the drum, it was cleaned with ethanol and acetone.

# 6 Surfactants influence the drop impact behavior of liquids[12]

Drop impact on liquid surfaces had been studied for more than 100 years. Reynolds [26, 27] and Thomson [28] were the first in the 1880s to report drop impacts on liquids, but the possibility of high-speed imaging ($\approx$1900) allowed for a more detailed study of impacting drops. Worthington [29] was one of the first who visualized splashing and jetting after drop impact in a deep pool of the same liquid in detail, using high-speed recording. Additionally to splashing and jetting drops, drops bouncing off a pool of the same liquid [31] or floating on the liquid surface [27, 30, 32–37] had been observed.

In contrast to a liquid pool as substrate, free-standing films can be strongly deformed during impact leading to softer impacts. Beside bouncing and coalescence, also known for impacts on liquid pools, passing was observed for impacts on free-standing films [38, 110, 111]. Also combinations of coalescence with one of the other phenomena were possible effects taking place, referred to as partial bouncing or partial passing. This means that only a part of the drop left the surface, either upwards or downwards. Regarding drops bouncing off the free-standing film, Courbin and Stone established the phrase "liquid trampoline" for those substrates [110]. Gilet and Bush also referred to liquid trampolines in their seminal work, where they investigated drop impacts on static and vibrating surfactant films [38]. They described all kinds of impacts, ranging from pure passing and bouncing to partial effects, and introduced the contact time $t_c$. The contact time described the time a drop was in contact with the substrate without any further process (either leaving or coalescing with the substrate) taking place. Gilet and Bush kept the drop to film radii ratio as well as the surfactant concentration in the film constant while varying the drop's falling height and therewith the impact velocity. By modeling the free-standing film as a linear spring, they found the contact time being proportional to the capillary time, but independent of the impact velocity of the drop.

For all impact phenomena, the presence of an air cushion separating drop and free-standing film/substrate is essential to prevent direct coalescence [31]. Already in the

[12]This chapter is based on "D. Fell, M. Sokuler, A. Lembach, T.F. Eibach, C. Liu, E. Bonaccurso, G.K. Auernhammer, H.-J. Butt *Drop impact on soap films and surfactant solutions*, Colloid & Polymer Science, submitted".

early works by Reynolds [40] and Lord Rayleigh [41, 42] the role of an air cushion was mentioned as a barrier between drop and liquid preventing coalescence, but they could not determine the detailed mechanism. In the cases where coalescence take place, the air has to flow out of the thinning gap between drop and surface (Section 6.4). This thinning proceeds until the gap reaches a thickness where van der Waals forces become relevant (10 - 100 nm) [31, 112, 113]. Hydrodynamic thinning of the air cushion does not only depend on impact velocity, drop size, and shape of the drop at impact [31], but also the hydrodynamic boundary conditions, influenced by e. g. the presence of surfactants on the surface, are important for the thinning process. It is assumed that even minute amounts of surfactants present in the water change the boundary condition effectively to no-slip [39, 114, 115]. This no-slip boundary condition is in good agreement with experimental results [31, 40]. However, it is known that a motion of the bulk liquid, either vertical or horizontal, with respect to the drop or electrolyte concentration in the solution can suppress coalescence for some time [31, 39, 43].

In this chapter, I test if surfactants influence the drop impact behavior by changing the boundary condition from slip to no-slip.

## 6.1 Coalescence, bouncing, and Co.

The behavior of the drops upon impact depend on the substrate, either liquid pool or free-standing film, as well as on the impact velocity. On a liquid pool, coalescence, bouncing, floating, or splashing can be observed. In splash impacts, drops break up into several smaller drops. Some of them coalesce with the substrate while others bounce. Splashing is only observed for impacts at high velocities. Drops impacting on free-standing films either show coalescence, bouncing, or passing.

Whether a drop coalesces, bounces, floats, or passes depends among other parameters on impact velocity $v_d$ and drop radius $r_d$. One widely used parameter to describe this dependency is the dimensionless Weber number $We$. It is, except of a factor of 1/6, the ratio of kinetic energy to surface energy of the drop ($\rho$: fluid density, $\gamma_d$: surface tension of the drop):

$$We = \frac{\rho v_d^2 r_d}{\gamma_d} \tag{6.1}$$

### Coalescence

The phenomena of a drop impacting on a substrate, touching it, and merging is called **coalescence**. Impacts on a liquid pool or free-standing film resulted in a

deformation of the substrate (Figure 6.1, yellow arrows). When drop and substrate came into direct contact, a surface wave was generated that expanded radially across the liquid surface starting from the impact point (red arrows). A better visualization of the film deformation and the merging between drop and substrate was gained by bending the film, so that impacts could be observed in side view (C). For these observations, black ink (Pelikan) was used to get a high contrast between liquid pool/free-standing film and impacting drop.Usual contact times for coalescing drops were between 0 and 15 ms.

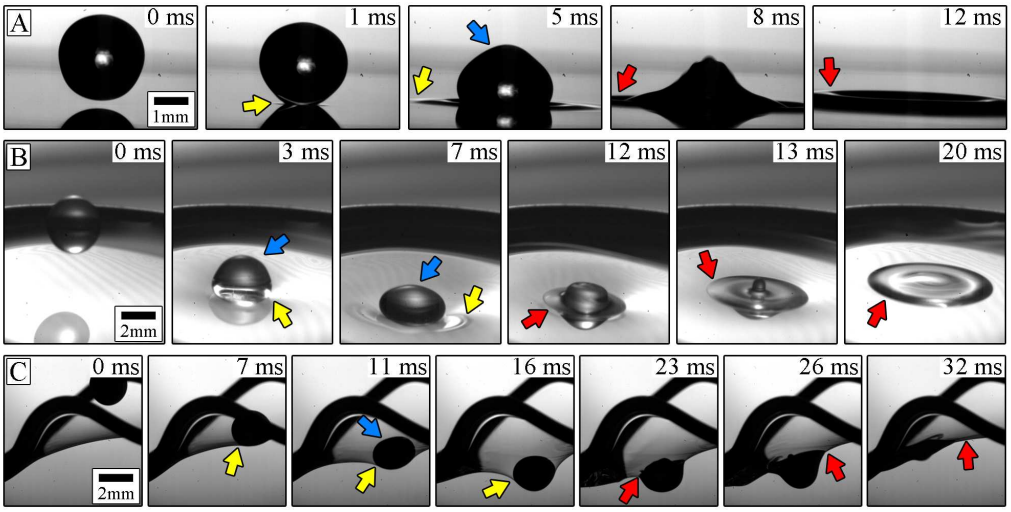


**Figure 6.1:** Coalescence describes the complete merging of an impacting drop with a substrate, leading to surface waves expanding radially from the point of impact (red arrows). Before direct contact between drop and substrate, the substrate (yellow arrows) as well as the drop (blue arrows) are deformed. (A) Coalescence on a liquid pool (water on water bath, $v_d = 0.2\,\mathrm{m/s}$). (B) Drop coalesces with a free-standing film (water on SDS film, $v_d = 0.4\,\mathrm{m/s}$) (C) Impact on a bended free-standing film to allow for observing the coalescence without a disturbing frame (ink on SDS film, $v_d = 0.3\,\mathrm{m/s}$).

## Bouncing

Completely from the substrate reflected drops are referred to as **bouncing** drops. When the drop came close to the substrate, the surface of the liquid pool or the free-standing film was deformed (Figure 6.2, yellow arrows) as well as the drop itself (blue arrows). During impact on a liquid pool, the drop was highly deformed and almost released a small droplet (A, 3 and 5 ms), while drops impacting on a free-standing film were only compressed (B, C). The difference in drop deformation/compression resulted from the different substrates - the free-standing film was flexible and there-

fore deformed readily while the surface of the liquid pool was more rigid. Due to this deformation of the film, the drop's downward motion was slowed down steadily in contrast to a sudden braking in case of the rigid liquid pool. When the substrate relaxed back to its initial state, the drop impacting on the free-standing film was compressed again, due to the upwards motion of the film (B - 15 ms, C - 29 ms).

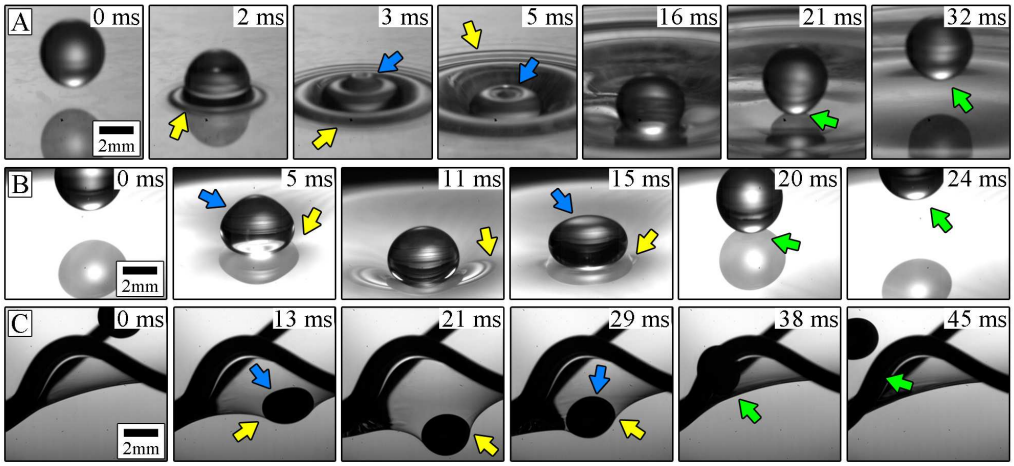


**Figure 6.2:** Bouncing describes the complete reflection of an impacting drop from a substrate without any material transfer. During impact, substrate (yellow arrows) and drop (blue arrows) are deformed. When the substrate relaxes again, it catapults the drop upwards. The drop leaves the substrate without ever being in contact with the substrate (green arrows). (A) Bouncing off a liquid pool (water on SDS solution, $v_d = 0.4\,\mathrm{m/s}$). (B) Drop bounces off a free-standing film (water on SDS film, $v_d = 0.3\,\mathrm{m/s}$). (C) Ink impacting on a bended film allows for observing the "contact region", where material transfer between drop and film should occur (ink on SDS film, $v_d = 0.2\,\mathrm{m/s}$).

In case of an impact on the liquid pool, the drop did not deform again while the liquid surface relaxed (A - 16 ms). Due to the relaxation of the liquid surface respectively the film, the drop was accelerated upwards and left the substrate (green arrows). During impact, drop and substrate were separated at any time by an air cushion preventing material transfer. Contact times for bouncing drops varied between 10 and 30 ms.

## Floating

**Floating** refers to drops sitting on the liquid surface for more than 15 ms before coalescing. It was only observed for impacts on a liquid pool. During impact, the drop as well as the liquid surface were deformed (Figure 6.3, blue and yellow arrows). When the liquid surface reached its initial state again, the spherical drop "sat" on top

of the liquid surface until the air separating the drop and liquid interface vanished and the drop merged with the subjacent liquid (190 ms, red arrow). This separating air layer is known as air cushion. At the beginning of the merging, a small "foot" formed at the bottom side of the drop (Figure 6.3, 190 ms).

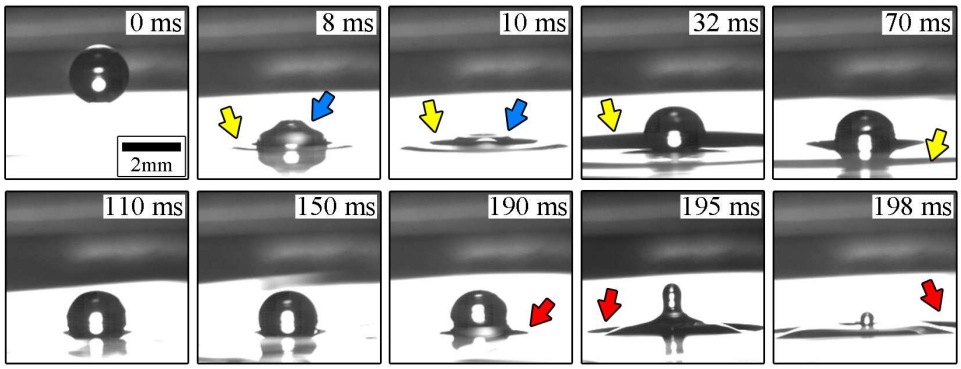


**Figure 6.3:** During floating impacts, drop and liquid surface were deformed (blue respectively yellow arrows) but relaxed to their initial state until the drop "sat" almost motionless on the liquid surface. When the separating layer (air cushion) between drop and liquid surface vanished, the drop merged and a surface wave was generated (red arrows). After coalescence often a smaller secondary drop was emitted from the surface (198 ms). The sequence shows a water drop impacting on a water pool at $v_d = 0.3\,\mathrm{m/s}$.

After the drop coalesced, often a smaller secondary drop was emitted from the surface, sitting on the liquid surface (198 ms) for some time, before another even smaller drop was emitted. The air cushion between drop and liquid surface was more stable for a moving liquid surface than for a calm one leading to longer floating times until coalescence took place [36]. Floating showed by far the longest contact times - starting with 15 ms and ranging up to 200 ms, as far as observed during experiments.

## Passing

Drops impacting on a free-standing film can show an additional phenomenon - **passing**. First the drop was compressed during impact (Figure 6.4, blue arrows) while it deformed the free-standing film (yellow arrows). When the energy of the impacting drop was high enough to deform the film so strongly that the drop was completely below the equilibrium state of the film, the drop elongated while a neck was formed between the drop and the equilibrium state of the film (orange arrows). The neck then narrowed and closed above the drop so that the drop pinched off the film (green arrows). Material was only transferred from the film to the drop, not vice

versa (Figure 6.4 B). While the drop passed the film, a surfactant layer wrapped around it (14.6 ms). When the neck pinched off (14.8 ms), not only film and drop were separated but also a surface wave propagated along the drop surface (14.8 - 15.4 ms, red arrows). This surface wave could result either from the pinch off or from a merging of the wrapping surfactant layer with the drop. Contact times for passing were comparable to those for coalescence, ranging from 5 to 15 ms.

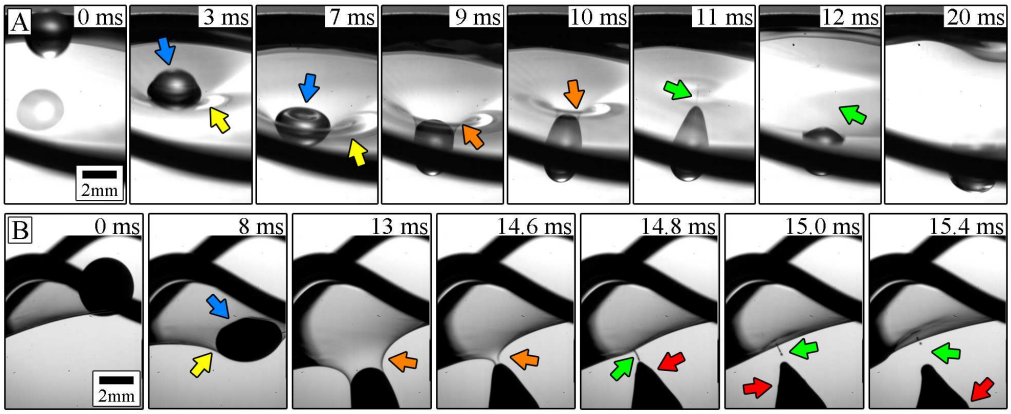


**Figure 6.4:** Passing refers to drop impacts on free-standing films resulting in film penetration of the drop without material transfer from drop to film. When the drop impacted on the film, it was at first compressed (blue arrows) while the film was deformed (yellow arrows). Due to the high impact energy, the drop was able to pass the film's equilibrium state resulting in an elongation of the drop while a neck was formed between drop and film (orange arrows). The neck narrowed and closed above the drop (green arrows). Material was only transferred from film to drop via a surfactant layer originating from the free-standing film (B, 14.8, 15.4 ms, red arrows). (A) Passing through a free-standing film (water on SDS film, $v_d = 0.8\,\mathrm{m/s}$). (B) Ink passing through a bended film to allow the observation of the neck narrowing and pinch off (ink on SDS film, $v_d = 0.6\,\mathrm{m/s}$).

## Partial effects

Beside the above mentioned phenomena, combinations of coalescence with either bouncing or passing could occur - called **partial bouncing** respectively **partial passing**. Partial refers to a drop that first coalesced and then split up into two parts: Only a part of the drop left the substrate either upwards (partial bouncing) or downwards (partial passing). The contact times for partial effects varied between those for the pure impact phenomena bouncing and passing, depending on the origin. Drops which bounced partially were usually in contact with the substrate between 15 and 30 ms, while drops which passed partially were only for 0 to 15 ms in contact with the free-standing film before merging.

### Contact time for separating impact phenomena

**Contact time** describes the time a drop was in contact with the substrate without any further process (leaving or coalescence with the substrate) taking place. The contact time varied depending on the occurring phenomena, e. g. a coalescing drop was in shorter contact with the substrate than a bouncing drop (Figure 6.5). For bouncing, the substrate reflected the drop and therefore it relaxed back to its initial state or bended upwards, what increased the contact time compared to coalescence. In contrast, when a drop passed a free-standing film, the film was bended downwards what corresponds to half the contact time necessary for bouncing effects and was about the contact time for coalescence. Floating drops had a much higher contact time, resulting from drops sitting on the liquid surface.

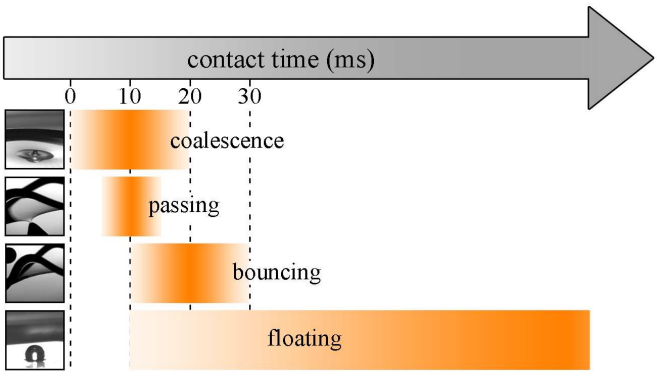


**Figure 6.5:** Impact phenomena dependent contact time shown for the four major effects - coalescence, passing, bouncing, and floating.

## 6.2 Impacts...

For observing drop impacts on either a liquid pool or a free-standing film, a simple setup was used: A syringe for generating the drops at a variable height above the substrate formed the basis. The impacts were recorded with a high-speed camera (Photron) at 5 400 frames per second under backlight illumination from a cold light source (Schott KL 2500) equipped with a diffuser (Figure 6.6).

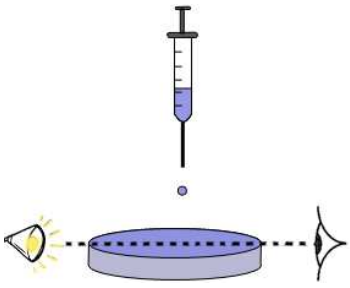

**Figure 6.6:** Single drops were generated by pressing the liquid carefully through a glass syringe. Impacts were recorded with a high-speed camera under backlight illumination.

The glass syringe was equipped with a steel needle ($\varnothing = 0.25\,\text{mm}$; Gesellschaft für Löttechnik mbH, Pforzheim, Germany) giving drops with a diameter of $2.4 \pm 0.4\,\text{mm}$. The distance between syringe and substrate could be varied between 0.5 to 10 cm, resulting in impact velocities ranging from 0.1 to 1.3 m/s (determined from the videos). The contact time was determined with a uncertainty about 0.5 ms from the video. All experiments were performed at ambient conditions. As impacting liquid, water or surfactant solutions (CTAB or SDS; 50 %, 100 %, 200 %, or 4 000 % cmc) were used. The same solutions were used for filling the liquid pool and for preparing the free-standing films.

### 6.2.1 Impacts on a liquid pool

For preparing the liquid pool, a petri dish ($\varnothing = 5\,\text{cm}$) was filled up to the edge with the liquid. This complete filling allowed for focusing on the air-liquid interface perpendicular to the drop impact without looking through the dish walls. Right after preparing the pool, the surface was in motion. Drop impacts on surfaces with a lateral relative motion with respect to the drops are known to favor floating instead of coalescence [30, 32, 36]. To prevent this favoring of one impact phenomenon, the liquid pool's surface was allowed to rest for at least 5 minutes to minimize the surface movement. The absence of surface waves on the pool was checked via a laser beam reflected from the air-liquid interface.

Drop impacts on a liquid pool resulted mainly in coalescence and floating (Figure 6.7), while (partial) bouncing only occurred in less than 2 % of the cases, so that they were not included in the further discussion.

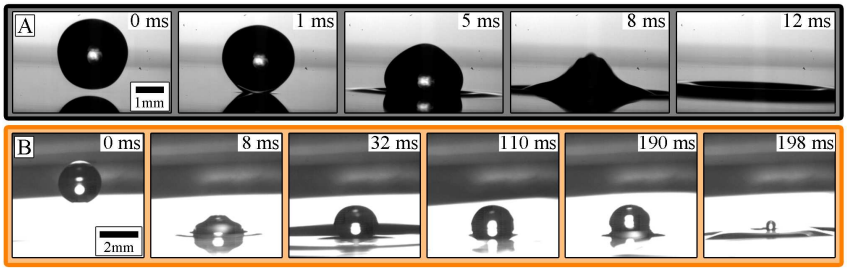


**Figure 6.7:** (A) Coalescence and (B) floating were the main effects on a liquid pool.

In Figure 6.8 all three cases - water on water, water on surfactant, and surfactant on surfactant - are shown in contact time versus Weber number plots ($t_c - We-$plots). At low Weber numbers floating as well as coalescence was observable, while with increasing Weber number coalescence got dominant. The blue line at $t_c = 15\,\text{ms}$ illustrates the separation between floating and coalescence.

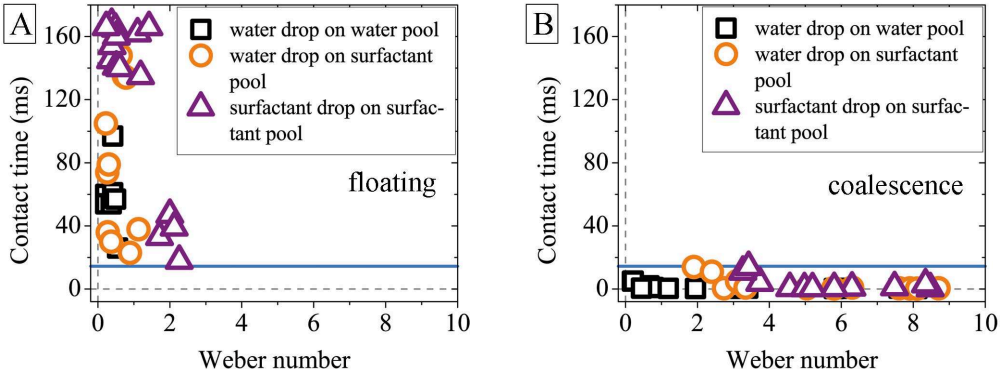


**Figure 6.8:** Drops impacted on a liquid pool either (A) floated and (B) coalesced. At low $We$ both phenomena took place, while at high $We$ only coalescence occurred. The blue line at $t_c = 15\,\text{ms}$ illustrates the separation between floating and coalescence.

Can the distribution between floating and coalescence be affected by surfactants being present in drop and/or liquid pool?

#### 6.2.1.1 Water drops impacting on a water pool

When water drops impacted on a water pool, a few floating events occurred at low Weber numbers ($We < 0.6$), while coalescence happened at the whole Weber number range (Figure 6.9). This means, floating was limited to low impact velocities ($v_d < 0.1\,\text{m/s}$) with contact times less than 100 ms. At these Weber numbers respectively low velocities, floating and coalescence occurred statistically.

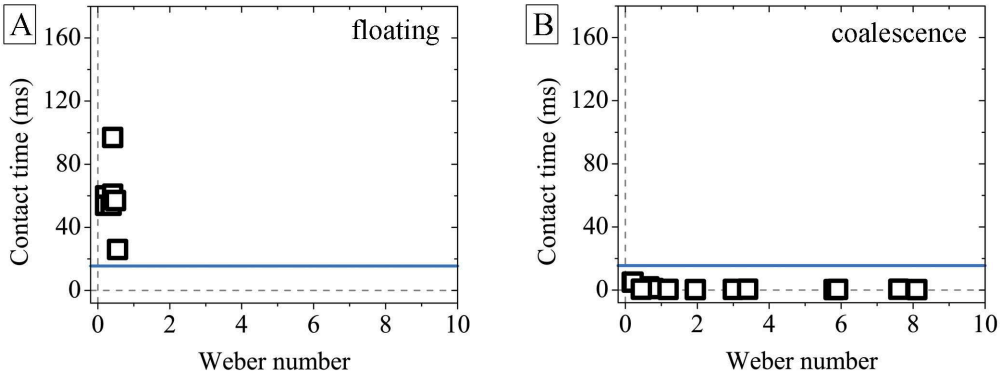


**Figure 6.9:** $t_c - We-$plot for water drops impacting on a water pool. The blue line at $t_c = 15\,\text{ms}$ illustrates the separation between (A) floating and (B) coalescence.

When floating compared to coalescence is favored in the presence of surfactants, the impact behavior shown in Figure 6.9 should change: The Weber numbers where floating occurs should shift to higher values.

#### 6.2.1.2 Water drops impacting on an aqueous surfactant pool

When surfactant was added to one of the components - for simplicity to the liquid pool - the floating/coalescence behavior changed (Figure 6.10). At low Weber numbers ($We < 1.3$), i. e. low impact velocities ($v_d < 0.2\,\mathrm{m/s}$), floating occurred not only statistically but almost exclusively at increased contact times (up to 150 ms). Further, floating could be observed up to higher Weber numbers than for impacts on pure water (the black shaded area illustrates the Weber numbers were floating occurred for water drops impacting on a water pool).

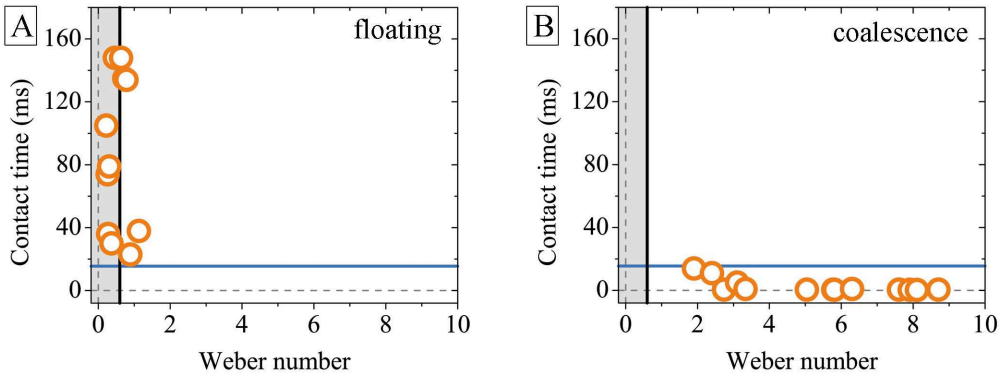


**Figure 6.10:** $t_c - We-$plot for water drops impacting on an aqueous surfactant pool. The blue line illustrates the separation between (A) floating and (B) coalescence. The black shading illustrates the area of water drops floating on pure water.

How can this increase of contact time as well as the dominating occurrence of floating at low Weber numbers be explained? Was it due to the presence of surfactant, i. e. due to the coverage of air-liquid interfaces with surfactant molecules? In this case, an addition of surfactant to the drop should further increase the contact times and shift floating to even higher $We$.

#### 6.2.1.3 Surfactant drops impacting on an aqueous surfactant pool

When surfactant was added to the drop as well as into the pool, a further shifting of the floating phenomena to higher $We$ could be observed (Figure 6.11). As already seen in the case of surfactant present in the pool, floating exclusively occurred at

low Weber numbers ($We < 3$ respectively $v_d < 0.3\,\mathrm{m/s}$). Here, the contact time for floating increased further, up to 180 ms, for $We < 2$, while for the floating phenomena at higher Weber numbers ($2 < We < 3$) only contact times below 80 ms could be observed. With further increasing the Weber number ($We > 3$) again only coalescence took place.

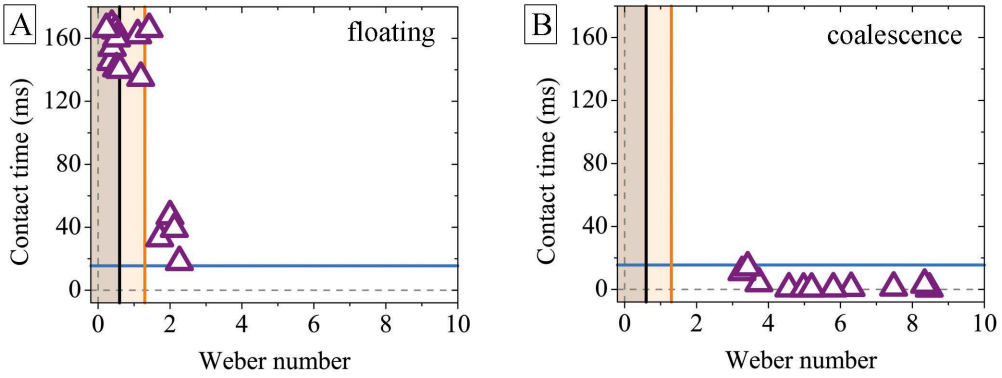


**Figure 6.11:** For surfactant drops impacting on surfactant solutions (A) floating and (B) coalescence is shown. The black and orange shadings indicate the area of water drops floating on water or surfactant solutions.

As speculated, the contact times for floating increased with adding surfactant not only to the drop but also to the liquid pool and floating was shifted to even higher Weber numbers. The presence of surfactants seemed to favor floating experiments at low Weber numbers and to suppress coalescence impacts.

#### 6.2.1.4 Surfactant favors floating impacts

Floating was favored in the presence of surfactant - in case of a surfactant-laden drop and/or pool surface floating exclusively occurred at low Weber numbers with long contact times in contrast to a statistically occurrence in the absence of any surfactant-laden surface. To give an overview of the three cases, $We$ is plotted versus the impacting case (Figure 6.12). Here, the symbol size represents the contact time - the larger the symbol, the larger the contact time. While adding surfactant to the system - either pool or drop and pool, floating became more and more dominant and coalescence was suppressed. In case of a surfactant-free system, only 35 % of all impact caes were floating impacts, while in case of surfactant being present in the drop as well as in the pool, floating occurred in 59 % of the impact cases. Further, when surfactant was present in the drop as well as in the pool, at low Weber numbers much larger contact times were observed for floating than in case of surfactant being

absent. Contact times decreased in all investigated cases (water on water, water on surfactant, and surfactant on surfactant) with increasing Weber number.

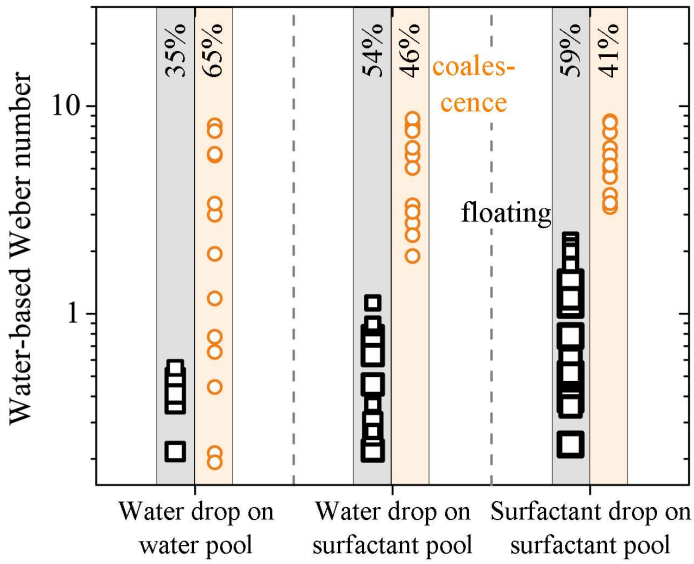


**Figure 6.12:** Overview of floating (black squares) and coalescence phenomena (orange circles) with respect to the different impact cases - water drop on water, water drop on surfactant, and surfactant drop on surfactant pool (left to right). Floating got more and more dominant and coalescence was suppressed at low $We$, with increasing the presence of surfactant. The symbol size increases with increasing contact time.

For the described experiments CTAB was used as surfactant. One could wonder if the experiments depend on the used surfactant, i. e. does SDS as anionic surfactant lead to similar observations like the cationic CTAB? Further, the question arises, if the contact times would decrease in case of SDS drops impacting on a CTAB pool or vice versa. The opposite charge of these two surfactants could lead to attractive forces minimizing the observed contact times in contrast to repulsive forces between equally charged molecules in drop and solution. But SDS as surfactant in the drop impact experiments showed no difference to the CTAB experiments. Further, crossed experiments (SDS drops on CTAB solutions or vice versa) did not lead to any differences in the observed contact times. This leads to the idea that the surfactant type/charge does not influence the impact behavior of the drops.

But what caused the floating impacts to get more dominant and “stable” in the presence of surfactant? To allow for coalescence, drop and pool have to come into contact with each other, but the separation layer seemed to be more efficient in the presence of surfactant as seen by the increased contact times. When surfactant is present, the hydrodynamic boundary condition is changed from a slip to a no-slip condition what seemed to stabilize the air cushion and therewith to slow down its

thinning and to suppress coalescence. The mechanisms for the air cushion-thinning is discussed in detail in Section 6.4.

### 6.2.2 Impacts on a free-standing surfactant film

The surfactant films were prepared by dipping a spherical frame ($\varnothing = 2\,\mathrm{cm}$) into the surfactant solution and slowly pulling it out again. The resulting films had a thickness in the order of a few micrometer, concluded from the interference rings visible under white illumination. After preparation, the films started to thin due to water evaporation, capillary forces, gravitation, etc. resulting in surfactant monolayers sandwiching only a few water molecules. During thinning, the interference colors of the film changed from rainbow colors to black, indicating very thin films right before bursting [116]. The usual lifetime of a free-standing film was about one minute. Drop impact experiments took place 15 to 20 s after film preparation, resulting in comparable films for each impact.

Drop impacts on free-standing films resulted mainly in coalescence, bouncing, and passing (Figure 6.13). Further, combinations of coalescence with bouncing and passing could be observed. The contact times varied between 5 and 25 ms.

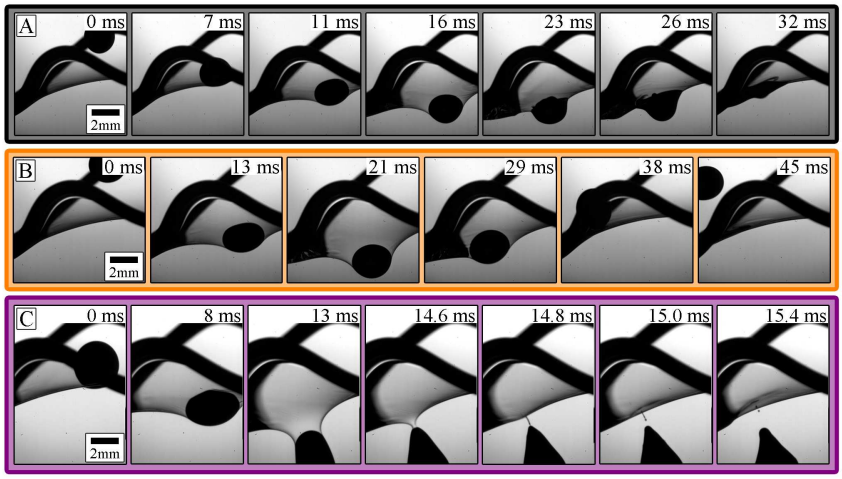


**Figure 6.13:** Main phenomena occurring during drop impact on a free-standing surfactant film - (A) coalescence, (B) bouncing, and (C) passing.

Does the observation of surfactants suppressing coalescence also hold true in case of impacts on free-standing surfactant films? When only the presence of surfactant molecules leads to the suppression, this should be true. This means that all effects involving coalescence should be suppressed or at least reduced, when surfactant drops impact on surfactant films compared to impacting water drops. In order to study

the influence of surfactant on the suppression on coalescence, the surfactant concentration inside the drop (0 % and 100 % cmc) and in the film (50 %, 100 %, 200 %, and 4 000 % cmc) was varied. The observations are presented in $t_c - We-$plots, separated into three cases - coalescence, passing, and bouncing.

#### 6.2.2.1 Water drops impacting on free-standing surfactant films

For water drops impacting on free-standing surfactant films all described phenomena were observed (Figure 6.14) - coalescence up to $We < 3.5$ (A, $t_c < 15\,\text{ms}$), (partial) passing at $We > 2.6$ (B, $5\,\text{ms} < t_c < 15\,\text{ms}$), and (partial) bouncing over the complete Weber number range (C, $t_c > 12\,\text{ms}$).

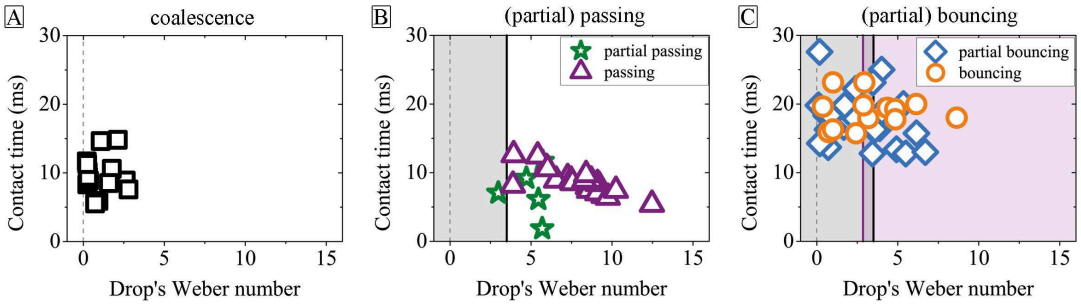


**Figure 6.14:** $t_c - We-$plots for water drops impacting on free-standing films separated in (A) coalescence, (B) (partial) passing, and (C) (partial) bouncing. The black and purple shading illustrates the area of coalescing and passing drops respectively.

While having a closer look at the Weber numbers where coalescence, passing and partial passing took place, one could observe an overlap of these phenomena (Figure 6.14 A and B). At low Weber numbers coalescence took place, while at high Weber numbers passing was observed. In the overlap regime ($We \approx 3$) mainly partial passing (green stars) - the combination of coalescence and passing - could be found, resulting in a gapless order of coalescence, partial passing, and passing. Bouncing and partial bouncing effects were observed in the whole Weber number range (C).

#### Does the type of surfactant influence the impact behavior?

The nature of the surfactant (SDS or CTAB) had no significant influence on the outcome of an impact experiment (Figure 6.15). CTAB and SDS showed no difference for coalescence, (partial) bouncing, and passing. The only exception was partial passing that was only observed for surfactant films containing SDS at a concentration below cmc. In addition, for SDS surfactant films, passing was shifted to little

higher Weber numbers compared to films containing CTAB. For films containing SDS, the Weber numbers for coalescence and passing were well separated while in CTAB surfactant films the regions partially overlapped.

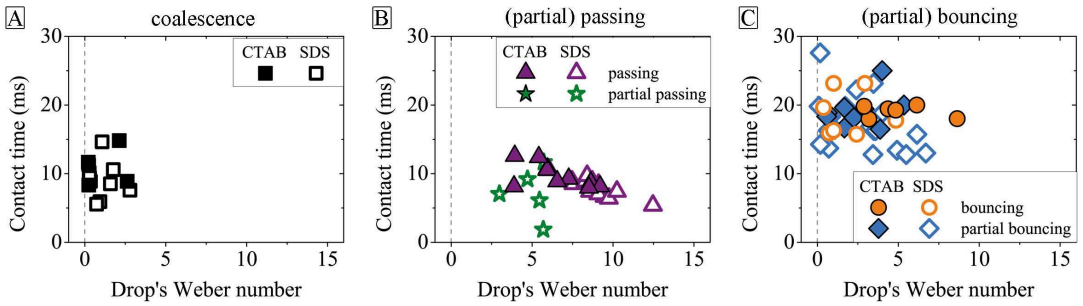


**Figure 6.15:** $t_c - We-$plots for pure water drops impacting on surfactant films. The surfactants in the were CTAB (filled symbols) and SDS (open symbols). (A) Coalescence, (B) (partial) passing, and (C) (partial) bouncing.

### Does the surfactant concentration influence the impact behavior?

In the range of surfactant concentrations studied, the outcome of the impact did not strongly depend on the surfactant concentration. As an example, Figure 6.16 shows the $t_c - We-$plots with respect to the surfactant concentration for films containing SDS. Two exceptions were observed: First, partial passing was only observed for concentrations below cmc; all results shown in Figure 6.15 for partial passing were recorded on free-standing SDS films at a concentration of 50% cmc. Second, bouncing occurred only for concentrations above cmc ($\geq$ 200 % cmc). Coalescence, passing, and partial bouncing were observed at all tested concentrations.

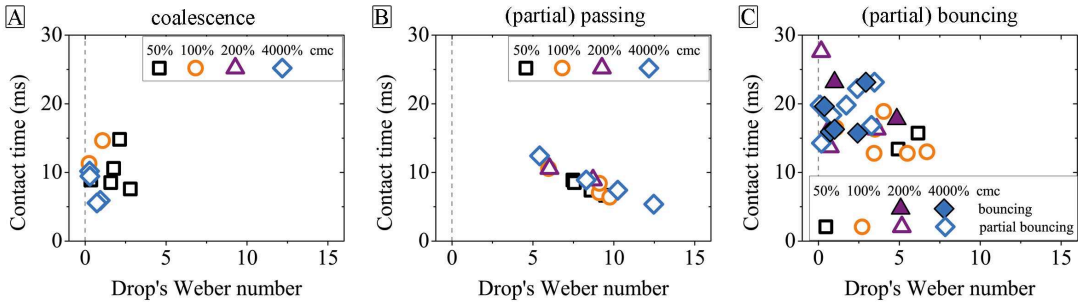


**Figure 6.16:** Parts of Figure 6.15 were replotted with respect to the surfactant concentration used for preparing the free-standing SDS films for water drop impacts. (A) Coalescence, (B) passing, and (C) (partial) bouncing.

For pure water drops impacting on free-standing surfactant films can be summarized:

- Coalescence was a dominating process at low Weber numbers.
- Coalescence and passing overlapped partially ($We \approx 3$).
- Neither surfactant type nor concentration showed a significant influence, except for partial passing that only occurred for SDS films below cmc. Bouncing was only observed for concentrations above cmc.

Are bouncing and passing favored for surfactant drops impacting on films in analogy to favored floating in case of surfactant drops impacting on a surfactant solution?

#### 6.2.2.2 Surfactant drops impacting on free-standing surfactant films

In contrast to water drops impacting on free-standing films, surfactant drops resulted mainly in passing ($We > 4.2$, $5\,\text{ms} < t_c < 15\,\text{ms}$; Figure 6.17 B) and (partial) bouncing (C). Coalescence was only rarely observed ($We < 1.2$; A), while partial passing could not be observed at all. In case of surfactant drops impacting on surfactant films, coalescence and passing impacts were well separated compared to impacting water drops (Figure 6.14). The hardly distinguishable bouncing and partial bouncing impacts occurred at the complete Weber number range.

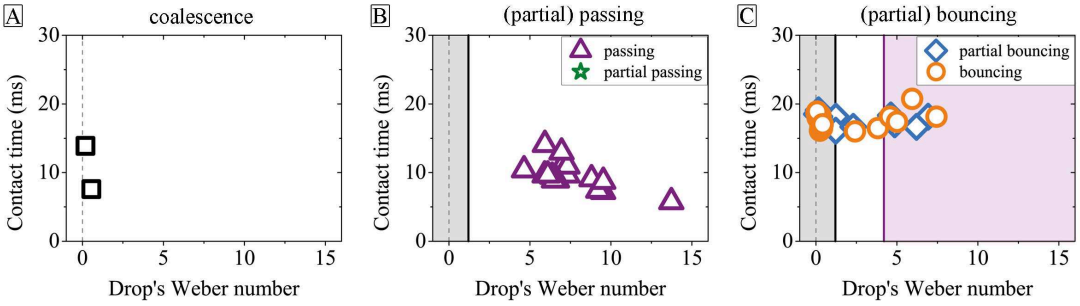


**Figure 6.17:** $t_c - We-$plots for surfactant drops impacting on free-standing surfactant films separated in (A) coalescence, (B) (partial) passing, and (C) (partial) bouncing. The black shading illustrates the area of drops coalescing while the purple shaded area illustrates the area of drops passing the film.

These results agree with observations of Gilet and Bush [38], who measured drop impacts ($r_d = 0.8\,\text{mm}$) on surfactant films ($\varnothing = 1.6\,\text{cm}$). For drops consisting of 79% water, 20% glycerol plus 1% Dove soap ($\gamma_d = 24\,\text{mN/m}$) impacting on a surfactant film of similar composition, they observed bouncing for low and passing for high $We$ with a transition at $We \approx 16$. Considering the different viscosities in the experiments of Gilet and Bush compared to my results, this value for the transition agrees with my value of $We \approx 10$ ($\gamma_d = 37\,\text{mN/m}$).

### Influence of surfactant type and concentration

Similar to the impacts of water drops on free-standing films, no dependency on the surfactant type (CTAB and SDS) was observed for impacting surfactant drops. Also a dependency of surfactant drops impacting on surfactant films of oppositely charged surfactants could not be observed. Varying the surfactant concentration did not significantly influence the outcome of the impact experiments. Only bouncing depended on the surfactant concentration that had to be larger than 100 % cmc.

#### 6.2.2.3 Surfactant suppresses coalescence

For surfactant drops impacting on free-standing films, coalescence as well as partial passing was suppressed (Figure 6.18) - only 4 % of all impacts were coalescence compared to 17 % coalescence in case of impacting water drops. As a consequence of impacting surfactant drops, the percentage of bouncing and passing events increased at the expense of coalescence and partial passing. Partial bouncing was not affected by surfactant being present in the drop.

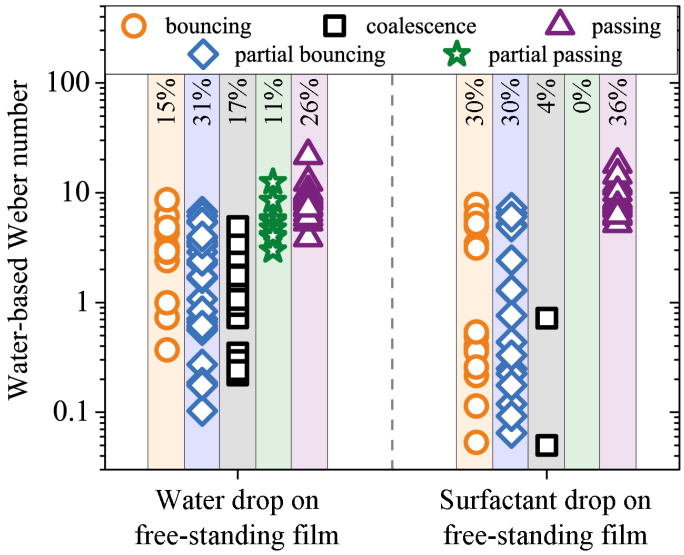


**Figure 6.18:** Overview of the impact phenomena bouncing, partial bouncing, coalescence, partial passing, and passing with respect to the different drops impacting on free-standing surfactant films. Coalescence and partial passing were suppressed when surfactant was added to the drop, while bouncing and passing were favored.

The phenomena - bouncing and passing - which need a stable air cushion as separation layer between drop and film were favored in case of surfactant drops impacting on free-standing surfactant films compared to impacting water drops.

### 6.2.3 Impacts and the influence of surfactants

In the presence of surfactant, floating as well as passing and bouncing were favored (Figures 6.12 and 6.18). These three impact phenomena had one common feature - the drops were not allowed to get in contact with the liquid respectively film underneath. This separation was given by an air cushion, whose thinning seemed to be more efficient in the absence of surfactants. The thinning mechanisms - hydrodynamic repulsion and gas diffusion into the liquid - is discussed in Section 6.4. Further, the stabilizing of the air cushion in presence of surfactants seemed to be independent of the surfactant type, at least given for SDS and CTAB.

## 6.3 Characteristic time scale of drop impacts

With respect to the kinetics of drop impact on free-standing surfactant films, two intrinsic characteristic times are important: The vibration period of the drop $\tau_d$ and the vibration of the surfactant film during drop impact $\tau_f$. The fundamental eigen vibration period of the initial drop [42, 117] in a gaseous environment or vacuum is given by

$$\tau_d = \pi\sqrt{\frac{\rho r_d^3}{2\gamma_d}}. \tag{6.2}$$

This vibration period is derived for the limit of an inviscid or only slightly viscous liquid and for small vibration amplitudes, as given for water or dilute surfactant solutions. The vibration time for water ($\gamma_d = 72\,\mathrm{mN/m}$, $\rho \approx 10^3\,\mathrm{kg/m^3}$, $r_d = 1.2\,\mathrm{mm}$) is given as $\tau_d = 10.9\,\mathrm{ms}$. For surfactant drops ($\gamma_d \approx 37\,\mathrm{mN/m}$) the vibration time increases to $\tau_d = 15.2\,\mathrm{ms}$.

The vibration period of a surfactant film during drop impact can be calculated with the mass of the drop $m$ and the spring constant $k$ of the film as

$$\tau_f = 2\pi\sqrt{\frac{m}{k}} \tag{6.3}$$

assuming that the mass of the film is negligible. The effective spring constant of a surfactant film can be calculated as $k = 8\pi\gamma_f/7$ assuming that the film maintains its equilibrium shape at all times during a central deflection. $\gamma_f$ is the surface tension of the surfactant film. The typical drop mass is given as $m = 4\pi r_d^3\rho/3 = 7.24\,\mathrm{mg}$. This results in a vibration period of the surfactant film of $\tau_f = 46\,\mathrm{ms}$.

**Theoretical contact times for bouncing and passing**

For bouncing one expects a contact time of half the vibration period of the film, $\tau_f/2 = 23\,\text{ms}$. This is in good agreement with the mean value of the measured contact time of $\bar{\tau}_{bouncing} = 19\,\text{ms}$ for bouncing impacts. Passing should be faster than a quarter vibration period of the film $\tau_f/4 = 11.5\,\text{ms}$. The mean passing time observed during experiments is with $\bar{\tau}_{passing} = 9.4\,\text{ms}$ in good agreement with the theoretical value.

**Estimating the film thickness**

Coalescence was always accompanied by a surface wave running through the surfactant film. The origin of this surface wave is most probably similar to surface (or capillary) waves observed in experiments of fast spontaneous wetting of drops with substrates. Upon contact of the drop with the substrate, the surface waves are generated due to fast motion of the contact line [118, 119]. Similar fast processes are expected when impacting drops coalesce with the surfactant films. The velocity of such a capillary wave $v_{cap}$ traveling along a liquid film [38] is given with the film thickness $d$ as

$$v_{cap} = \sqrt{\frac{\gamma_f}{\rho d}}. \tag{6.4}$$

This leads to a film thickness ranging from 1 to 4 µm ($v_{cap} = 3.2$ - $5.3\,\text{m/s}$), what is in good agreement with the observed interference fringes in the film.

## 6.4 Thinning of the air cushion

The air cushion that is necessary for preventing physical contact between drop and liquid/film and therefore preventing coalescence [31], was already mentioned by Reynolds and Lord Rayleigh [40, 41, 120]. Before the drop can coalesce with the liquid/film, the air has to flow out of the closing gap [31, 121] or diffuse into drop and liquid/film. This thinning proceeds until the gap has reached a thickness where van der Waals forces become relevant (10-100 nm) [31, 112, 113]. Hydrodynamic thinning of the air cushion does not only depend on impact velocity, drop size, and drop shape during impact [31], but also on the hydrodynamic boundary condition, that is influenced by the presence of surfactants on the surface. It is generally assumed, that even a minute amount of surfactant present in the water changes the boundary condition to effectively no-slip [39, 114, 115].

### 6.4.1 Influence of hydrodynamic repulsion

Not only in the described experimental results (Section 6.2), but also in impact experiments on a liquid pool observed by Amarouchene et al. [39], coalescence was hindered in presence of surfactants. They related this effect to surface elasticity caused by surfactants. Here, the suppression of coalescence in terms of a change in the hydrodynamic boundary condition due to surfactants will be considered.

The air flow in the gap between drop and liquid/film leads to a hydrodynamic repulsive force. The thinning of the gap can be described by hydrodynamics in the compressible lubrication approximation [31, 114, 115, 122–126]. The following is based on the results by Manor et al. [114] and Balmforth et al. [127]. In brief, the conservation of mass

$$\frac{\partial \rho}{\partial t} + \nabla(\rho \vec{v}) = 0 \tag{6.5}$$

and the conservation of momentum

$$\eta \frac{\partial^2 v_r}{\partial z^2} = \frac{\partial p}{\partial r} \tag{6.6}$$

are used. Here, $\vec{v}$ is the local velocity of the intervening air, and $v_r$ is the radial component of this velocity (Figure 6.19 A). In the lubrication approximation, the pressure is assumed to be constant over the gap thickness $h_g$ and to depend only on the radial coordinate $r$. Integrating momentum conservation twice over $z$ gives a parabolic flow profile

$$\eta v_r(z) = (a_v + b_v z + c_v z^2)\frac{\partial p}{\partial r} \tag{6.7}$$

with the parameters $a_v$, $b_v$, and $c_v$ depending on the flow boundary conditions at the liquid/film surface ($z = 0$) and at the drop surface ($z = h_g$). Inserting this result in the equation of mass conservation and integrating again over $z$ results in an equation describing the time dependence of the gap thickness.

$$\frac{\partial (h_g \rho)}{\partial t} = -\frac{1}{r}\frac{\partial}{\partial r}[rQ] \tag{6.8}$$

Here, $Q = \int_0^h \rho v_r dz$ denotes the hydrodynamic air flux in the gap. Density was assumed to depend only on the radial position ($\partial\rho/\partial z$).

A decisive parameter for determining $Q$ is the hydrodynamic boundary condition at the air-water interface. Despite the strong viscosity contrast between gas and liquid, the radial outflow of the gas can induce a flow in the liquid in the same

direction. Necessarily, such a flow brings new liquid to the surface, and creates a surface that is not covered by surfactant. Therefore, surface tension gradients along the surface of the liquid are created when surfactant molecules are present in the bulk [128, 129]. These surface tension gradients generate lateral stresses at the boundaries, which give an additional hindrance to any flow in the liquid phases and enforce no-slip boundary conditions on liquid surfaces covered with surfactant molecules [114, 129]. In the absence of surfactants, however, this restriction does not hold.

For a surface with a slip boundary condition the outflow of air should be faster than for a no-slip boundary condition. The case that one surface shows slip with a slip length $b$ (pure water) and the second surface shows a no-slip boundary condition (surfactant solution) is considered. Since the compressibility does enter the equation of momentum conservation, the result by Manor et al. can be applied [114]. They have shown that the air flux $Q$ out of the gap is increased by a factor of $(4b + h_g)/(b + h_g)$ in the presence of slip. This tells that a gap between mobile (pure water) boundaries thins faster than a gap between no-slip (surfactant solution) boundaries. A significant effect can only be expected if the slip length is comparable to or smaller than the gap thickness (Figure 6.19). As long as the slip length is small compared to the gap thickness, no effect of slip is expected and $(4b + h_g)/(b + h_g) \approx 1$. For thin gaps the flux $Q$ is increased by almost a factor of 4. Ultimately, slip allows for faster thinning of the air gap and favors coalescence.

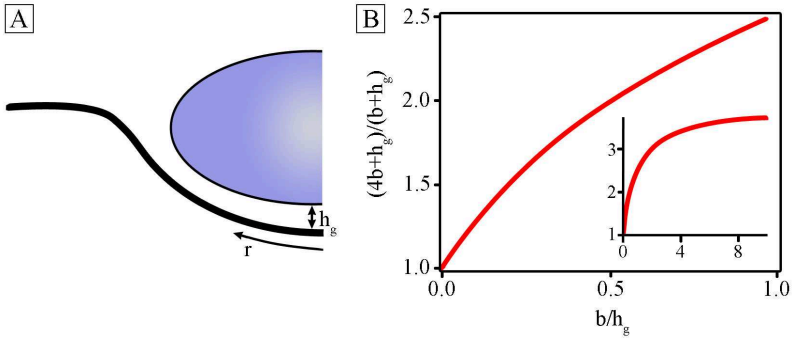


**Figure 6.19:** (A) Air gap of thickness $h_g$ separates the impacting drop from the surfactant film. The gap thickness depends on the radial position $r$. (B) The enhancement factor of the flux (as calculated by Manor et al. [114]) as a function of the ratio between slip length and gap height. Inset: The same function for large values of $b/h_g$.

Thus the experimental results can tentatively be interpreted in terms of increasing slip when changing from surfactant to pure water drops. In the first case most probably for both surfaces (in case of a surfactant pool/film) a no-slip boundary condition applies, resulting in a delayed coalescence. In the latter case, at least one

of the surfaces allows for slip and thus speeds up coalescence. The hypothesis that hydrodynamic effects and boundary conditions dominate the interaction is also in accordance with the observation that neither the type of surfactant nor the surfactant concentration had a strong influence on the outcome of an impact experiment. This was also observed in earlier experiments of rising bubbles [130–134] and surface forces [114, 129, 135]: Even little contamination of the air-liquid interfaces by any type of surface active molecules caused the boundary condition to change from slip to no-slip.

To study the flow inside the drop caused by the vanishing air cushion, silica particles (Kromasil 100) were dispersed in the drop in order to track their motion and thus the flow inside the drop. A slip boundary condition should induce a flow inside the drop. Consequently, after passing a soap film, the flow profile inside a water drop should differ from that inside a surfactant drop. From the Navier-Stokes equation, one would expect that the flow of the surface propagates a distance of about $\Delta x \sim \sqrt{\eta/\rho \Delta t}$ into the drop. For a contact time $\Delta t < 20\,\mathrm{ms}$, a thickness of the moving layer inside the drop in the order of 10 % of the drop radius is expected. The flow inside the drop was followed after they passed the surfactant film. It turned out that the flow due to the deformation of the drop (Figure 6.13) was so dominant that no change due to the boundary condition was observable. Therefore a visualization of the expected layer moving with a different velocity inside water or surfactant drops was not possible.

### 6.4.2 Gas diffusion into the liquid

Beside the hydrodynamic flow, diffusion of gas molecules into the liquid, drop as well as liquid/film, could be another possibility for the thinning of the air cushion. The solubility of a gas in a liquid is determined by the partial pressure of the gas above the gas-liquid interface. During impact the gas pressure in the intervening gap between drop and liquid/film is increased. Consequently, gas should diffuse into the liquid. Here, the effect of enhanced gas dissolution as reason for a gap thinning is discussed.

The equilibrium concentration $c^{eq}$ of gas dissolved in a liquid is, according to Henry's law, proportional to the partial pressure $p$ of the gas above the liquid gas interface with the Henry constant $k_H$ [54].

$$k_H p = c^{eq} \tag{6.9}$$

During drop impact the pressure increases in the gap between the two liquid surfaces. Air will diffuse into the liquid (that is saturated at ambient pressure). The

time scale to attain the new equilibrium is, however, determined by a number of factors, including the hydrodynamic flow profile in the liquid and the hindrance of the diffusion by surfactant molecules at the gas liquid interface [136].

To describe this quantitatively, a pressure jump of the (partial) pressure of the gas from $p_1$ to $p_2$ is considered. The concentration of the gas in the liquid then relaxes with characteristic constant $k_l$ to the new equilibrium [136, 137]

$$\frac{k_l}{h_l}\left[c^{eq}(p_2) - c(t)\right] \quad = \quad \frac{dc(t)}{dt}. \tag{6.10}$$

Here, $c(t)$ is the concentration of gas in the liquid as a function of time and $h_l$ is the thickness of the diffusively accessible liquid volume. The newly absorbed gas originated from the gap. When multiplying Equation (6.10) by 2 for the two gas-liquid interfaces available, the diffusive gas flux from the gap into the bulk of the drop and the liquid/film can be estimated.

The number of moles diffusing into the liquid per time interval $dt$ is given by $dN_l = V_l dc$, where $V_l$ is the volume of liquid that is accessible by diffusion during the impact of the drop. The same amount leaves the gas $dN_g = -dN_l = c_g dV_g$. Here, $c_g$ is the gas concentration in mol/m$^3$. Assuming that the gas behaves like an ideal gas $p = c_g RT$ (with gas constant $R = 8.31\,\mathrm{J/(mol\,K)}$ and temperature $T$), Equation (6.10) can be rewritten as

$$2\frac{k_l}{h_l}\left[c^{eq}(p_2) - c(t)\right] \;=\; \frac{dc(t)}{dt} \;=\; \frac{1}{V_l}\frac{dN_l(t)}{dt} \;=\; -\frac{c_g}{V_l}\frac{dV_g}{dt} \;=\; -\frac{p}{RTV_l}\frac{dV_g}{dt} \tag{6.11}$$

With $V_g = ah_g$ and $V_l = ah_l$ (a is the interfacial area and $h_g = h$ is the thickness of the gas layer) I get

$$\frac{dh_g}{dt} \quad = \quad -2k_l\frac{RT}{p}\left[c^{eq}(p_2) - c(t)\right] \tag{6.12}$$

as the contribution to the gap thinning due to the gas diffusion into the drop and the liquid/film. To estimate typical numbers, I took literature values for the Henry constants $k_l \approx 10^{-5}\,\mathrm{m/s}$ [138] and $k_H = 6.5 \cdot 10^{-6}\,\mathrm{mol/Nm}$ [139]. The absolute temperature is $T = 298\,\mathrm{K}$:

$$\frac{dh_g}{dt} \quad \approx \quad 2k_l k_H \frac{RT}{p_1}\left[p_2 - p_1\right] \quad \approx \quad 3.2 \cdot 10^{-7}\,\frac{p_2 - p_1}{p_1}\,\frac{\mathrm{m}}{\mathrm{s}}. \tag{6.13}$$

For films thick enough (thicker than a few tens of nm) that the disjoining pressure can be neglected, the pressure difference is taken from the Laplace equation $\Delta p = 2\gamma/r_d \approx 60\,\mathrm{Pa}$, leading to a negligible thinning due to diffusion (Figure 6.20). However, this can change significantly in nanometer thin gaps, when the disjoining pressure may add to the pressure in the gap. In conclusion, diffusion is only relevant for very thin films, i. e., in the very last moment before the merging of the drop takes place. Even if the mass transfer coefficient decreases with increasing surfactant concentration, I do not expect a strong influence of diffusion into the liquid on the lifetime of the gas film.

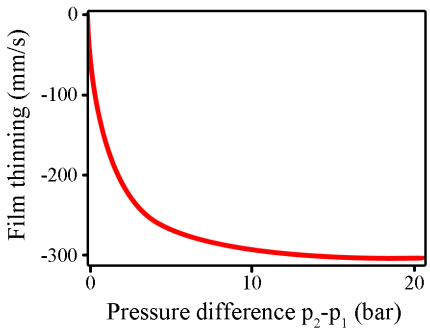


**Figure 6.20:** Film thinning velocity as estimated from Henry's law after a pressure jump of $p_2 - p_1$.

## 6.5 Conclusion

Liquid drops impacting on either a liquid pool or a free-standing surfactant film show different responses depending on their initial kinetic energy - coalescence, floating, bouncing, and passing. The characteristic time scales for bouncing on and passing through free-standing films could be related to the period $\tau_f$ of the oscillator with the film as a non-linear spring and the drop as an additional mass. The contact time for bouncing is roughly $\tau_f/2$. The upper boundary of the contact time in passing of the drop through the surfactant film is $\approx \tau_f/4$. When surfactant is added to the drop, coalescence and partial passing, i.e. the processes with relatively short contact times, were suppressed.

The outcome of the impact experiments was to a certain degree not deterministic but stochastic. At a given Weber number different phenomena could happen and only the probability of a certain outcome could be determined. Possible reasons for this uncertainty in the outcome of an experiment include:

- The Weber number might not be the only parameter determining the outcome of a drop impact. It could well be that the density, the size, the impact velocity, or the surface tension influence independently the outcome, and not only in the form of the Weber number.

- Additional factors such as the thickness of the soap film or humidity and thus the rate of evaporation, might influence the outcome of impact experiments.

In this work not all of these parameters were precisely controlled. But they are not accounted for in the Weber number.

As possible mechanisms for the gap thinning between drop and liquid/film, air diffusion into the liquid and hydrodynamic flow is discussed. It turned out that the diffusion of gas into the liquid due to the pressure increase is still very slow and only can become relevant in the very last stages before merging. As long as the gap is thick enough that contribution from diffusion can be neglected, hydrodynamics dominates the thinning of the gap, whereas the air flux depends on the hydrodynamic boundary condition. The hydrodynamic boundary condition is changed in presence of surfactants from a slip-like condition (pure water) to a no-slip boundary condition (surfactant solution). The more mobile the air-water interface is, the faster the flow of air out of the gap and the more efficiently the gap can thin.

## 6.6 Experimental details

### Drop impact...

Drops with an average diameter of $2.4 \pm 0.4\,\mathrm{mm}$ were generated by pressing liquid through a glass syringe equipped with a steel needle ($\varnothing = 0.25\,\mathrm{mm}$). These drops - pure water or surfactant drops (100 % cmc) - were allowed to impact either on a liquid pool or on a free-standing surfactant film. As surfactants CTAB (Sigma-Aldrich) and SDS (Acros Organics) were used as purchased.

The impact was observed with a high-speed camera (Photron, $12\times$ magnification) and light from the back. The usual frame rate was 5 400 Hz.

### ... on a liquid pool

A petri dish ($\varnothing = 5\,\mathrm{cm}$) was used as reservoir for the liquid pool. It was filled to the upper level with either pure water or a surfactant solution - CTAB or SDS. The surfactant solutions have a concentration of 50 %, 100 %, 200 %, and 4 000 % cmc. Before impact, the pool was allowed to rest for at least 5 minutes to suppress surface waves. The investigated combinations of drop and pool were:

- Water drop on water pool
- Water drop on surfactant solution
- Surfactant drop on surfactant solution

The impacts were usually observed at a frame rate of 5 400 Hz with the Photron high-speed camera (12 × magnification).

### ... on a free-standing film

In case of free-standing surfactant films as substrate, a spherical wire frame with a diameter of 2 cm was dipped into aqueous surfactant solutions and slowly pulled out again. This resulted in micrometer thick free-standing films with a usual lifetime about 60 seconds. As surfactant again CTAB or SDS was used at concentrations about 50 %, 100 %, 200 %, and 4 000 % cmc with impacting drops of either water or also a surfactant solution (100 %).

### Mass transfer between drop and free-standing film

For observing a possible mass transfer from drop to film while passing or bouncing, a slightly bend wire frame was used allowing for an undisturbed observation. Further black ink (Pelikan GmbH) was used as drop to provide a clear contrast between drop and film. The videos were recorded at 20 000 Hz.

### Drop's flow profile after passing a free-standing film

In order to investigate the flow profile in a drop before and after passing a free-standing surfactant film, small silica particles (Kromasil 100, $\varnothing = 7\,\mu m$, MZ Analysentechnik Mainz, Germany) were added as tracer particles to the drop. These particles reflected the light and appeared as bright spots inside the drop.

# Bibliography


[1] O. Voinov. *Hydrodynamics of wetting.* Fluid Dynamics, **11** (1976) 714. vii, ix, 17, 18, 48

[2] R. Cox. *The dynamics of the spreading of liquids on a solid surface. Part 1. Viscous flow.* Journal of Fluid Mechanics, **168** (1986) 169. vii, ix, 18, 48

[3] V. Starov, M. Velarde, and C. Radke. *Wetting and Spreading Dynamics.* CRC Press, **2007**. 1

[4] D. Bonn, J. Eggers, J. Indekeu, J. Meunier, and E. Rolley. *Wetting and spreading.* Reviews of Modern Physics, **81** (2009) 739. 1, 9, 12, 81

[5] R. Hill. *Superspreading.* Current Opinion in Colloid & Interface Science, **3** (1998) 247.

[6] A. Nikolov, D. Wasan, A. Chengara, K. Koczo, G. Policello, and I. Kolossvary. *Superspreading driven by Marangoni flow.* Advances in Colloid and Interface Science, **96** (2002) 325.

[7] K. Varanasi and S. Garoff. *Unsteady Motion of Receding Contact Lines of Surfactant Solutions: The Role of Surfactant Re-Self-Assembly.* Langmuir, **21** (2005) 9932. 1

[8] J. Hyypia. *Measurement of Rates of Spread of Solutions of Surface Active Agents.* Analytical Chemistry, **20** (1948) 1039. 1

[9] A. Marmur and M. Lelah. *The spreading of aqueous surfactant solutions on glass.* Chemical Engineering Communications, **13** (1981) 133.

[10] S. Troian, X. Wu, and S. Safran. *Fingering instability in thin wetting films.* Physical Review Letters, **62** (1989) 1496.

[11] W. Birch, M. Knewtson, S. Garoff, R. Suter, and S. Satiia. *The molecular structure of autophobed monolayers and precursing films of a cationic surfactant on the silicon oxide/silicon surface.* Colloids and Surfaces, A: Physicochemical and Engineering Aspects, **89** (1994) 145.

[12] B. Frank and S. Garoff. *Surfactant self-assembly near contact lines: control of advancing surfactant solutions*. Colloids and Surfaces, A: Physicochemical and Engineering Aspects, **116** (1996) 31.

[13] T. Stoebe, R. Hill, M. Ward, and H. Davis. *Enhanced Spreading of Aqueous Films Containing Ionic Surfactants on Solid Substrates*. Langmuir, **13** (1997) 7276.

[14] V. Dutschk, K. Sabbatovskiy, M. Stolz, K. Grundke, and V. Rudoy. *Unusual wetting dynamics of aqueous surfactant solutions on polymer surfaces*. Journal of Colloid and Interface Science, **267** (2003) 456. 1

[15] D. Quéré. *Fluid coating on a fiber*. Annual Review of Fluid Mechanics, **31** (1999) 347. 1, 19

[16] W. Wilkinson. *Entrainment of air by a solid surface entering a liquid/air interface*. Chemical Engineering Science, **30** (1975) 1227. 1, 21

[17] B. Bolton and S. Middleman. *Air entrainment in a roll coating system*. Chemical Engineering Science, **35** (1980) 597. 1, 21

[18] J. Sheats. *Manufacturing and commercialization issues in organic eletronics*. Journal of Materials Research, **19** (2004) 1974. 1

[19] N. Bornemann, H. Sauer, and E. Dörsam. *Gravure Printed Ultrathin Layers of Small-Molecule Semiconductors on Glass*. Journal of Imaging Science and Technology, **55** (2011) 040201–1. 1, 3, 4

[20] A. Blayo and B. Pineaux. *Printing Processes and their Potential for RFID Printing*. In *Joint sOc-EUSAI conference*. **2005**. 2

[21] A. Huebler, F. Doetz, H. Kempa, H. Katz, M. Bartzsch, N. Brandt, I. Hennig, U. Fuegmann, S. Vaidyanathan, J. Granstrum, S. Liu, A. Sydorenko, T. Zillger, G. Schmidt, K. Preissler, E. Reichmanis, P. Eckerle, F. Richter, T. Fischer, and U. Hahn. *Ring oscillator fabricated completely by means of mass-printing technologies*. Organic Electronics, **8** (2007) 480. 2

[22] A. Huebler, U. Hahn, W. Beier, N. Lasch, and T. Fischer. *High Volume Printing Technologies for the Production of Polymer Electronic Structures*. In *Proceedings of the 2nd International IEEE Conference on Polymers and Adhesives in Microelectronics and Photonics*, p. 172. **2002**.

[23] H. Kang, R. Kitsomboonloha, J. Jang, and V. Subramanian. *High-Performance Printed Transistors Realized Using Femtoliter Gravure-Printed*

*Sub-10 μm Metallic Nanoparticle Patterns and Highly Uniform Polymer Dielectric and Semiconductor Layers.* Advanced Materials, **24** (2012) 3065. 2, 3

[24] D.-Y. Chung, J. Huang, D. Bradley, and A. Campbell. *High performance, flexible polymer light-emitting diodes (PLEDs) with gravure contact printed hole injection and light emitting layers.* Organic Electronics, **11** (2010) 1088. 3

[25] P. Kopola, M. Tuomikoski, R. Suhonen, and A. Maaninen. *Gravure printed organic light emitting diodes for lighting applications.* Thin Solid Films, **517** (2009) 5757. 3

[26] O. Reynolds. *On the action of rain to calm the sea.* Proceedings of the Literary and Philosophical Society of Manchester, **14** (1875) 72. 3, 93

[27] O. Reynolds. *On the floating of drops on the surface of water depending only on the purity of the surface.* Proceedings of the Literary and Philosophical Society of Manchester, **21** (1881) 1. 93

[28] J. Thomson and H. Newall. *On the Formation of Vortex Rings by Drops Falling into Liquids, and Some Allied Phenomena.* Proceedings of the Royal Society of London, **39** (1885) 417. 93

[29] A. Worthington. *A Study of Splashes.* Longmans, Green, **1908**. 93

[30] J. Seth, C. Anand, and L. Mahajan. *Liquid Drops on the same Liquid Surface.* Philosophical Magazine, **7** (1929) 247. 3, 93, 100

[31] O. Jayaratne and B. Mason. *The Coalescence and Bouncing of Water Drops at an Air/Water Interface.* Proceedings of the Royal Society of London A, **280** (1964) 545. 3, 4, 93, 94, 111, 112

[32] J. Walker. *Drops of liquid can be made to float on the liquid. What enables them to do so?* Scientific American, **238** (1978) 151. 93, 100

[33] A. Prosperetti and H. Oguz. *The Impact of Drops on Liquid Surfaces and the Underwater Noise of Rain.* Annual Review of Fluid Mechanics, **32** (1993) 580.

[34] G. Neitzel and P. Dell'Aversana. *Noncoalescence and Nonwetting Behavior of Liquids.* Annual Review of Fluid Mechanics, **34** (2002) 267.

[35] S. Manzello and J. Yang. *An experimental study of water droplet impinging on a liquid surface.* Experiments in Fluids, **32** (2002) 580.

[36] Y. Couder, E. Fort, C. Gautier, and A. Boudaoud. *From Bouncing to Floating: Noncoalescence of Drops on a Fluid Bath.* Physical Review Letters, **94** (2005) 177801. 97, 100

[37] A. Yarin. *Drop Impact Dynamics: Splashing, Spreading, Receding, Bouncing.* Annual Review of Fluid Mechanics, **38** (2006) 159. 3, 93

[38] T. Gilet and J. Bush. *The fluid trampoline: droplets bouncing on a soap film.* Journal of Fluid Mechanics, **625** (2009) 167. 3, 93, 108, 111

[39] Y. Amarouchene, G. Cristobal, and H. Kellay. *Noncoalescing drops.* Physical Review Letters, **87** (2001) 206104. 4, 94, 111, 112

[40] O. Reynolds. *On the Theory of Lubrication and Its Application to Mr. Beauchamp Tower's Experiments, Including an Experimental Determination of the Viscosity of Olive Oil.* Philosophical Transactions of the Royal Society of London, **177** (1886) 157. 4, 94, 111

[41] L. Rayleigh. *Investigations in Capillarity: The size of drops. The liberation of gas from supersaturated solutions. Colliding jets. The tension of contaminated water-surfaces.* Philosophical Magazine Series 5, **48** (1899) 321. 4, 94, 111

[42] L. Rayleigh. *On the Capillary Phenomena of Jets.* Proceedings of the Royal Society of London, **29** (1879) 71. 4, 94, 110

[43] R. Horn, L. Del Castillo, and S. Ohnishi. *Coalescing map for bubbles in surfactant-free aqueous electrolyte solutions.* Advances in Colloid and Interface Science, **168** (2011) 85. 4, 94

[44] A. Hollemann and E. Wiberg. *Lehrbuch der Anorganischen Chemie.* de-Gruyter, **1995**. 5

[45] W. Eisner, P. Gietz, and J. Axel. *Elemente Chemie II.* Ernst Klett-Verlag, **2000**.

[46] C. Mortimer and U. Müller. *Chemie - Das Basiswissen der Chemie.* Thieme, **2001**. 8

[47] H.-J. Butt, K. Graf, and M. Kappl. *Physics and Chemistry of Interfaces.* Wiley-VCH, **2003**. 7, 8, 20, 33

[48] P. Atkins and J. de Paula. *Physikalische Chemie.* Wiley-VCH, **2006**. 5

[49] R. Laughlin. *The Aqueous Phase Behavior of Surfactants.* Academic Press, **1996**. 5

[50] W. Gelbart, A. Ben-Shaul, and D. Roux. *Micelles, Membranes, Microemulsions and Monolayers*. Springer, **1994**. 7

[51] J. Israelachvili. *Intermolecular & Surface Forces*. Academic Press, **1991**. 7

[52] R. Atkin, V. Craig, E. Wanless, and S. Biggs. *Mechanism of cationic surfactant adsorption at the solid-aqueous interface*. Advances in Colloid and Interface Science, **103** (2003) 219. 8

[53] T. Young. *An essay on the cohesion of fluids*. Philosophical Trnasactions of the Royal Society of London, **95** (1805) 65. 10

[54] P.-S. Laplace. *Mécanique Céleste*. Croucier, **1805**. 10

[55] J. Marsh, S. Garoff, and E. Dussan V. *Dynamic Contact Angles and Hydrodynamics near a Moving Contact Line*. Physical Review Letters, **70** (1993) 2778. 12, 21

[56] P. Thompson and M. Robbins. *Simulations of Contact-Line Motion: Slip and the Dynamic Contact Angle*. Physical Review Letters, **63** (1989) 766. 12

[57] W. Hardy. *The Spreading of Fluids on Glass*. Philosophical Magazine, **38** (1919) 49. 13

[58] M. Popescu, G. Oshanin, S. Dietrich, and A.-M. Cazabat. *Precursor films in wetting phenomena*. Journal of Physics: Condensed Matter, **24** (2012) 243102. 13

[59] A. Cazabat, S. Gerdes, M. Valignat, and S. Villette. *Dynamics of Wetting: From Theory to Experiment*. Interface Science, **5** (1997) 129. 13

[60] E. Dussan V. *On the spreading of liquids on solid surfaces: Static and dynamic contact lines*. Annual Review of Fluid Mechanics, **11** (1979) 371. 15, 17, 18, 37

[61] T. Blake and Y. Shikhmurzaev. *Dynamic Wetting by Liquids of Different Viscosity*. Journal of Colloid and Interface Science, **253** (2002) 196. 15, 16, 20

[62] R. Hoffman. *A Study of the Advancing Interface*. Journ, **50** (1975) 228. 15

[63] T. Blake. *The physics of moving wetting lines*. Journal of Colloid and Interface Science, **299** (2006) 1. 16, 17, 18

[64] T. Blake and J. De Coninck. *The influence of solid-liquid interactions on dynamic wetting*. Advances in Colloid and Interface Science, **96** (2002) 21. 16

[65] Y. Shikhmurzaev. *The moving contact line on a smooth solid surface*. International Journal of Multiphase Flow, **19** (1993) 589. 18

[66] Y. Shikhmurzaev. *Mathematical modeling of wetting hydrodynamics*. Fluid Dynamics Research, **13** (1994) 45. 18

[67] J. Billingham and A. King. *The interaction of a moving fluid/fluid interface with a flat plate*. Journal of Fluid Mechanics, **296** (1995) 325. 18

[68] A. King, J. Billingham, and D. Popple. *The moving contact line between two wegdes of fluid on a flat plate*. The Quarterly Journal of Mechanics and Applied Mathematics, **53** (1999) 453. 18

[69] J. Eggers and H. Stone. *Characteristic lengths at moving contact lines for a perfectly wetting fluid: the influence of speed on the dynamic contact angle*. Journal of Fluid Mechanics, **505** (2004) 309. 16

[70] G. Yarnold and B. Mason. *A Theory of the Angle of Contact*. Proceedings of the Physical Society, Section B, **62** (1949) 121. 16

[71] C. Huh and L. Scriven. *Hydrodynamic Model of Steady Movement of a Solid/Liquid/Fluid Contact Line*. Journal of Colloid and Interface Science, **35** (1971) 85. 17, 48

[72] M. Maleki, M. Reyssat, F. Restagno, D. Quéré, and C. Clanet. *Landau-Levich menisci*. Journal of Colloid and Interface Science, **354** (2011) 359. 18, 19

[73] J. Snoeijer, J. Ziegler, B. Andreotti, M. Fermigier, and J. Eggers. *Thick Films of Viscous Fluid Coating a Plate Withdrawn from a Liquid Reservoir*. Physical Review Letters, **100** (2008) 244502. 19, 24

[74] J. Delacotte, L. Montel, F. Restagno, B. Scheid, B. Dollet, H. Stone, D. Langevin, and E. Rio. *Plate Coating: Influence of Concentrated Surfactants on the Film Thickness*. Langmuir, **28** (2012) 3821. 19

[75] L. Wilhelmy. *Über die Abhängigkeit der Capillaritäts-Constanten des Alkohols von Substanz und Gestalt des benetzten festen Körpers*. Annalen der Physik und Chemie, **195** (1863) 177. 19

[76] R. Burley and B. Kennedy. *An experimental study of air entrainment at a solid/liquid/gas interface*. Chemical Engineering Science, **31** (1976) 901. 20

[77] T. Blake and K. Ruschak. *A maximum speed of wetting*. Nature, **282** (1979) 489.

[78] E. Gutoff and C. Kendrick. *Dynamic Contact Angles*. The American Institute of Chemical Engineers Journal, **28** (1982) 459. 20

[79] R. Ablett. *An investigation of the angle of contact between paraffin wax and water*. Philosophical Magazine, **46** (1923) 244. 21

[80] S. Nesic. *Horizontal rotating cylinder - A compact apparatus for studying the effect of water wetting on carbon dioxide corrosion of mild steel*. Corrosion, **59** (2003) 1085. 21

[81] G. Nadkarni and S. Garoff. *Reproducibility of Contact Line Motion on Surfaces Exhibiting Contact Angle Hysteresis*. Langmuir, **10** (1994) 1618. 24

[82] E. Decker and S. Garoff. *Contact Line Structure and Dynamics on Surfaces with Contact Angle Hysteresis*. Langmuir, **13** (1997) 6321. 24

[83] G. Delon, M. Fermingier, J. Snoeijer, and B. Andreotti. *Relaxation of a dewetting contact line. Part 2. Experiments*. Journal of Fluid Mechanics, **604** (2008) 55. 24

[84] G. Binnig, C. F. Quate, and C. Gerber. *Atomic Force Microscope*. Physical Review Letters, **56** (1986) 930. 32

[85] R. Chaudhuri and S. Paria. *Dynamic contact angles on PTFE surface by aqueous surfactant solution in the absence and presence of electrolytes*. Journal of Colloid and Interface Science, **337** (2009) 555. 35, 60

[86] D. Fell, G. Auernhammer, E. Bonaccurso, C. Liu, M. Sokuler, and H.-J. Butt. *Influence of Surfactant Concentration and Background Salt on Forced Dynamic Wetting and Dewetting*. Langmuir, **27** (2011) 2112. 41, 49, 54, 55, 72

[87] D. Keller, R. Carbonell, and P. Kilpatrick. *Adsorption Equilibria and Desorption Rates of Charged Ethoxylated Surfactants on Octadecyl Silica: Role of Electrostatics*. Journal of Colloid and Interface Science, **155** (1993) 124. 44

[88] B. Lindman, M.-C. Puyal, N. Kamenka, R. Rymdén, and P. Stilbs. *Micelle Formation of Anionic and Cationic Surfactants from Fourier Transform Hydrogen-1 and Lithium-7 Nuclear Magnetic Resonance and Tracer Self-Diffusion Studies*. The Journal of Physical Chemistry, **88** (1984) 5048. 55

[89] K. Mackie. *The Role of Surfactants in Aqueous Solution Diffusion in Hydrophobic Nanoporous Thin-Film Glasses*. NNIN REU Research Accomplishments, p. 66. 58

[90] R. Krechetnikov. *On application of lubrication approximations to nonunidirectional coating flows with clean and surfactant interfaces.* Physics of Fluids, **22** (2010) 92102. 58

[91] H. Mayer and R. Krechetnikov. *Flow visualization of the Landau-Levich problem - a resolution of the film thickening controversy.* In *American Physicle Society 63rd Annual Division of Fluid Dynamics Meeting.* **2010**. 58

[92] L. Gao and T. McCarthy. *Teflon is Hydrophilic. Comments on Definitions of Hydrophobic, Shear versus Tensile Hydrophobicity, and Wettability Characterization.* Langmuir, **24** (2008) 9183. 60

[93] M. Strobel, P. Thomas, and C. Lyons. *Plasma Fluorination of Polystyrene.* Journal of Polymer Science, Part A: Polymer Chemistry, **25** (1987) 3343. 60

[94] R. Cox. *The spreading of a liquid on a rough solid surface.* Journal of Fluid Mechanics, **131** (1983) 1. 75

[95] J. Bico, C. Marzolin, and D. Quéré. *Pearl drops.* Europhysics Letters, **47** (1999) 220.

[96] S. Herminghaus. *Roughness-induced non-wetting.* Europhysics Letters, **52** (2000) 165.

[97] K. Kubiak, M. Wilson, T. Mathia, and S. Carras. *Dynamics of contact line motion during the wetting of rough surfaces and correlation with topographical surface parameters.* Scanning, **33** (2011) 370. 75

[98] R. Wenzel. *Resistance of solid surfaces to wetting by water.* Industrial and engineering chemistry, **28** (1936) 988. 75, 80

[99] G. Wolansky and A. Marmur. *Apparent contact angles on rough surfaces: the Wenzel equation revisited.* Colloids and Surfaces A: Physicochemical and Engineering Aspects, **156** (1999) 381.

[100] D. Quéré. *Wetting and Roughness.* Annual Reviews of Materials Research, **38** (2008) 71. 75, 80, 81

[101] Z. Burton and B. Bhushan. *Hydrophobicity, Adhesion, and Friction Properties of Nanopatterned Polymers and Scale Dependence for Micro- and Nanoelectromechanical Systems.* Nano Letters, **5** (2005) 1607. 75

[102] Y. Kalinin, V. Berejnov, and R. Thorne. *Contact Line Pinning by Microfabricated Patterns: Effects of Microscale Topography.* Langmuir, **25** (2009) 5391. 75

[103] H. Modaressi-Esfeh. *Wetting on heterogeneous surfaces*. Ph.D. thesis, McGill University, Montréal, **2001**. 75

[104] S. Herminghaus, M. Brinkmann, and R. Seemann. *Wetting and Dewetting of Complex Surface Geometries*. Annual Reviews of Materials Research, **38** (2008) 101. 81

[105] V. H. G. R. B. Slavchov, R. Dutschk. *Justification of biexponential rate law of spreading over heterogeneous and rough surfaces*. Colloids and Surfaces A: Physicochemical and Engineering Aspects, **354** (2010) 252. 87

[106] P. Joanny, J.F. de Gennes. *A model for contact angle hysteresis*. Journal of Chemical Physics, **81** (1984) 552. 87

[107] S. Schwartz, L.W. Garoff. *Contact angle hysteresis on heterogeneous surfaces*. Langmuir, **1** (1985) 219. 87

[108] T. Eibach. *Messung des Kontaktwinkels bei erzwungener dynamischer Be- und Entnetzung unter Verwendung eines reflektierten Laserstrahls*. Staatsexamensarbeit, **2012**. 88

[109] T. Eibach, D. Fell, T.-H. Nguyen, R. Berger, H.-J. Butt, and G. Auernhammer. *Measuring contact angle and meniscus shape with a reflected laser beam*. under preparation. 88

[110] L. Courbin and H. Stone. *Impact, puncturing, and the self-healing of soap films*. Physics of Fluids, **18** (2006) 91105–1. 93

[111] S. Thoroddsen, K. Takehara, T. Etoh, and Y. Hatsuki. *Puncturing a drop using surfactants*. Journal of Fluid Mechanics, **530** (2005) 295. 93

[112] G. Charles and S. Mason. *The coalescence of liquid drops with flat liquid/liquid interfaces*. Journal of Colloid Science, **15** (1960) 236. 94, 111

[113] J. Israelachvili and D. Tabor. *The Measurement of Van Der Waals Dispersion Forces in the RAnge 1.5 to 130 nm*. Proceedings of the Royal Society of London A - Mathematical and Physical Sciences, **331** (1972) 19. 94, 111

[114] O. Manor, I. Vakarelski, G. Stevens, F. Grieser, R. Dagastine, and D. Chan. *Dynamic Forces between Bubbles and Surfaces and Hydrodynamic Boundary Conditions*. Langmuir, **24** (2008) 11533. 94, 111, 112, 113, 114

[115] D. Chan, E. Klaseboer, and R. Manica. *Dynamic deformations and forces in soft matter*. Soft Matter, **5** (2009) 2858. 94, 111, 112

[116] P.-G. de Gennes, F. Brochard-Wyart, and D. Quéré. *Capillarity and Wetting Phenomena*. Springer, **2002**. 105

[117] H. Lamb. *Hydrodynamics*. Cambridge Universtiy Press, **1879**. 110

[118] J. Bird, S. Mandre, and H. Stone. *Short-Time Dynamics of Partial Wetting*. Physical Review Letters, **100** (2008) 234501. 111

[119] L. Chen, G. Auernhammer, and E. Bonaccurso. *Short time wetting dynamics on soft surfaces*. Soft Matter, **7** (2011) 9084. 111

[120] L. Rayleigh. *Further Observations upon Liquid Jets, in Continuation of Those Recorded in the Royal Society's 'Proceedings' for March and May, 1879*. Proceedings of the Royal Society of London, **34** (1882) 130. 111

[121] R. Schotland. *Experimental results relating to the coalescence of water drops with water surfaces*. Discussions of the Faraday Society, **30** (1960) 72. 111

[122] G. Bach, D. Koch, and A. Gopinath. *Coalescence and bouncing of small aerosol droplets*. Journal of Fluid Mechanics, **518** (2004) 157. 112

[123] A. Gopinath and D. Koch. *Dynamics of droplet rebound from a weakly deformable gas-liquid interface*. Physics of Fluids, **13** (2001) 3526.

[124] A. Gopinath and D. Koch. *Collision and rebound of small droplets in an incompressible continuum gas*. Journal of Fluid Mechanics, **454** (2002) 145.

[125] P. Hicks and R. Purvis. *Air cushioning and bubble entrapment in three-dimensional droplet impacts*. Journal of Fluid Mechanics, **649** (2010) 135.

[126] M. Mani, S. Mandre, and M. Brenner. *Events before droplet splashing on a solid surface*. Journal of Fluid Mechanics, **647** (2010) 163. 112

[127] N. Balmforth, C. Cawthorn, and R. Craster. *Contact in a viscous fluid. Part 2. A compressible fluid and an elastic solid*. Journal of Fluid Mechanics, **646** (2010) 339. 112

[128] A. Javadi, D. Bastani, J. Krägel, and R. Miller. *Interfacial instability of growing drop: Experimental study and cenceptual analysis*. Colloids and Surfaces, A: Physicochemical and Engineering Aspects, **347** (2009) 167. 113

[129] O. Manor, I. Vakarelski, X. Tang, S. O'Shea, G. Stevens, F. Grieser, R. Dagastine, and D. Chan. *Hydrodynamic Boundary Conditions and Dynamic Forces between Bubbles and Surfaces*. Physical Review Letters, **101** (2008) 24501. 113, 114

[130] G. Kelsall, S. Tang, A. Smith, and S. Yurdakul. *Measurement of rise and electrophoretic velocities of gas bubbles.* Journal of the Chemical Society, Faraday Transactions, **92** (1996) 3879. 114

[131] L. Parkinson, R. Sedev, D. Fornasiero, and J. Ralston. *The terminal rise velocity of 10-100 $\mu$m diameter bubbles in water.* Journal of Colloid and Interface Science, **322** (2008) 168.

[132] Y. Pawar and K. Stebe. *Marangoni effects on drop deformation in an extensional flow: The role of surfactant physical chemistry. 1. Insoluble Surfactants.* Physics of Fluids, **8** (1996) 1738.

[133] S. Takagi, T. Ogasawara, and Y. Matsumoto. *The effects of surfactant on the multiscale structure of bubbly flows.* Philosophical Transactions of the Royal Society A - Mathematical, Physical and Engineering Sciences, **366** (2008) 2117.

[134] C. Ybert and J. di Meglio. *Ascencing air bubbles in solutions of surface-active molecules: Influence of desorption kinetics.* The European Physical Journal E: Soft Matter and Biological Physics, **3** (2000) 143. 114

[135] R. Dagastine, R. Manica, S. Carnie, D. Chan, and G. Stevens. *Dynamic Forces Between Two Deformable Oil Droplets in Water.* Science, **313** (2006) 210. 114

[136] G. Hebrard, J. Zeng, and K. Loubiere. *Effect of surfactants on liquid side mass transfer coefficients: A new insight.* Chemical Engineering Journal, **148** (2009) 132. 115

[137] R. Noyes, M. Rubin, and P. Bowers. *Transport of Carbon Dioxide between the Gas Phase and Water uner Well-Stirred Conditions: Rate Constatns and Mass Accommodation Coefficients.* The Journal of Physical Chemistry, **100** (1996) 4167. 115

[138] R. Noyes, M. Rubin, and P. Bowers. *An alternative model for transport of molecules between gas and solution.* The Journal of Physical Chemistry, **96** (1992) 1000. 115

[139] E. Wilhelm, R. Battino, and R. Wilcock. *Low-pressure solubility of gases in liquid water.* Chemical Reviews, **77** (1977) 219. 115

# List of abbreviations

| | |
|---|---|
| $a$ | interfacial area |
| $\Delta A$ | change in surface area |
| $b$ | slip length |
| $c$ | concentration |
| $c(t)$ | concentration as a function of time |
| $c^{eq}$ | equilibrium concentration |
| $c_g$ | gas concentration |
| $c_i$ | initial concentration |
| $\mathrm{C}_n$ | alkyl chain |
| $\mathrm{C}_n\mathrm{E}_m$ | alkyl glycole |
| $\mathrm{C}_n\mathrm{H}_{2n+1}$ | alkyl chain |
| $\mathrm{C}_4\mathrm{E}_1$ | butyl glycole |
| $\mathrm{C}_8\mathrm{E}_3$ | octyl triglycole |
| $\mathrm{C}_{12}\mathrm{E}_5$ | dodecyl pentaglycole |
| $\mathrm{C}_{12}\mathrm{H}_{25}\mathrm{OSO}_3\mathrm{Na}$ | sodium dodecyl sulfate |
| $\mathrm{C}_{16}\mathrm{H}_{33}\mathrm{N}(\mathrm{CH}_3)_3\mathrm{Br}$ | cetyl trimethyl ammonium bromide |
| $Ca$ | Capillary number |
| cmc | critical micelle concentration |
| CTAB | cetyl trimethyl ammonium bromide |
| $d$ | thickness of the free-standing film |
| $D$ | diffusion coefficient |
| $e$ | elementary charge |
| $\mathrm{E}_m$ | glycole chain |

| | |
|---|---|
| $F_{\gamma,\theta}$ | force resulting from Wilhelmy technique measurements |
| $g$ | gravity constant |
| $h$ | film thickness |
| $h_g$ | gap thickness |
| $h_l$ | diffusively accesible film thickness |
| HMDS | hexamethyl disilazane |
| $I$ | ionic strength |
| $k$ | spring constant |
| $k_B$ | Boltzmann constant |
| $k_H$ | Henry constant |
| $k_l$ | characteristic constant |
| $l$ | plate length |
| $L$ | macroscopic length |
| $L_m$ | microscopic length |
| $m$ | mass |
| $M_w$ | molecular weight |
| $n$ | number of carbon molecules |
| $N_A$ | Avogardo number |
| $N_g$ | number of moles diffusing into the gas |
| $N_l$ | number of moles diffusing into the liquid |
| NaCl | sodium chloride |
| $p$ | pressure |
| PFTE | poly(tetrafluoroethylene) |
| $Q$ | hydrodynamic air flux |
| $r$ | average roughness ratio |
| $r_d$ | drop radius |
| $R$ | gas constant |
| SDS | sodium dodecyl sulfate |

| | |
|---|---|
| SFM | scanning force microscopy |
| $t_c$ | contact time |
| $t_c - We-$plot | plot of contact time versus Weber number |
| $T$ | temperature |
| THF | tetrahydrofuran |
| $U$ | velocity |
| $U_c$ | critical velocity |
| $\vec{v}$ | local velocity of intervening air |
| $v_{cap}$ | velocity of a capillary wave |
| $v_d$ | impact velocity of a drop |
| $v_r$ | radial component of the velocity of intervening air |
| $V_g$ | diffusively accessible gas volume |
| $V_l$ | diffusively accessible liquid volume |
| $V_m$ | molecular flow volume |
| $W_a$ | work of adhesion |
| $\Delta W$ | performed work |
| $We$ | Weber number |
| wt % | weight percent |
| | |
| $\alpha$ | roll-off angle |
| $\gamma$ | surface tension |
| $\gamma_0$ | surface tension of pure water |
| $\gamma_d$ | surface tension of the drop |
| $\gamma_f$ | surface tension of the film |
| $\gamma_L$ | interfacial tension of the liquid |
| $\gamma_S$ | interfacial tension of the solid |
| $\gamma_{SL}$ | interfacial tension of the liquid-solid interface |
| $\Gamma$ | adsorption function |

| | |
|---|---|
| $\epsilon_0$ | permittivity of free space |
| $\epsilon_r$ | dielectric constant |
| $\eta$ | viscosity |
| $\theta$ | contact angle |
| $\theta_0$ | zero-velocity contact angle |
| $\theta_s$ | static contact angle |
| $\theta_{adv}$ | advancing contact angle |
| $\theta_{ap}$ | apparent contact angle |
| $\theta_{eq}$ | equilibrium contact angle |
| $\theta_m$ | microscopic contact angle |
| $\theta_{rec}$ | receding contact angle |
| $\theta - c-$plot | plot of contact angle versus concentration |
| $\theta - U-$plot | plot of contact angle versus velocity |
| $\lambda$ | average distance of displacement |
| $\lambda_D$ | Debye length |
| $\rho$ | fluid density |
| $\varsigma$ | three-phase contact line friction |
| $\bar{\tau}_{bouncing}$ | mean contact time for bouncing impacts |
| $\tau_d$ | vibration period of the drop |
| $\tau_f$ | vibration period of the film |
| $\tau_h$ | characteristic time to travel over a distance $h$ |
| $\bar{\tau}_{passing}$ | mean contact time for passing impacts |
| $\tau_x$ | characteristic time to travel over a thickness $x$ |
| | |
| $\varnothing$ | diameter |

# Acknowledgements

"Keine Schuld ist dringender, als die, Dank zu sagen."

*Marcus Tullius Cicero*

Getreu diesem Motto, möchte ich hiermit die Gelegenheit ergreifen und mich bei all denen bedanken, die zum Gelingen dieser Arbeit beigetragen haben - sei es durch Rat und Tat oder moralische Unterstützung:

# Curriculum vitae

# Publications

**2013**

D. Fell, N. Pawanrat, E. Bonaccurso, H.-J. Butt, G.K. Auernhammer, *Influence of surfactant transport suppression on dynamic contact angle hysteresis*, Colloid and Polymer Science **291**, 361 (2013).

D. Fell, M. Sokuler, A. Lembach, T.F. Eibach, C. Liu, E. Bonaccurso, G.K. Auernhammer, H.-J. Butt, *Drop impact on surfactant films and solutions*, Colloid and Polymer Science, DOI 10.1007/s00396-013-2931-z.

T.F. Eibach, D. Fell, T.-H. Nguyen, R. Berger, H.-J. Butt, G.K. Auernhammer, *Measuring contact angles and meniscus shape with a reflected laser beam*, in preparation.

**2012**

M. Anyfantakis, D. Fell, H.-J. Butt, G.K. Auernhammer, *Time-dependent dynamic receding contact angles during the flow of dilute aqueous surfactant solutions through fluorinated microtubes*, Chemistry Letters **41**, 1232 (2012).

C. Curschellas, R. Keller, R. Berger, U. Rietzler, D. Fell, H.-J. Butt, H.J. Limbach, *Scanning force microscopy as a tool to investigate the properties of polyglycerol ester foams*, Journal of Colloid and Interface Science **374**, 164 (2012).

**2011**

C. Liu, M.C. Lopes, S.A. Pihan, D. Fell, M. Sokuler, H.-J. Butt, G.K. Auernhammer, E. Bonaccurso, *Water diffusion in polymer nano-films measured with microcantilevers*, Sensors and Actuators B: Chemical **160**, 32 (2011).

J.P. Fernández-Blázquez, D. Fell, E. Bonaccurso, A. del Campo, *Superhydrophilic and superhydrophobic nanostructured surfaces via plasma treatment*, Journal of Colloid and Interface Science **357**, 234 (2011).

D. Fell, G.K. Auernhammer, E. Bonaccurso, C. Liu, M. Sokuler, H.-J. Butt, *Influence of surfactant concentration and background salt on forced dynamic wetting and dewetting*, Langmuir **27**, 2112 (2011).

**2010**

C. Liu, Y. Liu, M. Sokuler, D. Fell, S. Keller, A. Boisen, H.-J. Butt, G.K. Auernhammer, E. Bonaccurso, *Diffusion of water into SU-8 microcantilevers*, Physical Chemistry Chemical Physics **12**, 10577 (2010).

# International conference contributions

**2012**

05/2012 Conference of the International Association of Colloid and Interface Scientists (IACIS), Sendai, Japan: "Influence of surfactant concentration and transport on forced dynamic wetting", Talk.

03/2012 8th Zsigmondy-Kolloquium of the German Colloid Society, Darmstadt, Germany: "Influence of surfactant concentration and transport on forced dynamic wetting", Poster.

03/2012 Annual meeting of the German Physical Society (DPG), Berlin, Germany: "Influence of surfactant concentration and transport on forced dynamic wetting", Talk.

**2011**

09/2011 25th Conference of the European Colloid and Interface Society (ECIS), Berlin, Germany: "Influence of surfactant concentration on forced dynamic wetting and dewetting", Talk.

05/2011 18th Ostwald Kolloquium on Dynamic Wetting of Complex Liquids, Mainz, Germany: "Influence of surfactant concentration on forced dynamic wetting and dewetting", Talk.

03/2011 Annual meeting of the German Physical Society (DPG), Dresden, Germany: "Drop impact on free-standing surfactant films", Talk.

02/2011 7th Zsigmondy-Kolloquium of the German Colloid Society, Münster, Germany: "Influence of surfactant concentration on forced dynamic wetting and dewetting", Poster.

**2010**

07/2010 International Soft Matter Conference (ISMC), Granada, Spain: "Drop impact on free-standing surfactant films: Air cushion trapped by surfactant molecules", Poster.